Astronomy & Astrophysics

Gaia FGK benchmark stars: Effective temperatures and surface gravities

U. Heiter[1], P. Jofré[2], B. Gustafsson[1,4], A. J. Korn[1], C. Soubiran[3], and F. Thévenin[5]

[1] Institutionen för fysik och astronomi, Uppsala universitet, Box 516, 751 20 Uppsala, Sweden
  e-mail: ulrike.heiter@physics.uu.se
[2] Institute of Astronomy, University of Cambridge, Madingley Rd, Cambridge, CB3 0HA, UK
[3] Univ. Bordeaux, CNRS, LAB, UMR 5804, 33270 Floirac, France
[4] Nordita, Roslagstullsbacken 23, 106 91 Stockholm, Sweden
[5] Université de Nice-Sophia Antipolis, CNRS (UMR 7293), Observatoire de la Côte d'Azur, CS 34229, 06304 Nice Cedex 4, France

ABSTRACT

Context. In the era of large Galactic stellar surveys, carefully calibrating and validating the data sets has become an important and integral part of the data analysis. Moreover, new generations of stellar atmosphere models and spectral line formation computations need to be subjected to benchmark tests to assess any progress in predicting stellar properties.
Aims. We focus on cool stars and aim at establishing a sample of 34 *Gaia* FGK benchmark stars with a range of different metallicities. The goal was to determine the effective temperature and the surface gravity independently of spectroscopy and atmospheric models as far as possible. Most of the selected stars have been subjected to frequent spectroscopic investigations in the past, and almost all of them have previously been used as reference, calibration, or test objects.
Methods. Fundamental determinations of $T_{\rm eff}$ and $\log g$ were obtained in a systematic way from a compilation of angular diameter measurements and bolometric fluxes and from a homogeneous mass determination based on stellar evolution models. The derived parameters were compared to recent spectroscopic and photometric determinations and to gravity estimates based on seismic data.
Results. Most of the adopted diameter measurements have formal uncertainties around 1%, which translate into uncertainties in effective temperature of 0.5%. The measurements of bolometric flux seem to be accurate to 5% or better, which contributes about 1% or less to the uncertainties in effective temperature. The comparisons of parameter determinations with the literature in general show good agreements with a few exceptions, most notably for the coolest stars and for metal-poor stars.
Conclusions. The sample consists of 29 FGK-type stars and 5 M giants. Among the FGK stars, 21 have reliable parameters suitable for testing, validation, or calibration purposes. For four stars, future adjustments of the fundamental $T_{\rm eff}$ are required, and for five stars the $\log g$ determination needs to be improved. Future extensions of the sample of *Gaia* FGK benchmark stars are required to fill gaps in parameter space, and we include a list of suggested candidates.

Key words. stars: late-type – stars: fundamental parameters – stars: atmospheres – standards – surveys

1. Introduction

We are about to revolutionise our knowledge about the Milky Way Galaxy thanks to the recently launched *Gaia* mission (e.g. Perryman et al. 2001; Turon et al. 2005; Lindegren et al. 2008). With its exquisite precision of parallaxes and proper motions for millions of stars of our Galaxy, complemented with spectrophotometric and spectroscopic observations, a much improved picture of the kinematics and chemical composition of the Galactic populations will become available. This will allow us to understand the formation history of the Milky Way and its components in more detail. Achieving this goal requires proper calibration of the data sets.

In this context it is important to note that the system developed for the astrophysical parameter (AP) determination of *Gaia* sources will be almost entirely based on model spectra (Apsis[1], Bailer-Jones et al. 2013). Apsis uses methods that perform supervised classification, involving a comparison of the observed data with a set of templates. For the purpose of estimating stellar atmospheric parameters one may use either observed or synthetic

spectra as templates. Observed spectra are expected to represent individual *Gaia* spectrophotometric and spectroscopic observations better, but they do not cover the whole parameter range with sufficient density because of the small number of stars with accurately known APs. Synthetic templates allow one to deal with the latter issue, and also to attempt to classify sources that are very rare and possibly as yet unobserved. Furthermore, the effects of observational noise and interstellar extinction can be considered in a systematic way. However, synthetic spectra are based on simplified descriptions of the complex physical processes taking place in real stars. This causes a possible mismatch between synthetic and observed spectra, which may introduce large external errors in derived APs. Thus, the algorithms of Apsis using synthetic templates will need to be calibrated to account for deficiencies in the physics of the models used.

The calibration can be implemented by applying corrections either to the synthetic spectra before they are used or to the APs produced by each algorithm. For both approaches we need a set of reference objects, which will be observed by *Gaia*, but for which accurate APs have been determined by independent methods from ground-based observations (e.g. higher

---
[1] *Gaia* astrophysical parameters inference system.

resolution spectra). For those algorithms that estimate $T_{\rm eff}$, $\log g$, and [Fe/H], the reference objects will be divided into two goal levels. At the first level, we identify a small number of well-known bright benchmark stars. These will not necessarily be observed by *Gaia* owing to its bright magnitude limit, but their properties are being investigated in detail by ground-based observations. The second level consists of a large number (several hundred) of AP reference stars to ensure dense coverage of the AP space and to have magnitudes within the reach of *Gaia*. These stars will be characterised in an automated way using ground-based high-resolution spectroscopy with a calibration linking their APs to those of the benchmark stars.

Another approach to mitigating the spectrum mismatch problem is to improve the modelling of the synthetic spectra. For example, the synthetic stellar libraries currently in use for classification of FGK-type stars in Apsis (see Table 2 in Bailer-Jones et al. 2013) are mostly based on 1D hydrostatic model atmospheres where local thermodynamic equilibrium (LTE) is assumed. More realistic 3D radiation-hydrodynamics (RHD) simulations and results of detailed statistical equilibrium calculations are expected to be implemented in future versions of the libraries. It will be important to test the actual degree of improvement achieved with the new generations of atmospheric models. The benchmark stars may serve as test objects, for which synthetic observables generated from atmospheric models using different assumptions for the input physics can be compared with the observed data.

A set of stars with atmospheric parameters determined independently from spectroscopy will also be suitable to calibrate methods and input data for spectroscopic analyses, such as those based on the characterisation of thousands of spectra from ground-based surveys complementary to *Gaia*. Examples of such surveys are the *Gaia*-ESO Public Spectroscopic Survey (Gilmore et al. 2012; Randich et al. 2013), RAVE (Steinmetz et al. 2006), APOGEE (Allende Prieto et al. 2008), and GALAH (De Silva et al. 2015). To test that a method yields robust results, it should be applied to a set of spectra with known parameters to verify that the results agree.

However, after several decades of Galactic science using spectroscopic surveys, there is still no set of reference stars common to different data sets. In fact, the Sun has been used by most studies to calibrate methods of analysing the spectra of solar-type stars. Arcturus has also been widely used as a reference giant, although with varying stellar parameters. Some recent publications using Arcturus as a reference are Morel et al. (2014), Sbordone et al. (2014), Mészáros et al. (2013), Mortier et al. (2013), Ruchti et al. (2013), Thygesen et al. (2012), Worley et al. (2012), Boeche et al. (2011), Prugniel et al. (2011). The $T_{\rm eff}$ values used in these publications range from 4230 to 4340 K, the $\log g$ values from 1.5 to 1.9 dex, and the overall metallicities from -0.60 to -0.47 dex. Each of these publications used a different source for the parameters of Arcturus.

In this article, we aim at defining a sample of benchmark stars covering the range of F, G, and K spectral types at different metallicities, which is representative of a significant part of the stellar populations in our Galaxy. Stars of these spectral types will be the most numerous among the objects observed by *Gaia* – 86% of all stars with $V < 20$ according to estimations by Robin (2005). The benchmark stars are selected to have as much information as possible available to determine their effective temperature and surface gravity independently from spectroscopy. We refer to these stars as the *Gaia* FGK benchmark stars, as they will be used as pillars for the calibration of the *Gaia* parameter determination.

This is the first in a series of articles about the work on *Gaia* FGK benchmark stars, introducing the sample and describing the determination of effective temperature and surface gravity from fundamental relations. The second article of this series (Blanco-Cuaresma et al. 2014, hereafter Paper II) describes our libraries of observed high-resolution optical spectra for *Gaia* FGK benchmark stars and includes an assessment of the data quality. In the third article (Jofré et al. 2014b, hereafter Paper III), the fundamental $T_{\rm eff}$ and $\log g$ and the spectral libraries were used for metallicity determinations, based on the analysis of Fe lines by several methods. The three articles provide a full documentation, which is also summarised in Jofré et al. (2014a). In addition, an abundance analysis for more than 20 chemical elements accessible in the spectral libraries is in progress, and we are working on a future extension of the sample to improve the coverage of parameter space (cf. Appendix B).

The remainder of the article is organised as follows. In Sect. 2 we describe the selection of the current set of 34 *Gaia* FGK benchmark stars. In Sects. 3 and 4 we describe the determination of effective temperatures and surface gravities, respectively, based on angular diameters, bolometric fluxes, masses, and distances. In Sect. 5 we present our results and compare our set of parameters with spectroscopic and photometric determinations extracted from the literature. Section 6 contains a star-by-star summary of parameter quality and concludes the article.

2. Sample selection

The current sample of *Gaia* FGK benchmark stars was selected to cover the range of effective temperatures between about 4000 K and 6500 K. This region of the HR diagram was divided into the categories of F dwarfs, FGK subgiants, G dwarfs, FGK giants, and K dwarfs. For each of these categories we aimed at selecting at least two stars, one with solar and one with sub-solar metallicity. We also added a few M giants with $T_{\rm eff} \lesssim 4000$ K to enable an assessment of models and methods at the parameter range limits.

The main selection criteria are related to the availability of information required to determine the effective temperature and the surface gravity from fundamental relations (see Sects. 3 and 4). Angular diameter measurements should be available or expected in the near future, and bolometric fluxes should be reliably determined, in order to calculate the effective temperature. Accurate parallax measurements are a prerequisite for a fundamental $\log g$ determination. In addition, we considered stars that are members of visual or eclipsing binary systems and stars for which asteroseismic data are available or which are targets of asteroseismology missions or campaigns, such as CoRoT or *Kepler*. Finally, the stars were primarily chosen among those subjected to frequent spectroscopic investigations in the past.

Table 1 lists the identifiers and basic information for the current sample of *Gaia* FGK benchmark stars. The *V* magnitudes range from 0 to 8. About two thirds of the stars are fainter than 3 mag and will be included in the magnitude range observed by *Gaia* (see Martín-Fleitas et al. 2014 for a discussion of the detection of bright stars with *Gaia*). The stars are evenly distributed along the celestial equator, and all but ten stars have declinations within ±30 deg. Thus, a large part of the sample can be observed with telescopes on both hemispheres. The sample contains several visual binary stars. These are discussed in Sect. 4.2. A few active stars are also included, in case activity diagnostics need to be evaluated. Procyon, ϵ Eri, and 61 Cyg A were classified as active stars by Gray et al. (2003) based on Ca II H and K line emission, while μ Cas, 18 Sco, Gmb 1830, and 61 Cyg B were found

Table 1. General information for current sample of *Gaia* FGK benchmark stars.

Name	HD	RA (J2000)	Dec (J2000)	Spectral type	V mag	[Fe/H][†]	u([Fe/H])[‡]
F dwarfs							
Procyon	61421	07 39 18.119	+05 13 29.96	F5IV-V	0.4	0.01	0.08
HD 84937	84937	09 48 56.098	+13 44 39.32	sdF5	8.3	–2.03	0.08
HD 49933	49933	06 50 49.832	–00 32 27.17	F2V	5.8	–0.41	0.08
FGK subgiants							
δ Eri	23249	03 43 14.901	–09 45 48.21	K1III-IV	3.5	0.06	0.05
HD 140283	140283	15 43 03.097	–10 56 00.60	sdF3	7.2	–2.36	0.10
ε For	18907	03 01 37.637	–28 05 29.60	K2VFe-1.3CH-0.8	5.9	–0.60	0.10
η Boo	121370	13 54 41.079	+18 23 51.79	G0IV	2.7	0.32	0.08
β Hyi	2151	00 25 45.070	–77 15 15.29	G0V	2.8	–0.04	0.06
G dwarfs							
α Cen A	128620	14 39 36.494	–60 50 02.37	G2V	0.0	0.26	0.08
HD 22879	22879	03 40 22.064	–03 13 01.12	F9V	6.7	–0.86	0.05
Sun						0.03	0.05
μ Cas	6582	01 08 16.395	+54 55 13.23	G5Vb	5.2	–0.81	0.03
τ Cet	10700	01 44 04.083	–15 56 14.93	G8.5V	3.5	–0.49	0.03
α Cen B	128621	14 39 35.063	–60 50 15.10	K1V	1.4	0.22	0.10
18 Sco	146233	16 15 37.269	–08 22 09.99	G2Va	5.5	0.03	0.03
μ Ara	160691	17 44 08.701	–51 50 02.59	G3IV-V	5.1	0.35	0.13
β Vir	102870	11 50 41.718	+01 45 52.99	F9V	3.6	0.24	0.07
FGK giants							
Arcturus	124897	14 15 39.672	+19 10 56.67	K1.5III	–0.1	–0.52	0.08
HD 122563	122563	14 02 31.845	+09 41 09.95	F8IV	6.2	–2.64	0.22
μ Leo	85503	09 52 45.817	+26 00 25.03	K2III	3.9	0.25	0.15
β Gem	62509	07 45 18.950	+28 01 34.32	K0IIIb	1.1	0.13	0.16
ε Vir	113226	13 02 10.598	+10 57 32.94	G8III	2.8	0.15	0.16
ξ Hya	100407	11 33 00.115	–31 51 27.44	G7III	3.5	0.16	0.20
HD 107328	107328	12 20 20.981	+03 18 45.26	K0IIIb	5.0	–0.33	0.16
HD 220009	220009	23 20 20.583	+05 22 52.70	K2III	5.0	–0.74	0.13
M giants							
α Tau	29139	04 35 55.239	+16 30 33.49	K5III	0.9	–0.37	0.17
α Cet	18884	03 02 16.773	+04 05 23.06	M1.5IIIa	2.5	–0.45	0.47
β Ara	157244	17 25 17.988	–55 31 47.59	K3Ib-II	2.8	–0.05	0.39
γ Sge	189319	19 58 45.429	+19 29 31.73	M0III	3.5	–0.17	0.39
ψ Phe	11695	01 53 38.741	–46 18 09.60	M4III	4.4	–1.24	0.39
K dwarfs							
ε Eri	22049	03 32 55.845	–09 27 29.73	K2Vk:	3.7	–0.09	0.06
Gmb 1830	103095	11 52 58.769	+37 43 07.23	G8Vp	6.4	–1.46	0.39
61 Cyg A	201091	21 06 53.952	+38 44 57.99	K5V	5.2	–0.33	0.38
61 Cyg B	201092	21 06 55.264	+38 44 31.40	K7V	6.0	–0.38	0.03

Notes. Coordinates and spectral types are extracted from the SIMBAD database. The *V* magnitudes are mean values extracted from the General Catalogue of Photometric Data (GCPD[2], Mermilliod et al. 1997). [†] Non-LTE [Fe/H] value from Table 3 of Paper III. [‡] [Fe/H] uncertainty obtained by quadratically summing all σ and Δ columns in Table 3 of Paper III.

to be inactive. Surprisingly, HD 49933, the main asteroseismic target of the CoRoT mission, has been discovered as strongly active with surface spots (Mosser et al. 2005). This type of activity can modify the emergent stellar flux, leading to an increased uncertainty in T_{eff}. Beasley & Cram (1993) measured an activity index based on Ca II H and K line emission for ξ Hya. For ten stars, an X-ray luminosity was measured by ROSAT (Hünsch et al. 1998), which is given relative to bolometric luminosity in Sect. 4.1.

Almost all stars in the current sample fulfil the main criteria, with two exceptions. We included two dwarf stars with extreme metallicities, even though their angular diameters do not lie within reach of current interferometers. HD 84937 is the faintest star ($V = 8$), and it has a predicted angular diameter of 0.15 mas (O. Creevey, priv. comm.). Thus, it is too small and too faint to be measured with currently existing interferometers. At

a distance of ~70 pc, it is, however, the closest dwarf star with a metallicity around −2 dex, and one of the most studied halo dwarfs (e.g. Bergemann et al. 2012b; Mashonkina et al. 2008). It remains an important candidate benchmark star, awaiting future improvements in capabilities of interferometers, e.g. the Navy Precision Optical Interferometer (NPOI, Armstrong et al. 2013). The most metal-rich star in the sample, μ Ara, would be feasible for being measured with an instrument such as the CHARA array at Mount Wilson Observatory (California), but is not accessible with the latter owing to its position in the sky. This star has been the target of an asteroseismology campaign (Bouchy et al. 2005, and Sect. 4.2). The sample should be complemented in the future with a northern dwarf star of similar metallicity, magnitude, and angular size as μ Ara (see Appendix B).

Almost all of the stars in our sample have previously been used as reference, calibration, or test objects. In the following, we give some examples. Similar to Arcturus (see Sect. 1),

[2] http://obswww.unige.ch/gcpd/gcpd.html

Procyon has been widely used as a standard star in various studies. Some recent publications using Procyon as a calibration or test object are Porto de Mello et al. (2014), Doyle et al. (2013), Bergemann et al. (2012a), Worley et al. (2012), Lobel (2011), Mashonkina et al. (2011), Quirion et al. (2010), Bruntt et al. (2010), Gebran et al. (2010). The $T_{\rm eff}$ values used in these publications range from 6490 K to 6650 K, and the $\log g$ values from 3.96 dex to 4.05 dex. Each of these publications used a different source for the parameters.

Apart from Arcturus, several giants have been used as reference objects in differential abundance analyses, illustrated in the following three examples. In an abundance study of barium stars Smiljanic et al. (2007) adopted the solar-metallicity giant ϵ Vir as the standard star for a differential analysis[3]. The stellar parameters of the reference star were determined from photometric calibrations and stellar evolution models. Hill et al. (2011) studied the formation of the Galactic bulge by determining metallicities for clump giants in Baade's window relative to the metal-rich giant μ Leo. The effective temperature adopted for the reference star was obtained by the infrared flux method, and the $\log g$ value was estimated from various independent methods (Lecureur et al. 2007). Westin et al. (2000) studied nucleosynthesis signatures of neutron-capture elements through a line-by-line differential abundance comparison of an r-process enriched low-metallicity giant (HD 115444) with the metal-poor giant HD 122563. The atmospheric parameters of both stars were determined by demanding excitation and ionization equilibrium of Fe line abundances.

Arcturus, α Cen A, α Cet, and α Tau are among the standard sources that were used for the flux calibration of the Short-Wavelength Spectrometer on the Infrared Space Observatory by means of synthetic spectra. The stellar spectra and calibration issues were discussed by Decin et al. (2003), for example, who used atmospheric parameters from the literature for α Cen A and determined parameters from the infrared spectra for the other stars. These four stars, as well as β Gem, are also included in the sample of 12 standard stars used for calibration purposes in a procedure for creating template spectral energy distributions in the infrared for arbitrary effective temperatures (*autoshape* procedure, 1–35 μm, Engelke et al. 2006). Procyon and ϵ Eri were used by Lobel (2011) to calibrate oscillator strengths of over 900 lines of neutral species in the wavelength range 400 to 680 nm. The star 18 Sco is one of six fundamental stars that are being used for calibrating atomic and molecular line lists for producing theoretical stellar libraries (Martins et al. 2014)[4]. Procyon, β Vir, ϵ Eri, η Boo, μ Cas, and τ Cet were used among other stars by Cayrel et al. (2011, cf. their Table 2) for a calibration between effective temperatures derived from Hα line-profile fitting and direct effective temperatures based on interferometric angular diameters and bolometric fluxes.

Subsets of the *Gaia* FGK benchmark stars have been used in numerous works for tests of various modelling and analysis techniques. Bruntt et al. (2010) compared direct and indirect methods to determine astrophysical parameters for Procyon, α Cen A and B, β Hyi, β Vir, δ Eri, η Boo, ξ Hya, μ Ara, and τ Cet. Their direct parameters were based on interferometric and asteroseismic data. HD 22879 was used by Jofré et al. (2010) as part of a sample of stars with high-resolution spectra to validate

the MAχ tool, which had been applied to low-resolution spectra of over 17 000 metal-poor dwarfs from the SEGUE survey to estimate atmospheric parameters. Procyon, α Cen A and B, β Hyi, η Boo, and τ Cet appear in a test of automatic determination of stellar parameters from asteroseismic data (Quirion et al. 2010), where various sources were used for the reference stellar parameters.

Eleven of the current *Gaia* FGK benchmark stars are included in one of the stellar samples that were used to validate the SDSS/SEGUE stellar parameter pipeline by Lee et al. (2011). This sample was selected from the ELODIE spectral library (Prugniel & Soubiran 2001, 2004; Moultaka et al. 2004). These *Gaia* FGK benchmark stars are Procyon, β Gem, β Vir, ϵ Eri, μ Cas, τ Cet, 18 Sco, Gmb 1830, HD 22879, HD 84937, and HD 140283. The reference parameters were those supplied with the ELODIE library. Arcturus and μ Leo were used together with two other nearby red giants by Mészáros et al. (2013) as standard stars to test the results of the APOGEE Stellar Parameters and Chemical Abundances Pipeline. Arcturus, α Cen A, β Vir, γ Sge, ξ Hya, μ Cas, and μ Leo were used by Valentini et al. (2013) to validate the GAUFRE tool for measuring atmospheric parameters from spectra by comparing the results of the tool with average spectroscopic parameters from the literature. In a similar way, Arcturus and HD 140283 were used by Sbordone et al. (2014) to validate the MyGIsFOS code for spectroscopic derivation of atmospheric parameters, using various sources for the reference parameters.

Procyon and the metal-poor stars Gmb 1830, HD 84937, HD 122563, and HD 140283 were used (in different combinations) as test objects in a series of investigations of non-LTE line formation for several chemical elements (Ca I and Ca II in Mashonkina et al. 2007; eight elements in Mashonkina et al. 2008; Mn I in Bergemann & Gehren 2008; Co I and Co II in Bergemann et al. 2010; Mg I in Mashonkina 2013). In most cases, the reference $T_{\rm eff}$ values were based on Balmer line-profile fitting, and the $\log g$ values were determined with the parallax method (cf. Sect. 5.4). In Bergemann et al. (2012b) non-LTE line formation of Fe was studied in 1D hydrostatic and averaged 3D hydrodynamic model atmospheres, using photometric parameters for the metal-poor test objects. The analysis of Ba by Mashonkina & Zhao (2006) included HD 22879 as well, and β Vir and τ Cet were added in the study of Fe I and Fe II by Mashonkina et al. (2011). In the latter work, $T_{\rm eff}$ and $\log g$ were determined from methods that are largely independent of the model atmosphere.

The M giants α Tau and α Cet were used as test objects by Lebzelter et al. (2012) in a comparative study of stellar spectrum modelling involving 11 different analysis methods. Arcturus, α Tau, μ Leo, Gmb 1830, HD 122563, and HD 140283 are included in the catalogue of observed and synthetic hydrogen line profiles (Pδ, Pγ, Hα) by Huang et al. (2012). The stellar parameters were taken from various sources, but mainly from the spectroscopic study by Fulbright (2000). Arcturus, Procyon, ϵ Eri, and τ Cet were used by Gray (2010) to analyse the shapes of spectral line bisectors and to measure basic properties of stellar granulation. The local metal-poor dwarf Gmb 1830 was used by VandenBerg et al. (2000) and follow-up publications to validate predictions of stellar models for old stars.

Furthermore, 18 of the *Gaia* FGK benchmark stars are included in the MILES library of medium-resolution spectra. The atmospheric parameters for most of the 985 stars in the MILES library were determined by Prugniel et al. (2011) using an automatic routine. However, for some stars, parameters from the literature were adopted, which the authors judged to be more

---

[3] The history of ϵ Vir as a standard star goes much further back in time. For example, it was used as a reference star in a differential curve-of-growth analysis by Cayrel de Strobel & Pasinetti (1975).

[4] http://archive.eso.org/wdb/wdb/eso/sched_rep_arc/query?progid=087.B-0308(A)

Table 2. Fundamental parameters and data for the Sun, and physical constants.

Description	Value	Uncertainty	Unit	Ref.
Solar radius	$6.9577 \times 10^{+08}$	$1.4 \times 10^{+05}$	m	(1)
Solar constant	1360.8	0.5	$\mathrm{W\,m^{-2}}$	(2)
Solar mass parameter $GM_\odot$	$1.3271244210 \times 10^{+20}$	$1 \times 10^{+10}$	$\mathrm{m^3\,s^{-2}}$	(3)
Astronomical unit of length	$1.49597870700 \times 10^{+11}$		m	(4)
Stefan-Boltzmann constant	5.670373×10^{-08}	2.1×10^{-13}	$\mathrm{W\,m^{-2}\,K^{-4}}$	(5)
Newtonian constant of gravitation	6.67384×10^{-11}	8.0×10^{-15}	$\mathrm{m^3\,kg^{-1}\,s^{-2}}$	(5)
Zero point L_0 for bolometric flux	$3.055 \times 10^{+28}$		W	(6)

References. (1) Meftah et al. (2014), Haberreiter et al. (2008); (2) Kopp & Lean (2011); (3) Konopliv et al. (2011), and Resolution B3 adopted at IAU General Assembly 2006[6]; (4) Resolution B2 adopted at IAU General Assembly 2012[7]; (5) 2010 CODATA recommended values[8]; (6) Andersen (1999).

credible than the results of the automatic analysis. Among the *Gaia* FGK benchmark stars this was the case for Arcturus, HD 122563, and HD 140283. Procyon and β Gem are included as two of eight iconic cool stars in the Advanced Spectral Library (ASTRAL, Ayres 2013), a library of high-quality UV atlases obtained with HST/STIS. The star ϵ For is included in the X-Shooter spectral library (Chen et al. 2014).

As can be seen from these examples, the stars included in our sample of *Gaia* FGK benchmark stars have been widely used in the literature. However, different authors considered different values for the fundamental parameters T_{eff} and $\log g$. The aim of this work is to provide a set of recommended values for calibration purposes, based on interferometric, photometric, and seismic data.

3. Effective temperature

We employed the fundamental relation $L = 4\pi R^2 \sigma T_{\mathrm{eff}}^4$, where L is the luminosity, R the radius, and σ the Stefan-Boltzmann constant, to determine the effective temperature. In fact, the Sun is the only object for which we used the relation in this form. For the other stars, we used the bolometric flux[5] F_{bol} and the limb-darkened angular diameter θ_{LD} instead of L and R, and calculated T_{eff} directly from these two measured quantities:

$$T_{\mathrm{eff}} = \left(\frac{F_{\mathrm{bol}}}{\sigma}\right)^{0.25} (0.5\,\theta_{\mathrm{LD}})^{-0.5}. \tag{1}$$

The input data for T_{eff} were compiled from the sources described in the following sections.

When possible, interferometric measurements of θ_{LD} and F_{bol} determinations based on integrations of absolute flux measurements across the stellar spectrum were extracted from the literature. We refer to these as direct data. For the cases where direct data are not yet available, we resorted to indirect determinations based on various calibrations available in the literature.

3.1. The Sun

The fundamental parameters used for calculating the effective temperature of the Sun are given in Table 2. The solar radius

is based on the recent measurements by Meftah et al. (2014). These authors used a ground-based facility to measure the position of the inflection point of the solar intensity at the limb from 2011 to 2013. The measurements were corrected for the effects of refraction and turbulence in the Earth's atmosphere. We used their result of 959.78 ± 0.19 arcsec for the angular radius, obtained at a wavelength of 535.7 nm. The radius defined by the inflection point position is somewhat larger than the radius where the optical depth in the photosphere is equal to 1, which is the definition commonly used for stellar (atmosphere) modelling (e.g. Gustafsson et al. 2008). The correction needs to be derived from radiative-transfer modelling of the solar limb, and we used a value of -340 ± 10 km based on the calculations by Haberreiter et al. (2008). This corresponds to a difference in effective temperature of about 2 K.

The solar luminosity was computed from the solar constant (total solar irradiance) and the astronomical unit. A recent measurement of the solar constant from the Total Irradiance Monitor on NASA's Solar Radiation and Climate Experiment during the 2008 solar minimum period is given by Kopp & Lean (2011)[9]. For a discussion of solar luminosity, mass, and radius, see also Harmanec & Prša (2011).

3.2. Angular diameters

Direct measurements. The catalogues of Pasinetti Fracassini et al. (2001) and Richichi et al. (2005) and the literature were searched for angular diameter determinations, and the data were extracted from the original references. The compiled θ_{LD} values include the effects of limb darkening. For 27 stars we found θ_{LD} values, which are given in Table 4 together with their references. In the case of multiple measurements by different authors, we adopted the most recent one or the one with the lowest formal uncertainty. The measurements were done with several different instruments, mainly in the infrared, but in a few cases in optical wavelength regions. Various approaches to account for limb darkening were used. The most common one was to apply limb-darkening coefficients taken from Claret (2000) or Claret et al. (1995).

The measurements for β Gem and ϵ Vir were done by Mozurkewich et al. (2003) at four optical wavelengths between 450 and 800 nm with the Mark III Stellar Interferometer on Mount Wilson (California, Shao et al. 1988). *R*-band (700 nm) observations were obtained with the Sydney University Stellar

---

[5] The term "bolometric flux" refers to the total radiative flux from the star received at the Earth.

[6] http://www.iau.org/static/resolutions/IAU2006_Resol3.pdf

[7] http://www.iau.org/static/resolutions/IAU2012_English.pdf

[8] http://physics.nist.gov/cuu/Constants/bibliography.html

[9] The same value is obtained by calculating the median of the 4080 measurements taken by the same instrument between 2003-02-25 and 2015-02-18, available at http://lasp.colorado.edu/lisird/sorce/sorce_tsi/index.html.

Table 3. Broad-band photometry for *Gaia* FGK benchmark stars used for indirect determinations of θ_{LD} and/or F_{bol}.

Name	V	$\sigma(V)$	BC_V	$(B-V)$	J	K
HD 84937	8.324	0.021		0.389	7.359	7.062
ϵ For	5.883	0.005	−0.25	0.790	4.364	3.824
HD 22879	6.689	0.009		0.540	5.588	5.179
μ Ara	5.131	0.012		0.700	4.158	3.683
HD 122563	6.200	0.009	−0.47			
μ Leo	3.880	0.005	−0.51			
HD 107328	4.970	0.012	−0.49			
HD 220009	5.047	0.008	−0.64			
β Ara	2.842	0.004	−0.75			

Notes. The V magnitudes and $B-V$ colour indices are mean values and $\sigma(V)$ the standard deviation extracted from the GCPD (Mermilliod et al. 1997). The bolometric corrections BC_V were calculated as described in the text, Sect. 3.3. The J and K magnitudes are taken from the 2MASS catalogue (Cutri et al. 2003).

Interferometer (SUSI, New South Wales, Australia, Davis et al. 1999) by North et al. (2007, 2009) for β Hyi and β Vir. In that work, limb-darkening corrections from Davis et al. (2000) based on Kurucz stellar atmosphere models were applied. The angular diameters of the two dwarf stars 18 Sco and HD 49933, the subgiant HD 140283, and the giant HD 220009 were measured in the near-infrared with the CHARA Array at Mount Wilson Observatory (California, ten Brummelaar et al. 2005) and either the PAVO or the VEGA instruments by Bazot et al. (2011, PAVO), Bigot et al. (2011, VEGA), Creevey et al. (2015, VEGA), and Thévenin et al. (in prep., VEGA), respectively. Bigot et al. (2011) used 3D-RHD atmospheric models to determine the limb-darkening effect.

The most recent diameter of Arcturus was obtained by Lacour et al. (2008) in the H-band (1.5 to 1.8 μm) with the IOTA (Infrared-Optical Telescope Array) interferometer (Arizona, Traub et al. 2003). The diameters of the remaining stars were measured in the K-band (2.2 μm) with either the VLT Interferometer (VLTI, VINCI instrument, Kervella et al. 2003a) or the CHARA Array using the Classic or FLUOR instrument, and in two cases, data from the Palomar Testbed Interferometer (PTI, California, Colavita et al. 1999) were used (for HD 122563 by Creevey et al. 2012 and for η Boo by van Belle et al. 2007). For the 61 Cyg components we used the VINCI measurement by Kervella et al. (2008). The system was also observed with the PTI by van Belle & von Braun (2009), who determined $\theta_{LD} = 1.63 \pm 0.05$ mas for 61 Cyg A and $\theta_{LD} = 1.67 \pm 0.05$ mas for 61 Cyg B. These values are 8% lower and 5% higher, respectively, than the values we used. We prefer the values by Kervella et al. (2008) because van Belle & von Braun (2009) derived a significant extinction for the K7V component ($A_V = 0.23 \pm 0.01$ mag, while $A_V = 0$ for the K5V component as expected for this nearby system), and their angular diameter for the K7V component is larger than that of the K5V component (although they are equal within the uncertainties). Limb darkening was taken into account using individual atmospheric models in the cases of ψ Phe, α Cet, and γ Sge (Wittkowski et al. 2004, 2006a,b), for which spherical PHOENIX models (Hauschildt & Baron 1999, version 13) were computed. In the case of Procyon, α Cen B, and HD 122563, 3D-RHD simulations were applied by Chiavassa et al. (2012), Bigot et al. (2006), and Creevey et al. (2012), respectively.

Indirect determinations. For two giants in our sample, Cohen et al. (1999) determined angular diameters by scaling spectra of reference stars with absolute flux calibration in the infrared region (1.2 to 35 μm) to infrared photometry of the target stars with similar type (μ Leo with reference Arcturus, and HD 107328 with reference β Gem). The diameters of the target stars were obtained by multiplying the diameters of the reference stars by the square root of the scale factors. This method was applied to a large sample of giant stars and verified to be accurate to within 2% by comparison to direct measurements (see their Fig. 8).

For four of the dwarf and subgiant stars (HD 22879, HD 84937, ϵ For, μ Ara), we used the surface-brightness relations by Kervella et al. (2004a) to estimate the angular diameters. We used the average of the results from the relations for the $(B-K)$ and $(V-K)$ colour indices (Eqs. (22) and (23) in Kervella et al. 2004a), because those present the smallest dispersions ($\leq$1% in Table 4 of Kervella et al. 2004a). Interstellar extinction was assumed to be negligible for these four stars. Lallement et al. (2014) derived maps of the local interstellar medium (ISM) from inversion of individual colour excess measurements. These show that interstellar reddening is negligible within about 40 pc, applicable to three of the stars. Also the fourth star, HD 84937, seems to be located within a local cavity with negligible reddening. The photometry is given in Table 3. The K magnitudes from 2MASS were transformed to the Johnson system using Eqs. (12) and (14) from Carpenter (2001), followed by Eqs. (13) and (14), as well as Eqs. (6) and (7), from Alonso et al. (1994). For the uncertainties of the angular diameters we adopted 2% in the case of ϵ For and μ Ara and 3% for HD 22879 and HD 84937. The last two are metal-poor dwarf stars with diameter values of less than 0.4 mas, which is well below the lowest value (0.7 mas) measured for the sample of stars that Kervella et al. (2004a) used for calibrating their relations. Furthermore, the calibration sample was biased against metal-poor stars (only three of the 20 dwarf star calibrators had [Fe/H] below −0.5 dex, with a lower limit of −1.4 dex), and there are indications that the predicted diameters might be slightly underestimated for metal-poor stars (Creevey et al. 2012, 2015). The indirectly determined angular diameters are given in Table 4.

3.3. Bolometric flux

Direct measurements. F_{bol} values based on integrations of the observed spectral energy distribution (SED) were found in the literature for 24 stars. These are given in Table 4 together with their references. For about half of these stars, the data were taken from Blackwell & Lynas-Gray (1998), after adopting uncertainties of 1.1% for dwarfs and 2.6% for giants and subgiants following di Benedetto (1998, Sect. 3.2, p. 863). For Procyon, the F_{bol} value was taken from Aufdenberg et al. (2005), and for Arcturus

Table 4. Measured or calibrated angular diameters and bolometric fluxes, and their uncertainties (absolute, *u*, and in percent, %*u*) for *Gaia* FGK benchmark stars.

Name	$\theta_{\rm LD}$ [mas]	$u(\theta_{\rm LD})$	%$u(\theta_{\rm LD})$	Band	Ref($\theta_{\rm LD}$)	$F_{\rm bol}$ [10^{-9} W m^{-2}]	$u(F_{\rm bol})$	%$u(F_{\rm bol})$	Ref($F_{\rm bol}$)
F dwarfs									
Procyon	5.390	0.030	0.6	*K*	Ch	17.8600	0.8900	5.0	A
HD 84937	0.153	0.005	3.0	–	K04*	0.0127	0.0001	1.1	B98
HD 49933	0.445	0.012	2.7	735 nm	B11	0.1279	0.0014	1.1	B98
FGK subgiants									
δ Eri	2.394	0.029	1.2	*K*	T	1.1500	0.0008	0.1	Bo13
HD 140283	0.353	0.013	3.7	720 nm	C15	0.0386	0.0008	2.0	A96*
ϵ For	0.788	0.016	2.0	–	K04*	0.1425	0.0066	4.6	H*
η Boo	2.189	0.014	0.6	*K*	vB	2.2100	0.0282	1.3	vB
β Hyi	2.257	0.019	0.8	700 nm	N07	2.0190	0.0525	2.6	B98
G dwarfs									
α Cen A	8.511	0.020	0.2	*K*	*K*	27.1600	0.2670	1.0	Bo13
HD 22879	0.382	0.011	3.0	–	K04*	0.0577	0.0006	1.1	B98
μ Cas	0.973	0.009	0.9	*K′*	Bo08	0.2504	0.0028	1.1	B98
τ Cet	2.015	0.011	0.5	*K′*	D	1.1620	0.0128	1.1	B98
α Cen B	6.000	0.021	0.4	*K*	B06	8.9800	0.1220	1.4	Bo13
18 Sco	0.676	0.006	0.9	700 nm	Ba	0.1734	0.0090	5.2	Bo13
μ Ara	0.763	0.015	2.0	–	K04*	0.2354	0.0047	2.0	A95*
β Vir	1.450	0.018	1.2	700 nm	N09	0.9590	0.0105	1.1	B98
FGK giants									
Arcturus	21.050	0.210	1.0	H	L	49.8000	1.2948	2.6	G
HD 122563	0.940	0.011	1.2	*K*	C12	0.1303	0.0061	4.7	H*
μ Leo	2.930	0.040	1.4	–	C99*	1.1458	0.0530	4.6	H*
β Gem	7.980	0.080	1.0	opt	M	11.8200	0.5319	4.5	M
ϵ Vir	3.280	0.030	0.9	opt	M	2.2100	0.0994	4.5	M
ξ Hya	2.386	0.021	0.9	*K*	T	1.2280	0.0319	2.6	B98
HD 107328	1.740	0.020	1.1	–	C99*	0.4122	0.0195	4.7	H*
HD 220009	2.045	0.034	1.7	800 nm	Tp	0.4409	0.0206	4.7	H*
M giants									
α Tau	20.580	0.030	0.1	*K*	RR	33.5700	1.3500	4.0	RR
α Cet	12.200	0.040	0.3	*K*	W4	10.3000	0.7000	6.8	W4
β Ara	5.997	0.037	0.6	*K*	Tp	3.7179	0.1718	4.6	H*
γ Sge	6.060	0.020	0.3	*K*	W3	2.5700	0.1300	5.1	W3
ψ Phe	8.130	0.200	2.5	*K*	W2	3.2000	0.3000	9.4	W2
K dwarfs									
ϵ Eri	2.126	0.014	0.7	*K′*	D	1.0000	0.0200	2.0	A96*
Gmb 1830	0.679	0.015	2.2	*K*	C12	0.0834	0.0009	1.1	B98
61 Cyg A	1.775	0.013	0.7	*K*	K08	0.3844	0.0051	1.3	M13
61 Cyg B	1.581	0.022	1.4	*K*	K08	0.2228	0.0032	1.4	M13

Notes. See text for description, and table notes for references. An asterisk indicates indirect determinations of $\theta_{\rm LD}$ and $F_{\rm bol}$ values determined from calibrations. The column headed "Band" indicates the wavelength band of the interferometric observations – "opt" for several optical wavelengths, H for several wavelengths from 1.5 to 1.8 μm, *K* or *K′* for *K*-band (about 2 μm), or wavelength in nm.

References. For $\theta_{\rm LD}$: B06 ... Bigot et al. (2006); B11 ... Bigot et al. (2011); Ba ... Bazot et al. (2011); Bo08 ... Boyajian et al. (2008); C12 ... Creevey et al. (2012); C15 ... Creevey et al. (2015); C99 ... Cohen et al. (1999); Ch ... Chiavassa et al. (2012); D ... di Folco et al. (2007); K ... Kervella et al. (2003b); K08 ... Kervella et al. (2008); K04 ... indirect, using surface-brightness relations by Kervella et al. (2004a); M ... Mozurkewich et al. (2003); L ... Lacour et al. (2008, $\tau_{\rm Ross}$ = 1 diameter); N07 ... North et al. (2007); N09 ... North et al. (2009); RR ... Richichi & Roccatagliata (2005); T ... Thévenin et al. (2005); Tp ... Thévenin et al., in prep., VLTI/AMBER measurement for β Ara, CHARA/VEGA for HD 220009; vB ... van Belle et al. (2007); W2/W3/W4 ... Wittkowski et al. (2004, 2006b,a, $\tau_{\rm Ross}$ = 1 diameter). Additional references for $F_{\rm bol}$: A ... Aufdenberg et al. (2005); A95 ... Alonso et al. (1995) calibration for dwarf stars; A96 ... Alonso et al. (1996a, their Table 4); B98 ... Blackwell & Lynas-Gray (1998), uncertainties of 1.1% for dwarfs and 2.6% for giants and subgiants following di Benedetto (1998, Sect. 3.2, p. 863); Bo13 ... Boyajian et al. (2013), G ... Griffin & Lynas-Gray (1999), uncertainty of 2.6% from Koch & McWilliam (2008); H ... from the *V* magnitude and the bolometric correction BC$_V$ derived from the calibration of Alonso et al. (1999b); M13 ... Mann et al. (2013).

from Griffin & Lynas-Gray (1999), adopting an uncertainty of 2.6% as derived by Koch & McWilliam (2008). For α Cen A and B, δ Eri, and 18 Sco, we adopted the measurements by Boyajian et al. (2013), and for 61 Cyg A and B those by Mann et al. (2013). For the remaining stars, the $F_{\rm bol}$ determinations were taken from the publications for the interferometric angular diameters discussed in Sect. 3.2.

Calibrations. The K dwarf ϵ Eri and the metal-poor subgiant HD 140283 are included in Table 4 of Alonso et al. (1996a), which lists bolometric fluxes derived with the calibration of Alonso et al. (1995), and we adopted these values with uncertainties of 2%. For the dwarf star μ Ara, we used the calibration of Alonso et al. (1995, their Eqs. (8)–(10)) of the bolometric flux as a function of the *K* magnitude, ($V − K$) and

Table 5. Other interferometric measurements of angular diameter, which are compared to the adopted values in Fig. 1.

Name	θ_{LD} [mas]	$u(\theta_{LD})$	$\%u(\theta_{LD})$	Band	Reference
α Cet	13.2	0.3	1.9	opt	Mozurkewich et al. (2003)
α Cet	11.9	0.4	3.5	K	Dyck et al. (1998)
γ Sge	6.22	0.06	1.0	opt	Mozurkewich et al. (2003)
α Tau	21.1	0.2	1.0	opt	Mozurkewich et al. (2003)
α Tau	20.2	0.3	1.5	K	di Benedetto & Rabbia (1987)
Arcturus	21.4	0.2	1.2	opt	Mozurkewich et al. (2003)
Arcturus	21.0	0.2	1.0	K	di Benedetto & Foy (1986)
Arcturus	19.5	1.	5.1	K	Dyck et al. (1996)
Arcturus	20.9	0.08	0.4	K	Perrin et al. (1998)
Arcturus	21.2	0.2	1.0	K	Verhoelst et al. (2005)
Gmb1830	0.696	0.005	0.7	K'	Boyajian et al. (2012a)
β Gem	7.97	0.1	1.4	800	Nordgren et al. (2001)
β Gem	7.90	0.3	3.9	K	di Benedetto & Rabbia (1987)
β Gem	7.95	0.09	1.1	740	Nordgren et al. (2001)
ϵ Vir	3.28	0.05	1.5	800	Nordgren et al. (2001)
ϵ Vir	3.23	0.05	1.5	740	Nordgren et al. (2001)
ϵ Eri	2.15	0.03	1.4	K	di Folco et al. (2004)
τ Cet	2.07	0.01	0.5	opt	Baines et al. (2014)
τ Cet	2.08	0.03	1.5	K	di Folco et al. (2004)
18Sco	0.780	0.02	2.2	K'	Boyajian et al. (2012a)
η Boo	2.20	0.03	1.4	K	Thévenin et al. (2005)
η Boo	2.28	0.07	3.1	740	Nordgren et al. (2001)
η Boo	2.13	0.01	0.6	opt	Baines et al. (2014)
η Boo	2.27	0.03	1.1	opt	Mozurkewich et al. (2003)
η Boo	2.17	0.03	1.4	800	Nordgren et al. (2001)
Procyon	5.46	0.08	1.5	800	Nordgren et al. (2001)
Procyon	5.40	0.03	0.6	K	Aufdenberg et al. (2005)
Procyon	5.45	0.05	1.0	K	Kervella et al. (2004b)
Procyon	5.45	0.05	1.0	opt	Mozurkewich et al. (2003)
Procyon	5.43	0.07	1.3	740	Nordgren et al. (2001)

Notes. The column headed "Band" indicates the wavelength band of the interferometric observations – "opt" stands for several optical wavelengths, K or K' for K-band (about 2 μm), numbers give the wavelength in nm.

[Fe/H][10], with uncertainties of 2%. The photometry can be found in Table 3. The K magnitudes from 2MASS were transformed to the Johnson system in the same way as for the surface-brightness relations described above. The metallicity was set to +0.2 dex, which corresponds to the upper validity limit of the calibration.

For several giants and subgiants, we computed the bolometric flux from the V magnitudes and the bolometric corrections BC_V[11]. The latter were derived from the calibration of Alonso et al. (1999b) of BC_V as a function of T_{eff} and [Fe/H]. Since F_{bol} is used to compute T_{eff}, we iterated until we obtained consistent values for T_{eff} and BC_V. For the uncertainty in BC_V, we adopted a value of 0.05 mag. The photometry can be found in Table 3. The metallicities were those derived in Paper III of this series. The bolometric fluxes determined from calibrations are given in Table 4.

3.4. Additional determinations of angular diameter and bolometric flux

We compiled additional measurements of angular diameter and bolometric flux in Tables 5 and 6. The differences from the adopted values are less than 3% for angular diameter and less than 5% for bolometric flux for most stars, as shown in Fig. 1. For θ_{LD}, the deviations are comparable to the uncertainties

quoted for the adopted values (Table 4), with three outliers discussed below. Uncertainties in θ_{LD} of 3% translate into uncertainties in effective temperature of 1.5%. Also in the case of F_{bol}, the differences shown in Fig. 1 are comparable to the relative uncertainties quoted in Table 4. The two stars with the largest differences are discussed below. Uncertainties in F_{bol} of 5% translate into uncertainties in effective temperature of about 1%.

One of the outliers in the angular diameter comparison is 18 Sco with a difference of 15% between the K-band measurement of Boyajian et al. (2012a) and the R-band measurement of Bazot et al. (2011, adopted here), corresponding to about five times the combined uncertainty[12]. We compare the visibility measurements by the two authors in Fig. 2. It is obvious that these measurements are affected by systematic differences, which cannot be explained by the uncertainties in the linear limb-darkening coefficients used by both authors. A more complex modelling of limb darkening might diminish the discrepancy, since the deviation of realistic limb darkening from 1D approximations could be wavelength dependent. For example, Bigot et al. (2006) find that for K-band observations of the somewhat cooler star α Cen B, the diameter using 1D models for limb darkening was only 0.3% larger than when using 3D-RHD models. On the other hand, for R-band observations of the somewhat hotter star HD 49933, Bigot et al. (2011) derived a 2% larger diameter from 1D compared to 3D models. Most of the difference in the measurements may, however, be due to

---

[10] Note that the original Eq. (8) must be divided by 10 to obtain F_{bol} in units of mW m^{-2}.

[11] $F_{bol} = \frac{1}{4\pi(10\mathrm{pc})^2} \cdot L_0 \cdot 10^{-0.4(V+BC_V)}$, where L_0 is the zero-point luminosity, given in Table 2.

[12] With "combined uncertainty" we refer to the uncertainties added in quadrature.

Table 6. Other measurements of bolometric flux, which are compared to the adopted values in Fig. 1.

Name	F_{bol} [10^{-9} W m^{-2}]	$u(F_{bol})$	$\%u(F_{bol})$	Reference
α Cet	9.57	0.4	4.5	Mozurkewich et al. (2003)
γ Sge	2.86	0.1	4.5	Mozurkewich et al. (2003)
61Cyg B	0.223	0.004	2.0	Alonso et al. (1996a)
61Cyg B	0.203	0.001	0.5	Boyajian et al. (2012b)
Arcturus	48.6	2.	4.5	Mozurkewich et al. (2003)
61Cyg A	0.377	0.002	0.5	Boyajian et al. (2012b)
61Cyg A	0.372	0.007	2.0	Alonso et al. (1996a)
Gmb1830	0.0838	0.002	2.0	Alonso et al. (1996a)
Gmb1830	0.0827	0.0008	1.0	Boyajian et al. (2012a)
δ Eri	1.18	0.05	3.9	Bruntt et al. (2010)
ξ Hya	1.17	0.05	3.9	Bruntt et al. (2010)
α Cen B	8.37	0.3	4.2	Bruntt et al. (2010)
μ Cas	0.253	0.005	2.0	Alonso et al. (1996a)
τ Cet	1.12	0.0007	0.1	Boyajian et al. (2013)
τ Cet	1.16	0.02	2.0	Alonso et al. (1996a)
τ Cet	1.14	0.04	3.3	Bruntt et al. (2010)
τ Cet	1.13	0.003	0.3	Baines et al. (2014)
α Cen A	26.3	0.9	3.4	Bruntt et al. (2010)
18Sco	0.165	0.003	2.0	Alonso et al. (1995)
HD 22879	0.0590	0.001	2.0	Alonso et al. (1996a)
β Hyi	1.97	0.07	3.7	Bruntt et al. (2010)
β Vir	0.942	0.02	2.0	Alonso et al. (1996a)
β Vir	0.915	0.03	3.5	Bruntt et al. (2010)
β Vir	0.944	0.02	2.1	North et al. (2009)
η Boo	2.17	0.01	0.5	Mozurkewich et al. (2003)
η Boo	2.14	0.06	2.9	Bruntt et al. (2010)
η Boo	2.14	0.007	0.3	Baines et al. (2014)
HD 84937	0.0136	0.0003	2.0	Alonso et al. (1996a)
Procyon	18.4	0.4	2.0	Alonso et al. (1996a)
Procyon	18.2	0.8	4.5	Mozurkewich et al. (2003)
Procyon	17.6	0.5	2.7	Bruntt et al. (2010)
Procyon	18.3	0.02	0.1	Boyajian et al. (2013)
HD 49933	0.127	0.0008	0.6	Boyajian et al. (2013)
HD 49933	0.144	0.003	2.0	Alonso et al. (1996a)

Notes. The values with reference Alonso et al. (1995) or Alonso et al. (1996a) are based on calibrations using broad-band photometry. All others are determined by integrating over SEDs.

calibration errors (see Sect. 2.2 in Boyajian et al. 2013). Bazot et al. (2011) and Boyajian et al. (2012a) used three and two calibrator stars, respectively, with one star in common. For that star (HD 145607), they assumed slightly different angular diameters, but they agree within the uncertainties. In any case, the measurements by Bazot et al. (2011) show a much smaller scatter, and the model curve using their θ_{LD} value passes through a few of the points by Boyajian et al. (2012a), while the opposite case is not true.

The two other outliers in the angular diameter comparison (Fig. 1, upper panel) are Arcturus and α Cet, with the largest and third largest angular diameters. For each star, one of the measurements shows a deviation of 7–8% from the adopted value (Dyck et al. 1996 and Mozurkewich et al. 2003, respectively). For Arcturus, the difference is less than two times the combined uncertainties, while the difference is at the 3σ level for α Cet. For the latter star, the deviating observation was obtained at optical wavelengths as compared to the infrared. However, there are five other stars with angular diameter determinations at optical wavelengths by the same author (Mozurkewich et al. 2003) with good agreement with determinations in the infrared.

Regarding the F_{bol} comparison, the largest differences from the adopted values are found for γ Sge and 61 Cyg B. For γ Sge Mozurkewich et al. (2003) obtained a bolometric flux that is 11% higher (or twice the combined uncertainty)
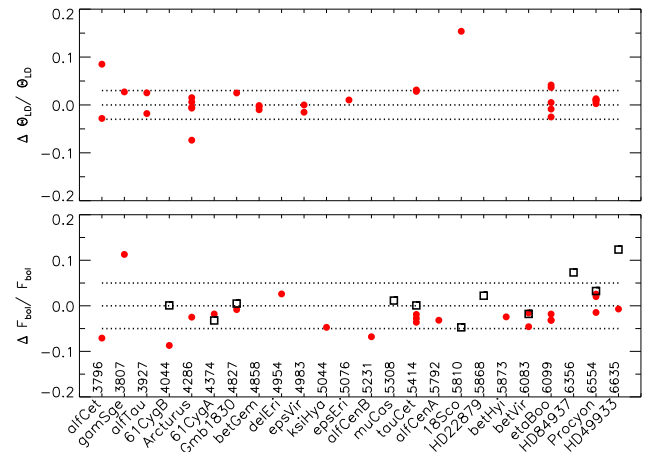

Fig. 1. Relative difference between additional and adopted values of angular diameter (*upper panel*) and bolometric flux (*lower panel*), for *Gaia* FGK benchmark stars with multiple measurements, sorted by T_{eff}. Red full circles are direct measurements, black open squares are calibrated values (see Tables 5 and 6). Dotted lines indicate differences of ±3% (*upper panel*) and ±5% (*lower panel*).

than Wittkowski et al. (2006b, adopted here). Mozurkewich et al. (2003) integrated over the SED derived from broad-band photometry alone, while Wittkowski et al. (2006b) used

Table 7. Masses M, parallaxes π, and luminosities L, and their uncertainties (absolute, u, and in percent, $\%u$), for *Gaia* FGK benchmark stars.

Name	$M\ [M_\odot]$	$u(M)$	$\%u(M)$	π [mas]	$u(\pi)$	$\%u(\pi)$	$\log L/L_\odot$	$u(\log L/L_\odot)$	$L_X/L\ [10^{-6}]$
F dwarfs									
Procyon	1.50	0.07	5	284.52	1.27	0.45	0.839	0.022	0.72
HD 84937	0.75	0.04	5	12.24	0.20	1.63	0.424	0.005	
HD 49933	1.17	0.06	5	33.68	0.42	1.25	0.547	0.005	23
FGK subgiants									
δ Eri	1.13	0.05	5	110.62	0.22	0.20	0.468	0.000	0.08
HD 140283	0.68	0.17	24	17.18	0.26	1.51	0.612	0.009	
ϵ For	0.91	0.16	17	31.05	0.36	1.16	0.665	0.020	
η Boo	1.64	0.07	5	87.77	1.24	1.41	0.953	0.006	0.31
β Hyi	1.15	0.04	3	134.07	0.11	0.08	0.546	0.011	0.48
G dwarfs									
α Cen A	1.11	0.04	3	747.10	1.20	0.16	0.182	0.004	0.38
HD 22879	0.75	0.06	7	39.13	0.57	1.46	0.071	0.005	
μ Cas	0.58	0.08	15	132.40	0.82	0.62	–0.350	0.005	
τ Cet	0.71	0.03	4	273.96	0.17	0.06	–0.315	0.005	0.59
α Cen B	0.93	0.06	6	747.10	1.20	0.16	–0.298	0.006	
18 Sco	1.02	0.06	6	71.93	0.37	0.51	0.020	0.023	
μ Ara	1.19	0.06	5	64.48	0.31	0.48	0.248	0.009	
β Vir	1.34	0.04	3	91.50	0.22	0.24	0.554	0.005	1.8
FGK giants									
Arcturus	1.03	0.21	20	88.83	0.53	0.60	2.295	0.011	
HD 122563	0.86	0.03	3	4.22	0.35	8.29	2.360	0.020	
μ Leo	1.69	0.42	25	26.27	0.16	0.61	1.715	0.020	
β Gem	2.30	0.40	18	96.52	0.24	0.25	1.598	0.020	
ϵ Vir	3.02	0.11	4	29.75	0.14	0.47	1.892	0.020	
ξ Hya	2.84	0.12	4	25.14	0.16	0.64	1.784	0.011	
HD 107328	1.41	0.41	29	10.60	0.25	2.36	2.060	0.021	
HD 220009	0.83	0.21	26	7.55	0.40	5.30	2.383	0.020	
M giants									
α Tau	0.96	0.41	43	48.92	0.77	1.57	2.642	0.017	
α Cet	1.76	0.91	52	13.10	0.44	3.36	3.273	0.030	
β Ara	8.21	1.88	23	4.54	0.61	13.44	3.751	0.020	
γ Sge	1.11	0.82	75	12.61	0.18	1.43	2.704	0.022	
ψ Phe	1.00	0.40	40	9.54	0.20	2.10	3.041	0.041	
K dwarfs									
ϵ Eri	0.80	0.06	8	310.95	0.16	0.05	–0.490	0.009	17
Gmb 1830	0.64	0.03	4	109.98	0.41	0.37	–0.666	0.005	
61 Cyg A	0.69	0.05	7	286.83	6.77	2.36	–0.835	0.006	5
61 Cyg B	0.61	0.05	8	285.89	0.55	0.19	–1.069	0.006	

Notes. See text for description and references. Column L_X/L gives the ratio of X-ray luminosity measured by ROSAT (Hünsch et al. 1998) to bolometric luminosity.

narrow-band spectrophotometry in the optical/near-infrared region complemented by broad-band photometry in other regions. Thus, the flux estimated by the latter group of authors should be more realistic.

For 61 Cyg B Boyajian et al. (2012b) obtained a bolometric flux 9% lower (or six times the combined uncertainty) than Mann et al. (2013, adopted here). Mann et al. (2013) measured F_{bol} for about 20 K- and M-type dwarfs in common with Boyajian et al. (2012b) and obtained 4% higher values on average. Both authors used a similar method of integrating over stellar SEDs. The difference is that Mann et al. (2013) had spectra observed for each star, while Boyajian et al. (2012b) used spectral templates from an empirical library. Mann et al. (2013) show that the use of templates results in an underestimation of the infrared flux level and argue that this explains the discrepancy for most of the stars. For the extreme cases, such as 61 Cyg B, the different input photometry used to determine the absolute flux scale of the spectra might also play a role.

Figure 1 shows that bolometric fluxes determined with the calibration by Alonso et al. (1995, 1996a) for dwarf stars agree to

within 5% with those determined from SED integration, except for the hottest stars ($T_{eff} \gtrsim 6300$ K). This justifies using these calibrations for some of the stars in our sample without "direct" determinations.

4. Surface gravity

We used the fundamental relation $g = GM/R^2$, where M is the stellar mass, R the stellar radius, and G the Newtonian constant of gravitation (Table 2), to determine the surface gravity. The linear radius R was calculated for each star from the angular diameter (see Sect. 3.2) and the parallax. The parallaxes (see Table 7) were taken from van Leeuwen (2007), from Söderhjelm (1999) for the α Cen system, and from VandenBerg et al. (2014) for the halo stars HD 84937 and HD 140283.

For the Sun, the surface gravity was calculated from the solar mass parameter given in Table 2 and the radius. The parameter $GM_\odot$ is measured in the process of planetary ephemeris determination with a considerably higher relative accuracy ($\approx 10^{-11}$) than that of the constant of gravitation G (10^{-4}). The latter is the

Table 8. Mean α-element abundances and mass corrections determined from *Yonsei-Yale* grids: $\Delta M = M(+0.3) - M(0.0)$.

Name	$[\alpha/\mathrm{Fe}]$	Elements	Ref.	$\Delta M[M_\odot]$
HD 84937	+0.4	Mg, Ca	1	0.00
HD 140283	+0.3	Mg, Ca	1	+0.02
ϵ For	+0.25	Si, Ti	2	−0.02
HD 22879	+0.3	Si, Ti	2	0.00
μ Cas	+0.3	Mg, Si, Ca, Ti	3	0.00†
τ Cet	+0.2	Si, Ca, Ti	2, 3	+0.01
HD 220009	+0.2	Si, Ca, Ti	4	−0.03

Notes. References: (1) Mashonkina et al. (2007); (2) Valenti & Fischer (2005); (3) Luck & Heiter (2005); (4) Luck & Heiter (2007). (†) For μ Cas only the $[\alpha/\mathrm{Fe}] = +0.3$ *Yonsei-Yale* grid could be used, and the $[\alpha/\mathrm{Fe}]$ correction was assumed to be zero, as found for HD 22879.

limiting factor for the achievable accuracy of the solar mass. A recent measurement of $GM_\odot$ based on tracking data from Mars-orbiting spacecraft is given in Konopliv et al. (2011)[13]. The solar radius is given in Table 2 and described in Sect. 3.1, and its uncertainty by far dominates the uncertainty in the solar surface gravity.

4.1. Mass determination from evolutionary tracks

For all stars apart from the Sun, we aimed to determine the mass (in solar units) in a homogeneous way by visual interpolation in two different grids of evolutionary tracks. We used the fundamental T_{eff} value (Sect. 5.1), the stellar luminosity, and the spectroscopic metallicity as constraints. The luminosity was calculated from the bolometric flux (see Sect. 3.3) and the parallax (see Table 7). For the metallicity, we used the [Fe/H] value from Table 3 in Paper III, with an uncertainty obtained by quadratically summing all σ and Δ columns in that table (see Table 1). For the two stars HD 122563 and Gmb 1830, and the two components of 61 Cyg, the T_{eff} and L values lie outside the range of the selected grids. Thus, we adopted the masses determined by Creevey et al. (2012) and Kervella et al. (2008), respectively, which are based on CESAM2k stellar evolution models (Morel 1997; Morel & Lebreton 2008).

Throughout the discussion in this section, one should keep in mind that the possible uncertainties in the mass are less important for determining surface gravity than the uncertainty of the radius. We selected the *Padova* stellar evolution models by Bertelli et al. (2008, 2009)[14] and the *Yonsei-Yale* models by Yi et al. (2003), Demarque et al. (2004)[15]. These groups have published grids of stellar evolution tracks for a wide range of masses and metallicities. The grid metallicities are given by [Fe/H] = $\log_{10}(Z_0/X_0) - \log_{10}(Z_{0,\odot}/X_{0,\odot})$, where Z_0 and X_0 are the initial mass fractions of metals and hydrogen, respectively. For the *Padova* models, $Z_{0,\odot} = 0.017$ and $X_{0,\odot} = 0.723$, and the metallicities range from +0.75 to −2.26 dex. For the *Yonsei-Yale* models, $Z_{0,\odot} = 0.0181$ and $X_{0,\odot} = 0.7149$ (Yi et al. 2001), and the metallicities range from +0.78 to −3.29 dex. The initial mass fraction of helium Y_0 was set to $Y_0 = 0.23 + 2Z_0$. For the *Yonsei-Yale* models, grids for different α-element abundances are available.
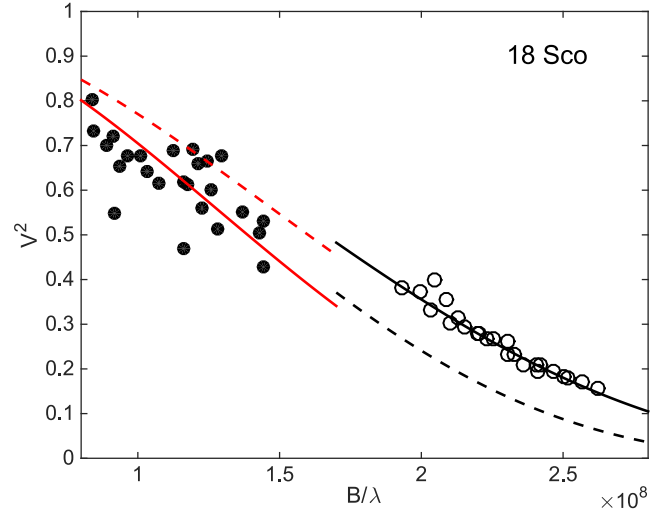
Fig. 2. 18 Sco: squared visibility as a function of the ratio of projected baseline and wavelength. Open circles: measurements from Bazot et al. (2011); full circles: measurements from Boyajian et al. (2012a). Lines are calculations using the same model as in the two references. Solid lines: using the author's determination of θ_{LD}; dashed lines: swapped θ_{LD} values. Red and black lines: using limb-darkening coefficients for K and R filters, respectively.
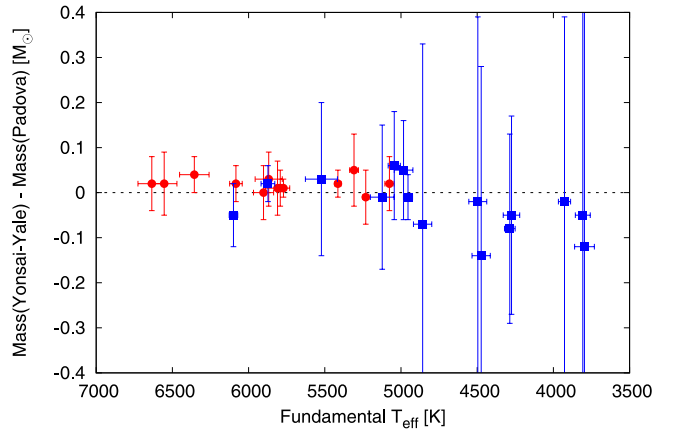

Fig. 3. Difference between masses determined from *Yonsei-Yale* and *Padova* grids as a function of fundamental T_{eff}. Red circles are dwarfs ($\log g \geq 4$), blue squares are giants and subgiants.

For stars with enhanced $[\alpha/\mathrm{Fe}]$ ratios, *Yonsei-Yale* tracks with $[\alpha/\mathrm{Fe}] = +0.3$ were used, based on α-element abundances from the literature (see Table 8). In these cases, the mass was also determined from solar $[\alpha/\mathrm{Fe}]$ tracks, and a correction determined in this way was applied to the masses obtained from the *Padova* tracks. The correction values are given in Table 8 and are found to be insignificant.

The final adopted mass value is the average from the *Padova* and *Yonsei-Yale* grids (except for β Ara, see below) and is given in Table 7, where we also list the parallaxes, luminosities, and relative X-ray luminosities. The uncertainties of the masses were determined for each grid based on the uncertainties of T_{eff}, L, and [Fe/H]. See Appendix A for more details and examples. The uncertainties of the adopted masses were then estimated using the maximum possible deviation from the mean in any one of
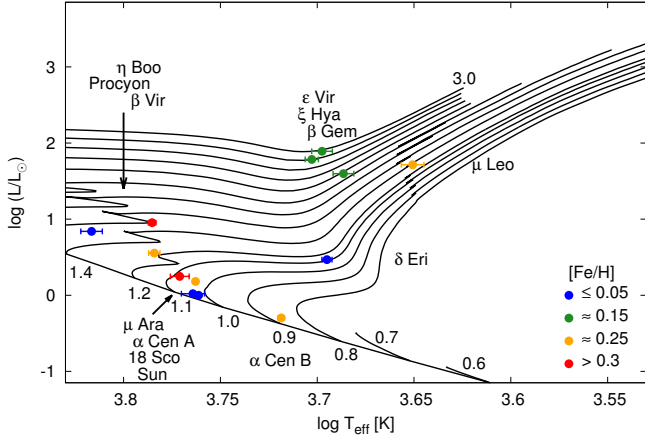
Fig. 4. HR-diagram with fundamental $T_{\rm eff}$, and L from $F_{\rm bol}$ and parallax for *Gaia* FGK benchmark stars with metallicities between +0.4 and 0.0 dex. *Yonsei-Yale* evolutionary tracks for [Fe/H] = +0.05 and [α/Fe] = +0.0, labelled with mass in $M_\odot$. Between 1.4 and 3.0 $M_\odot$ the step is 0.2 $M_\odot$. The mass can be read off the figure only for δ Eri, which has the same metallicity as the tracks. For lower metallicities (blue points) the tracks shift towards higher $T_{\rm eff}$ and L, and the points will be located on tracks with lower masses (cf. Fig. 7). The opposite applies to stars with higher metallicities (green, orange, red points), which will fall on tracks with higher masses than those shown (e.g. ≈1.2 $M_\odot$ for μ Ara).
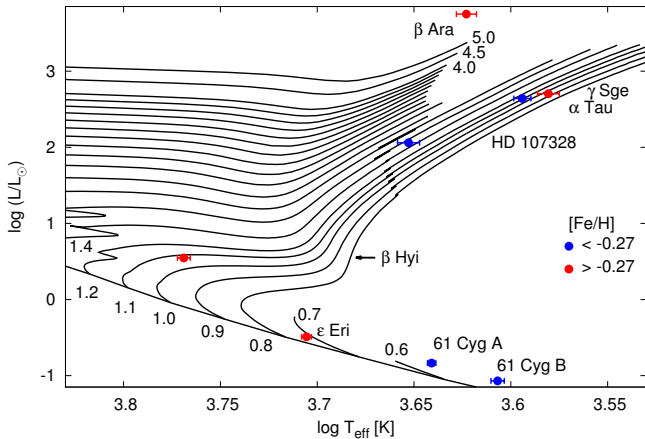
Fig. 5. Same as Fig. 4 for stars with metallicities between 0.0 and −0.4 dex. *Yonsei-Yale* evolutionary tracks for [Fe/H] = −0.27 and [α/Fe] = +0.0, labelled with mass in $M_\odot$. Between 1.4 and 4.0 $M_\odot$ the step is 0.2 $M_\odot$. Note that none of the stars has exactly the same metallicity as the shown tracks.

Fig. 6. Same as Fig. 4 for stars with metallicities between −0.4 and −0.9 dex. *Yonsei-Yale* evolutionary tracks for [Fe/H] = −0.68 and [α/Fe] = +0.3, labelled with mass in $M_\odot$. The step is 0.2 $M_\odot$ between 1.4 and 2.0 $M_\odot$. HD 220009 with $M \approx 0.8\ M_\odot$ has a metallicity closest to that of the shown tracks. HD 49933 and HD 22879 lie at the maximum and the minimum of the metallicity range, thus falling on higher (1.2 $M_\odot$) and lower mass (0.7 $M_\odot$) tracks, respectively, than those shown.
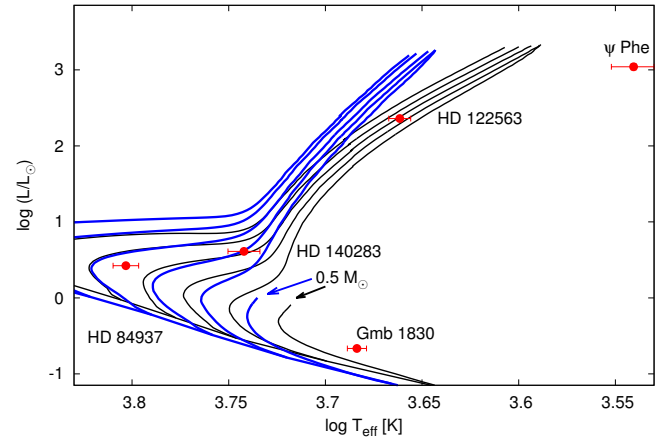
Fig. 7. Same as Fig. 4 for stars with metallicities lower than −1.2 dex. *Yonsei-Yale* evolutionary tracks for [Fe/H] = −1.29 (black, to the right) and −2.29 (blue, to the left), and [α/Fe] = +0.3, for masses between 0.5 and 1.0 $M_\odot$, in steps of 0.1 $M_\odot$. Clearly, ψ Phe ([Fe/H] = −1.2), Gmb 1830 (−1.5) and HD 122563 (−2.6) lie outside the range of the tracks with corresponding metallicities. HD 84937 and HD 140283 have metallicities close to the −2.29 tracks, resulting in derived masses of about 0.75 and 0.7 $M_\odot$, respectively.

the two grids[16]. Applying the same method using the solar $T_{\rm eff}$ and L results in a mass of 1.01 ± 0.02 $M_\odot$.

The main difference between the two sets of evolutionary tracks is that the *Yonsei-Yale* models take the diffusion of helium into account, while the *Padova* models do not include diffusion at all. Other differences can be found in the assumptions for microscopic physics, in the treatment of convective core overshoot, or in the boundary conditions at the surface. However, Figure 3 shows that the differences between the masses determined from the two grids are much lower than the uncertainties. Figures 4 to 7 show the locations of all *Gaia* FGK benchmark stars in the

theoretical HR-diagram for several metallicity groups, together with *Yonsei-Yale* evolutionary tracks.

We note that the best possible modelling of a star's location in the HR-diagram should take other parameters into account apart from metallicity and α-element abundances. Examples of these are the mixing length used for modelling convection, the initial helium abundance, or diffusion of chemical elements other than helium. When using a fixed set of evolutionary tracks for all stars, we do not have the possibility of arbitrarily varying these parameters, but detailed modelling of each star is beyond the scope of this article. Another shortcoming of the method is that we did not consider evolution beyond the red giant stage. Stars with luminosities greater than about 1.6 $L_\odot$ could be in a stage after the onset of core helium burning. Tracks for the corresponding "horizontal branch" (HB) models are included

---

[16] If M is the adopted mass, M_P and M_Y the masses from the *Padova* and *Yonsei-Yale* grids, respectively, and σ_P and σ_Y the corresponding uncertainties, then $\sigma_M = \max(|M - (M_P - \sigma_P)|, |M - (M_P + \sigma_P)|, |M - (M_Y - \sigma_Y)|, |M - (M_Y + \sigma_Y)|)$.
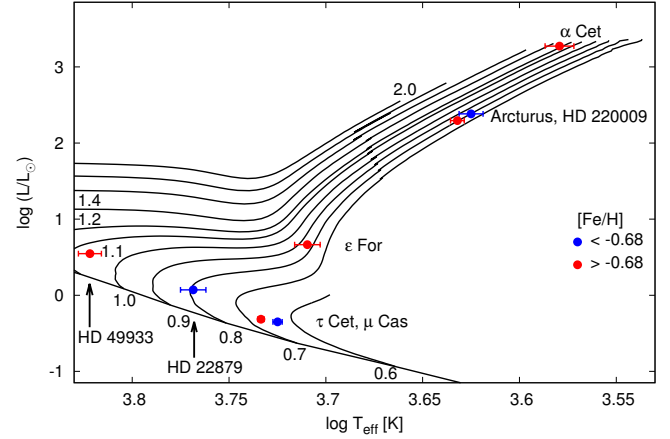
in the *Padova* grid, and we used these to evaluate the effect of ambiguous evolutionary stages on mass determination for the giants in our sample. Most of the stars are in fact not located on the HB tracks. The only affected stars are γ Sge, for which the mass derived from HB tracks would be lower by about 0.1 $M_\odot$, as well as μ Leo and HD 107328, for which the HB mass would be lower by about 0.4 $M_\odot$.

The interpolation between evolutionary tracks was only made with respect to mass. We did not try to estimate an age for any of the stars. However, the model grids include models with assigned ages that are greater than the age of the Universe, and we noticed that a few of the stars lie close to or in the areas in the HR diagram corresponding to such models. This points towards problems with the model physics. Two of the metal-poor dwarfs, HD 22879 (Fig. 6) and HD 84937 (Fig. 7), are located at the main-sequence turn-off for their masses of ~0.7 $M_\odot$, and neighbouring models have presumed ages between 12 and 24 Gyr. HD 84937 has a metallicity similar to the globular cluster NGC 6397, for which Korn et al. (2007) estimated the effects of atomic diffusion. They find a surface iron abundance of turn-off stars on average 0.16 dex lower than that of red-giant-branch stars. This indicates that more metal-rich evolutionary models would be more appropriate for determining the mass of HD 84937. A slightly higher mass would be derived in this case with models of more reasonable ages. For more details on the effects of atomic diffusion see also Jofré & Weiss (2011) or Creevey et al. (2015). In the case of the metal-poor subgiant HD 140283 (Fig. 7), which has passed the turn-off of the 0.7 $M_\odot$ track, the neighbouring models have ages between 14 and 37 Gyr. For the metal-deficient dwarfs μ Cas and τ Cet (Fig. 6), which are located on the main sequence near 0.6 to 0.7 $M_\odot$, the models would predict ages that are too large (more than 20 Gyr).

In the following, we give further comments on the mass determination for a few individual stars. For HD 140283 the mass determined from the *Padova* models was obtained by extrapolation in metallicity, because the lowest metallicity of the grid is 0.1 dex higher than the stellar metallicity. Both η Boo and β Vir (Fig. 4) lie in a post-main-sequence region of the HR diagram where the evolutionary tracks form a loop. The range of masses given by the high-L and the low-L parts of the loop provides the main contribution to the uncertainty in mass in this case. For α Cet (Fig. 6), the gravity used in Paper III was calculated with a mass determined for solar metallicity (3 $M_\odot$), while the low metallicity determined in Paper III ([Fe/H] = −0.45 dex) results in a mass of 1.8 $M_\odot$ and a gravity that is lower by 0.2 dex. For β Ara, only the *Padova* grids were used, since the *Yonsei-Yale* grids are only available up to 5 $M_\odot$ (Fig. 5). This star lies in a region that is crossed several times by the model tracks. This, together with the uncertain metallicity, results in a more than 20% uncertainty on the mass. For ψ Phe, the $T_{\rm eff}$ and L values lie outside the range of the grid values for metallicities lower than −0.3 dex (Fig. 7). Thus, the mass cannot be determined using the metallicity determination from Paper III (−1.2 ± 0.4 dex). Possible mass values range from 1.3 ± 0.3 $M_\odot$ at solar metallicity to 0.8 ± 0.2 $M_\odot$ at [Fe/H] = −0.3 dex, corresponding to $\log g$(cm s^{-2}) = 0.6 and 0.4, respectively.

For the 61 Cyg system, the $T_{\rm eff}$ and L values lie outside the range of the grid values. That is, the *Padova* models indicate a mass lower than 0.6 $M_\odot$ for both components. In the *Yonsei-Yale* grids, the 61 Cyg A values lie close to the 0.6 $M_\odot$ track, and the 61 Cyg B values close to 0.5 $M_\odot$, but beyond the point with the highest age of 30 Gyr (Fig. 5). Thus, we resorted to using the masses derived by Kervella et al. (2008) for this

system. Since Kervella et al. (2008) did not derive uncertainties for the masses, we adopted uncertainties of 0.05 $M_\odot$ for both components (similar to ϵ Eri)[17].

4.2. Other determinations of mass

Our sample includes both components or the primary ones of several visual binary systems. The masses of the two components of 61 Cyg were derived by Gorshanov et al. (2006) from dynamical modelling of astrometric observations to be 0.74 and 0.46 $M_\odot$. The observations span 40 yr, that is, about 6% of the 700-yr orbit. Gorshanov et al. (2006) derived a somewhat higher mass ratio (1.6) than Kervella et al. (2008, 1.1, adopted here), while the values for the total mass of the system are similar (1.2 and 1.3 $M_\odot$, respectively). For α Cen, precise masses were determined by Pourbaix et al. (2002) from dynamical modelling of combined astrometric and spectroscopic observations. These masses (A: 1.105±0.007 $M_\odot$, B: 0.934 ± 0.006 $M_\odot$) are in excellent agreement with the ones derived here from the stellar model grids. Drummond et al. (1995) used astrometric data for μ Cas and its 5 mag fainter M-dwarf companion GJ 53 B to derive a mass of 0.74±0.06 $M_\odot$ for μ Cas, which is somewhat higher than the one determined here. The mass of Procyon was determined by Girard et al. (2000) and Gatewood & Han (2006) from astrometric measurements of the 40-year orbit with its white-dwarf companion. The authors obtained values of 1.50 ± 0.04 $M_\odot$ and 1.43 ± 0.03 $M_\odot$ from observations spanning 83 and 18 yr, respectively. These values agree with the one derived from the stellar model grids.

As an alternative method for determining masses of single stars we can make use of measured pulsation frequencies (asteroseismology). For solar-like oscillations (convection-powered p-modes), the power spectrum shows a series of peaks with constant frequency separation $\Delta\nu$. These correspond to pulsation modes with the same spherical harmonic degree l, but different radial orders n. It has been shown (e.g. Kjeldsen & Bedding 1995) that this so-called large frequency separation is proportional to the square root of the mean stellar density. Thus, we can use $\Delta\nu$ measurements, together with the radius determined from $\theta_{\rm LD}$ and the parallax, for a *seismic* mass estimation:

$$\frac{\Delta\nu}{\Delta\nu_\odot} \approx \left(\frac{\bar{\rho}}{\bar{\rho}_\odot}\right)^{1/2} \Rightarrow \frac{M}{M_\odot} \approx \left(\frac{\Delta\nu}{\Delta\nu_\odot}\right)^2 \left(\frac{R}{R_\odot}\right)^3, \qquad (2)$$

where $\Delta\nu_\odot$ = 135.229 ± 0.003 μHz (Bazot et al. 2011). We compiled measurements of $\Delta\nu$ for about half of our sample from the literature, starting from the references given in Bruntt et al. (2010) and Kallinger et al. (2010). All of these stars except μ Ara have interferometric measurements of $\theta_{\rm LD}$. The data, references, and seismic masses are given in Table 9. For most stars, the seismic masses agree with those determined from the stellar model grids within ±0.1 $M_\odot$. Larger deviations are obtained for δ Eri, μ Ara, and Arcturus (+0.2, −0.3, and −0.4 $M_\odot$, respectively). As mentioned above, the $T_{\rm eff}$ and radius of μ Ara are uncertain owing to a calibrated angular diameter. In the case of Arcturus, the $\Delta\nu$ value (the lowest one of the sample) is rather uncertain, since it is close to the observational frequency resolution. Also, it is not yet certain that the regularities in the observed time series of Arcturus are due to p-mode oscillations (Retter et al. 2003).

---

[17] For the metallicity determination in Paper III, we used gravities based on extrapolated masses of 0.4 $M_\odot$ for both components, which are probably too low. However, for these stars, the change in metallicity caused by a change in $\log g$ is negligible (see Table 3 in Paper III).

Table 9. Seismic data (large frequency separation $\Delta\nu$), masses (M) from Eq. (2), and their uncertainties (u), for a subset of *Gaia* FGK benchmark stars.

Name	M [$M_\odot$]	$u(M)$	$\Delta\nu$ [μHz]	$u(\Delta\nu)$	Ref.
Procyon	1.40	0.06	55	1	1
HD 49933	1.14	0.10	85.2	0.5	2
δ Eri	1.32	0.04	43.8	0.1	3
η Boo	1.68	0.08	39.9	0.1	4
β Hyi	1.06	0.03	57.24	0.16	5
α Cen A	1.13	0.02	106	1	6
τ Cet	0.78	0.01	169.3	0.3	7
α Cen B	0.92	0.01	161.38	0.06	8
18 Sco	1.02	0.03	134.4	0.3	9
μ Ara	0.91	0.06	90	1	10
β Vir	1.41	0.05	72.07	0.10	11
Arcturus	0.62	0.08	0.83	0.05	12
β Gem	1.96	0.09	7.14	0.12	13
ξ Hya	2.94	0.15	7.11	0.14	14

Notes. References for $\Delta\nu$: 1) Bedding et al. (2010), estimated from their Fig. 11; 2) Kallinger et al. (2010); 3) Bouchy & Carrier (2003); 4) Carrier et al. (2005a); 5) Bedding et al. (2007); 6) Bouchy & Carrier (2001); 7) Teixeira et al. (2009), estimated from the mean density of 2.21 ± 0.01 g cm^{-3} determined by the authors; 8) Kjeldsen et al. (2005), oscillations discovered by Carrier & Bourban (2003); 9) Bazot et al. (2011); 10) Bouchy et al. (2005); 11) Carrier et al. (2005b); 12) Retter et al. (2003); 13) Hatzes et al. (2012); 14) Frandsen et al. (2002), their Eq. (1).

For several stars, detailed investigations of the evolutionary state have been done with the CESAM2k code (Morel 1997; Morel & Lebreton 2008), taking seismic data into account when available. For α Cen A and B, Thévenin et al. (2002) constrained their models by measured values of $T_{\rm eff}$, L, [Fe/H], and both the large and small frequency separations. The age, initial helium content, initial metallicity, mixing length parameter, and mass were varied, and the best-fit masses were 1.100 ± 0.006 and 0.907 ± 0.006 $M_\odot$ for the A and B components, respectively. Kervella et al. (2004b) explored evolutionary models for Procyon with two different masses and find that models with a mass of 1.42 $M_\odot$, with or without diffusion of heavy elements, predicted oscillation frequencies consistent with the observed large frequency separation. The model with a higher mass of 1.5 $M_\odot$ predicted a $\Delta\nu$ value that was too high by about 3%. For δ Eri, η Boo, and ξ Hya, Thévenin et al. (2005) computed best-fit $T_{\rm eff}$, L, and [Fe/H] values by adjusting the model parameters of mass, age, and initial metallicity. The derived masses (1.215, 1.70, and 2.65 $M_\odot$, respectively) were not affected by including diffusion. The models for δ Eri and ξ Hya predicted $\Delta\nu$ values similar to the observed ones within 2–3%, while the values predicted for η Boo were too large by about 5%.

The CoRoT target HD 49933 was modelled by Bigot et al. (2011), who reproduced the interferometric radius and the observed large and small frequency separations by adjusting the mass, initial helium content, initial metallicity, and the core-overshoot and mixing-length parameters. They arrived at 1.20 ± 0.08 $M_\odot$. Roxburgh (2015) used a different stellar evolution code (Roxburgh 2008) and applied a model-fitting technique to the observed frequencies of HD 49933, which uses constraints that do not depend on the structure of the stellar surface layers. Best-fit models with masses ranging from 1.1 to 1.3 $M_\odot$ were found. Finally, the metal-poor subgiant HD 140283 was investigated in detail by Creevey et al. (2015). Interferometric, spectroscopic, and photometric data were used to fine-tune stellar evolution models including diffusion. The correlated effects

Table 10. Fundamental $T_{\rm eff}$ and $\log g$ values and their uncertainties (absolute, u, and in percent, $\%u$) for *Gaia* FGK benchmark stars.

Name	$T_{\rm eff}$ [K]	$u(T_{\rm eff})$	$\%u(T_{\rm eff})$	$\log g$ [cm s^{-2}]	$u(\log g)$
F dwarfs					
Procyon	6554	84	1.28	4.00	0.02
HD 84937	6356	97	1.52	4.06	0.04
HD 49933	6635	91	1.38	4.20	0.03
FGK subgiants					
δ Eri	4954	30	0.61	3.76	0.02
HD 140283	[5522]	[105]	[1.91]	3.58	0.11
ϵ For	5123	78	1.53	[3.52]	[0.08]
η Boo	6099	28	0.45	3.79	0.02
β Hyi	5873	45	0.77	3.98	0.02
G dwarfs					
α Cen A	5792	16	0.27	4.31	0.01
HD 22879	5868	89	1.52	4.27	0.04
Sun	5771	1	0.01	4.4380	0.0002
μ Cas	5308	29	0.54	[4.41]	[0.06]
τ Cet	5414	21	0.39	[4.49]	[0.02]
α Cen B	5231	20	0.38	4.53	0.03
18 Sco	5810	80	1.38	4.44	0.03
μ Ara	[5902]	[66]	[1.12]	4.30	0.03
β Vir	6083	41	0.68	4.10	0.02
FGK giants					
Arcturus	4286	35	0.82	[1.64]	[0.09]
HD 122563	4587	60	1.31	1.61	0.07
μ Leo	4474	60	1.34	2.51	0.11
β Gem	4858	60	1.23	2.90	0.08
ϵ Vir	4983	61	1.21	2.77	0.02
ξ Hya	5044	40	0.78	2.87	0.02
HD 107328	4496	59	1.32	2.09	0.13
HD 220009	[4217]	[60]	[1.43]	[1.43]	[0.12]
M giants					
α Tau	3927	40	1.01	1.11	0.19
α Cet	3796	65	1.71	0.68	0.23
β Ara	[4197]	[50]	[1.20]	[1.05]	[0.15]
γ Sge	3807	49	1.28	1.05	0.32
ψ Phe	[3472]	[92]	[2.65]	[0.51]	[0.18]
K dwarfs					
ϵ Eri	5076	30	0.60	4.61	0.03
Gmb 1830	[4827]	[55]	[1.14]	4.60	0.03
61 Cyg A	4374	22	0.49	4.63	0.04
61 Cyg B	4044	32	0.78	4.67	0.04

Notes. Values in square brackets are uncertain and should not be used as a reference for calibration or validation purposes (see Sect. 6.1).

of varying mass, initial helium abundance, and mixing-length parameter were evaluated. Best-fit models with masses ranging from 0.77 to 0.81 $M_\odot$ were obtained. In most of these cases, the masses obtained by detailed modelling agree with the masses estimated from the *Padova* and *Yonsei-Yale* grids within the uncertainties (Table 7). The masses for δ Eri and ξ Hya show marginally significant discrepancies of 7–8%. The largest difference of 13–19% is seen for HD 140283, which is, however, expected considering the estimated uncertainty of 24%.

5. Results and comparisons

5.1. Fundamental effective temperature and surface gravity

The input data discussed in Sects. 3 and 4 and listed in Tables 4 and 7 were used to calculate the adopted fundamental values of $T_{\rm eff}$ and $\log g$ for the current sample of *Gaia* FGK benchmark stars. These values and their uncertainties are given
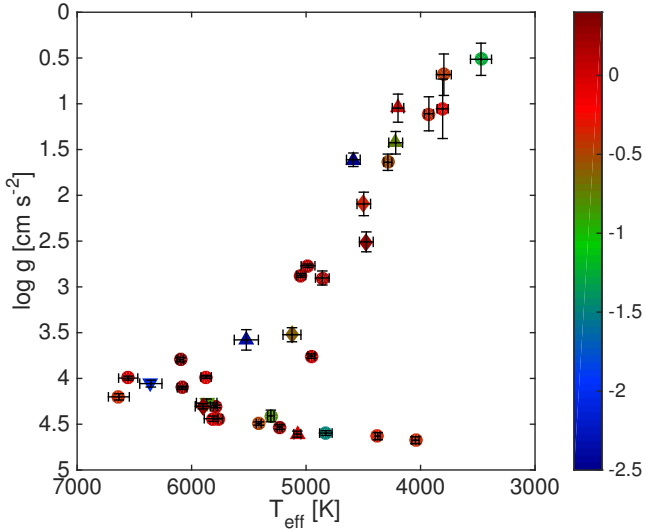
Fig. 8. Fundamental T_{eff} and $\log g$ values for *Gaia* FGK benchmark stars. Colour indicates [Fe/H] (non-LTE) as determined in Paper III. Circles: stars for which both θ_{LD} and F_{bol} have been measured; triangles up: stars with only θ_{LD} measured; triangles down: stars with only F_{bol} measured; diamonds: both calibrated.

Fig. 9. Fundamental T_{eff} as a function of $V - K$ colour index. Symbols and colours are as in Fig. 8. V magnitudes are mean values extracted from the GCPD (Mermilliod et al. 1997). K magnitudes were taken from the 2MASS catalogue (Cutri et al. 2003) if the entry had quality flag (Qflg) "A". Otherwise they are mean values taken from the Catalog of Infrared Observations (Gezari et al. 2000), if available, and transformed to the 2MASS system (Carpenter 2001, Eq. (A1)). Stars with large error bars in $V - K$ have K magnitudes from 2MASS with Qflg "D". $V - K$ for the Sun was taken from Casagrande et al. (2012). Grey line: empirical relation derived by Boyajian et al. (2013, their Eq. (2) and Table 8, row $(V - K)^c$).

in Table 10. Figure 8 shows the distribution of the stars in the T_{eff}–$\log g$ plane, with metallicity indicated by the symbol's colour (cf. Table 1). The sample covers the expected locations of FGK-type dwarfs, subgiants, and giants fairly well. It is obvious that stars with metallicities around the solar value dominate. However, the metal-poor stars are distributed regularly over the parameter space. The uncertainties in θ_{LD} and F_{bol} listed in Table 4 are below 5% for all stars (except F_{bol} for two M giants), propagating to T_{eff} uncertainties below 1% for half of the stars and below 2% otherwise (except for ψ Phe). Uncertainties in $\log g$ are below 0.1 dex except for the coolest giants (up to 0.3 dex).

In Fig. 8, the shape of the symbol indicates the quality of the input angular diameters and bolometric fluxes. Twenty-two stars have both measured angular diameters and integrated bolometric flux values, which is two thirds of the current sample (disregarding the Sun, see Table 4, rows without asterisks). Five stars have measured θ_{LD} values, but calibrated bolometric fluxes: the K dwarf ϵ Eri, the metal-poor (sub)giants HD 140283, HD 122563, and HD 220009, and the M giant β Ara. Two metal-poor dwarfs have integrated bolometric fluxes, but indirect θ_{LD} values (HD 22879, HD 84937). Lastly, for four stars the angular diameter is currently not directly measured, and the bolometric flux is determined from a calibration (the metal-rich dwarf μ Ara, the subgiant ϵ For, and the giants μ Leo and HD 107328).

The colour index $V - K$ has high sensitivity to effective temperature and low sensitivity to metallicity (see e.g. Boyajian et al. 2013). As can be seen in Fig. 9, the stars in our sample follow a tight relation in the $V - K$ versus fundamental T_{eff} diagram. Figure 9 shows the empirical relation derived by Boyajian et al. (2013) based on 111 FGK dwarfs with measured angular diameters and represented by a third-order polynomial (their Eq. (2)) using the coefficients given in their Table 8, row $(V - K)^c$. Excellent agreement is evident, except for the warmest and coolest stars. We note the deviating point at $V - K \approx 2$ corresponding to Gmb 1830, which is discussed in Sect. 5.2.6.

In Sects. 5.2 to 5.4, we present comparisons of the fundamental T_{eff} and $\log g$ values with spectroscopic and photometric
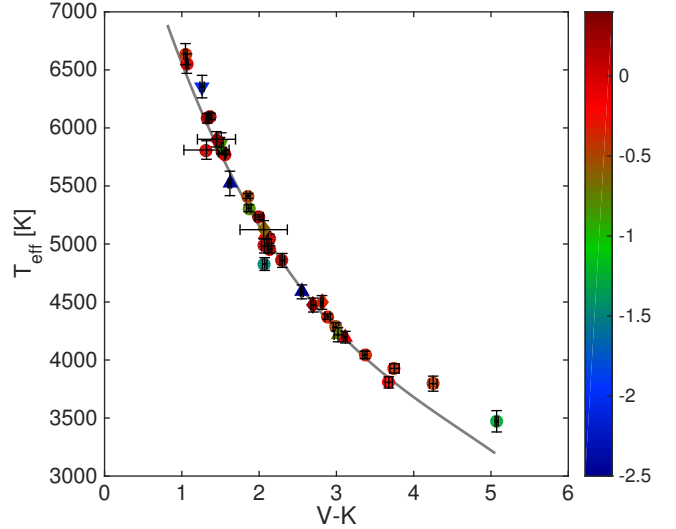
determinations, and with estimates based on parallaxes and asteroseismic data, and we discuss several cases in detail. The impatient reader may at this point skip to Sect. 6.1, where we give a brief summary of the status and conclusions for each star, and refer to the detailed discussions, as appropriate.

5.2. Comparison of fundamental T_{eff} to other methods

The sample of *Gaia* FGK benchmark stars was selected to include bright and well-known stars. Thus, many studies reporting temperatures can be found in the literature. In addition to our fundamental method the two main approaches to determine effective temperatures are through spectroscopic analysis or relations with photometric colour indices, the latter mostly based on the infrared flux method (IRFM). Spectroscopic temperature determinations are usually based on the requirement of excitation equilibrium of neutral iron lines or on fitting the profiles of Balmer lines. We queried the PASTEL catalogue[18] (Soubiran et al. 2010) for temperatures of *Gaia* FGK benchmark stars published between 2000 and 2012. We supplemented the results with some additional data and classified the T_{eff} determinations by method. Duplicate values and those outside the two categories were removed. We compiled 191 T_{eff} determinations using spectroscopic methods and 108 values using photometric calibrations. Ten or more *Gaia* FGK benchmark stars were analysed spectroscopically by Valenti & Fischer (2005), Luck & Heiter (2005), and Bruntt et al. (2010), while photometric temperature determinations have been published for more than ten stars by Allende Prieto et al. (2004), Ramírez & Meléndez (2005), Ramírez et al. (2007), and Casagrande et al. (2011).

---

[18] http://vizier.u-strasbg.fr/viz-bin/Cat?B/pastel, Version 17-May-2013.

Table 11. Mean T_{eff} and $\log g$ values from a compilation of spectroscopic, photometric, and parallax-based determinations published between 2000 and 2012.

Name	T_{eff} [K] spectroscopic	σ	N	T_{eff} [K] photometric	σ	N	$\log g$ [cm s^{-2}] spectroscopic	σ	N	$\log g$ [cm s^{-2}] parallax	σ	N
α Cet	3834	220	7	3724	87	2	1.29	0.43	7	0.73	0.30	1
γ Sge	4064	106	2	3877	41	1	1.52	0.32	2			
α Tau	3987	246	14	3887	86	2	1.42	0.31	14	1.20	0.30	1
61 Cyg B	4400	100	1				4.20	0.10	1			
HD 220009	4402	111	2	4484	100	1	1.95	0.34	2	2.03	0.10	1
Arcturus	4326	68	6	4274	83	5	1.70	0.20	6	1.82	0.15	5
61 Cyg A	4655	138	3	4300	170	2	4.49	0.17	3	4.50	0.20	1
μ Leo	4590	65	5	4425	100	1	2.65	0.22	5	2.24	0.10	1
HD 107328	4514	100	1	4436	125	2	1.94	0.10	1	2.09	0.27	2
HD 122563	4509	75	5	4795	107	1	1.23	0.30	4	1.44	0.24	2
Gmb 1830	5087	100	11	5133	36	4	4.75	0.21	9	4.69	0.05	6
β Gem	4952	33	4	4795	87	4	3.10	0.04	4	2.76	0.06	3
δ Eri	5085	51	9	5004	20	3	3.89	0.12	10	3.92	0.24	3
ϵ Vir	5115	29	3	5055	24	3	3.05	0.11	3	2.78	0.17	2
ξ Hya	5045	80	1				2.81	0.08	1			
ϵ Eri	5114	68	11	5063	80	6	4.51	0.14	12	4.61	0.02	4
ϵ For	5093	14	4	5135	155	4	4.07	0.30	5	3.61	0.10	5
α Cen B	5194	33	5	5131	110	4	4.49	0.07	5	4.58	0.06	2
μ Cas	5341	92	7	5338	82	4	4.51	0.20	8	4.62	0.09	4
τ Cet	5326	45	12	5395	92	5	4.56	0.18	14	4.62	0.07	2
HD 140283	5692	102	7	5774	77	7	3.54	0.15	3	3.69	0.03	8
α Cen A	5816	39	6	5681	117	6	4.30	0.13	7	4.32	0.10	2
18 Sco	5789	30	9	5759	72	5	4.39	0.07	10	4.45	0.05	4
HD 22879	5840	73	9	5844	87	10	4.37	0.15	8	4.33	0.10	9
β Hyi	5875	87	3	5815	95	3	4.07	0.21	4	3.98	0.03	3
μ Ara	5783	46	9	5703	93	3	4.29	0.13	9	4.26	0.12	2
β Vir	6138	54	6	6154	89	4	4.13	0.14	7	4.14	0.04	3
η Boo	6085	106	8	6041	140	2	3.94	0.18	8	3.77	0.10	2
HD 84937	6340	41	7	6352	63	6	4.02	0.09	6	4.05	0.05	6
Procyon	6601	148	9	6610	82	6	4.16	0.30	9	4.01	0.05	4
HD 49933	6661	110	5	6741	106	2	4.23	0.10	5	4.21	0.50	1

Notes. The stars are ordered by increasing fundamental temperature. Columns headed σ give standard deviations if number of determinations $N \geq 3$, or combined linear uncertainties ($N = 2$) or individual uncertainties ($N = 1$) quoted in the publications. T_{eff} values from González Hernández & Bonifacio (2009) with uncertainties larger than 200 K due to large uncertainties in 2MASS magnitudes were not included.
References for spectroscopic T_{eff} and $\log g$: Smith & Ruck (2000), Mashonkina & Gehren (2000); Fulbright (2000); Westin et al. (2000); Feltzing & Gonzalez (2001); Mishenina & Kovtyukh (2001); Santos et al. (2001); Stephens & Boesgaard (2002); Santos et al. (2003); Laws et al. (2003); Heiter & Luck (2003); Mishenina et al. (2003); Ryan & Smith (2003); Santos et al. (2004); Bruntt et al. (2004); Fuhrmann (2004); Santos et al. (2005); Luck & Heiter (2005); Valenti & Fischer (2005); Takeda et al. (2005); Gillon & Magain (2006); da Silva et al. (2006); Takeda et al. (2007); Hekker & Meléndez (2007); Mashonkina et al. (2008); Sousa et al. (2008); Porto de Mello et al. (2008); Fuhrmann (2008); Bruntt (2009); Gonzalez et al. (2010); Bruntt et al. (2010); da Silva et al. (2011); Sousa et al. (2011); Bruntt et al. (2011); Maldonado et al. (2012); da Silva et al. (2012); Britavskiy et al. (2012); Thygesen et al. (2012); Lebzelter et al. (2012); Pavlenko et al. (2012).
References for photometric T_{eff} and parallax-based $\log g$: Nissen et al. (2000); Gratton et al. (2000); Zhao & Gehren (2000); Nissen et al. (2002); Zhao et al. (2002); Allende Prieto et al. (2004); Galeev et al. (2004); Jonsell et al. (2005); Zhang & Zhao (2005); Zhang & Zhao (2006); Kotoneva et al. (2006); Bean et al. (2006); Reddy et al. (2006); Ramírez et al. (2007); Meléndez et al. (2008); Ramírez et al. (2009); Nissen & Schuster (2010); Casagrande et al. (2011).
References for spectroscopic T_{eff} and parallax-based $\log g$: Gratton et al. (2003); Korn et al. (2003); Bensby et al. (2003); Gehren et al. (2006); Roederer (2012); Roederer et al. (2012).
References for photometric T_{eff} and spectroscopic $\log g$: Bond et al. (2006); Ishigaki et al. (2012).
References for photometric T_{eff} only: Ramírez & Meléndez (2005); Masana et al. (2006); González Hernández & Bonifacio (2009); Casagrande et al. (2010); Gebran et al. (2010).
References for spectroscopic $\log g$ only: Mishenina et al. (2004); Thorén et al. (2004); Kovtyukh et al. (2004).
References for parallax-based $\log g$ only: Mishenina et al. (2008); Bergemann & Gehren (2008); Ramírez & Allende Prieto (2011).
References containing values in three or four categories: Affer et al. (2005); Smiljanic et al. (2007); Luck & Heiter (2007).

In Table 11 we list the mean and standard deviation or quoted uncertainties of the compiled T_{eff} values, as well as the number of determinations used for each star and method. References are given in the table notes. These values are compared in Fig. 10, where we plot the difference between the spectroscopic and the fundamental T_{eff} values (cf. Table 10) in the top panel, and the difference between the photometric and fundamental values in the middle panel. The uncertainties in the fundamental values and the σ values from Table 11 are represented as separate error bars. The bottom panel shows the difference between the mean spectroscopic and photometric values with combined uncertainties. The stars are ordered by increasing fundamental
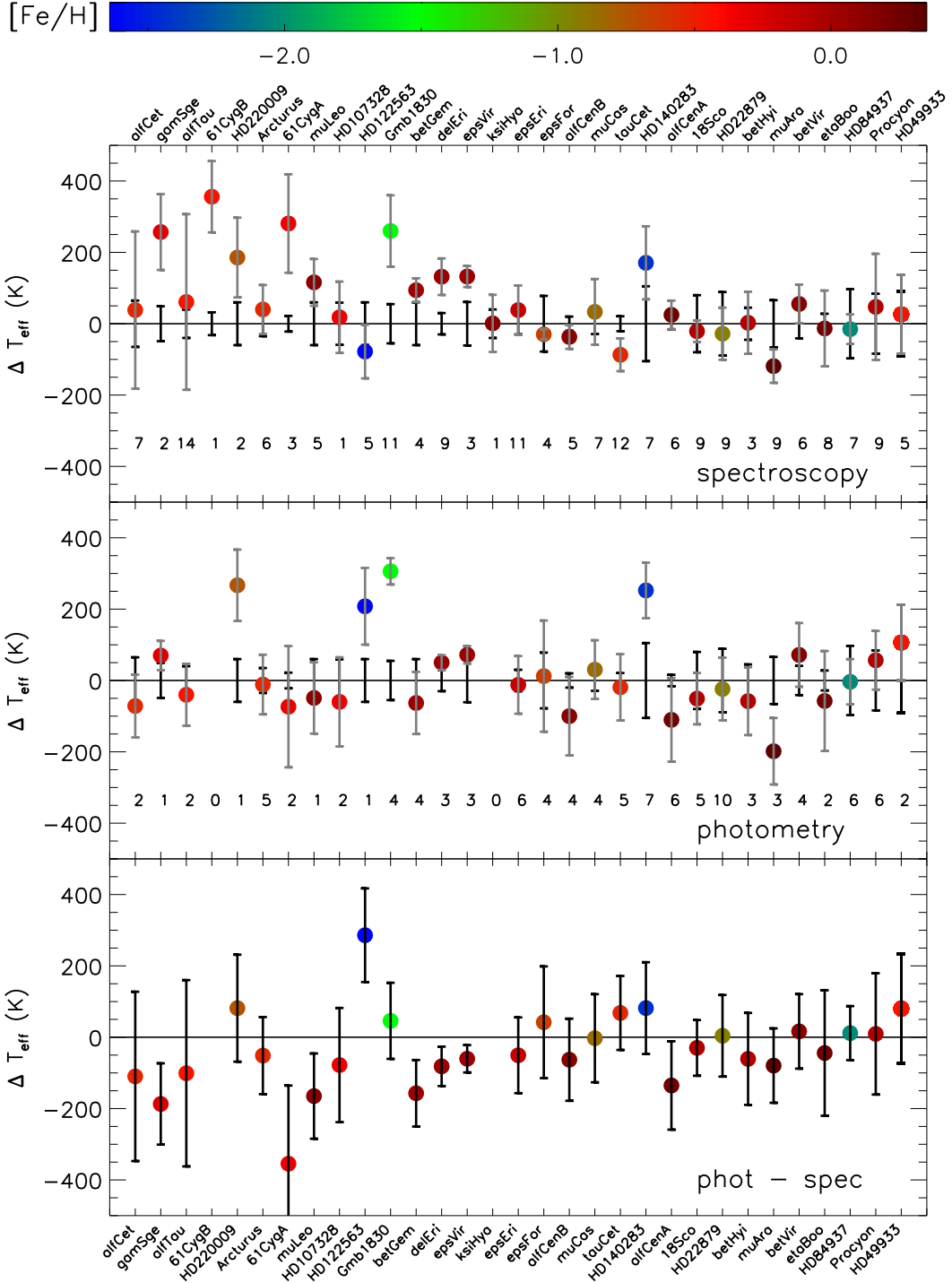
Fig. 10. Comparison of the fundamental temperature values with mean values of spectroscopic and photometric determinations compiled from the literature. The stars are ordered by increasing fundamental temperature *from left to right*. The *two upper panels* display the difference in the literature T_{eff} from the fundamental T_{eff}. Black error bars centred on zero represent the uncertainty in fundamental T_{eff} for each star, while grey error bars represent the standard deviation of the mean for $N \geq 3$, and combined and individual uncertainties in the case of two and one determinations, respectively. The number of determinations for each star are indicated in the two panels. The *bottom panel* compares the photometric and spectroscopic temperature measurements with error bars representing combined standard deviations. Symbol colour indicates metallicity from Table 1. See text and Table 11 for data, references, and discussion.

temperature from left to right and the colour of the symbol indicates the metallicity. Two stars, ψ Phe and β Ara, are not included in this comparison. The reason is that ψ Phe has no entry in PASTEL, while for β Ara there is only one entry: Luck (1979) quotes a temperature about 400 K higher than the fundamental one.

There is generally good agreement between the T_{eff} values obtained from the different approaches, when taking the uncertainties into account. For stars with $T_{eff} < 5000$ K, the mean spectroscopic T_{eff} values are almost always greater than the fundamental values, although the difference is not significant in most cases. Also, the error bars for spectroscopic

methods become larger towards cooler stars. At the hot end, the spectroscopic T_{eff} values of Procyon and HD 49933 show somewhat larger than typical scatter. For the FG dwarfs 18 Sco, HD 22879, and HD 84937, all three values agree very well, and the standard deviations of the spectroscopic and photometric values (each based on five to ten determinations) are smaller than the uncertainties in the fundamental values. Also for Arcturus, the most widely used giant among the *Gaia* FGK benchmark stars, the three T_{eff} values agree well. Furthermore, Ramírez & Allende Prieto (2011) used an additional method to derive the effective temperature of Arcturus from a fit of model SEDs scaled by the square of the angular diameter (21.06 ± 0.17 mas) to the observed SED. They obtained $T_{\mathrm{eff}} = 4286 \pm 30$ K, which is in excellent agreement with the value given in Table 10. In the following, we discuss those stars with discrepant values (non-overlapping error bars). For the spectroscopic methods, all of these have fundamental T_{eff} lower than 5000 K. An extensive discussion of the parameters of α Tau and α Cet can be found in Lebzelter et al. (2012).

5.2.1. The M giant γ Sge

For γ Sge, da Silva et al. (2006) and Hekker & Meléndez (2007) obtained a higher spectroscopic T_{eff} than the fundamental one: by 170 K or 2σ[19], and by 340 K or more than 3σ, respectively. Both used excitation equilibrium of Fe I lines as a constraint for T_{eff}, based on equivalent widths determined by two different procedures from spectra with similar quality ($R = \lambda/\Delta\lambda = 50\,000$–$60\,000$), and different line lists, atmospheric models, and radiative transfer codes. Using different selections of Fe lines and atomic data can have a large impact on the result of a spectroscopic analysis, in particular for cool stars (e.g. Lebzelter et al. 2012). This and other differences in analysis could explain the difference between the two spectroscopic values. Furthermore, Hekker & Meléndez (2007) compared in their Fig. 2 their T_{eff} values for 250 stars from their sample with literature determinations, and found differences of up to 300 K at temperatures around 4000 K. On the other hand, the photometric T_{eff} by Ramírez & Meléndez (2005) agrees with the fundamental value. We conclude that spectroscopic T_{eff} determinations for γ Sge are probably overestimated.

5.2.2. The 61 Cyg system

For 61 Cyg A, the spectroscopic T_{eff} determined in three publications is on average 280 K (2σ) higher than the fundamental value (4370 K), which is based on direct measurements of both angular diameter and bolometric flux and has a small formal uncertainty. The three individual values determined by Heiter & Luck (2003), Luck & Heiter (2005), and Affer et al. (2005) are 4800 K, 4640 K, and 4525 K, respectively. All studies are based on an equivalent width analysis, and in all cases, the effective temperature was determined by forcing the excitation equilibrium of Fe I lines (about 240 lines in the first two studies and 26 in the third one). Affer et al. (2005) did not measure any Fe II lines and could not simultaneously solve for ionization balance, as was done in the other two studies (based on 3–4 Fe II lines).

Equivalent width analyses of stars with such low temperatures are questionable, because most lines will be blended, not the least by molecular bands. Heiter & Luck (2003) compare

their temperatures with previous studies in their Fig. 10, which shows that their temperatures might be overestimated by up to 350 K for stars around 5000 K. Also the comparison with Fuhrmann (2004) in Fig. 9 of Luck & Heiter (2005) shows a systematic offset of 80 K towards higher T_{eff} values over the whole T_{eff} range. On the other hand, the T_{eff} value published by Mishenina et al. (2008) using a different method ($T_{\mathrm{eff}} = 4236 \pm 11$ K) is lower than the fundamental value. It is based on a calibration of line-depth ratios with a very low formal uncertainty. The absolute scale is given by the T_{eff} values of their calibrator stars, which are determined by the IRFM (Kovtyukh et al. 2004). The better agreement of this latter method with the fundamental value is in line with the good agreement of the photometric T_{eff} determination by Casagrande et al. (2011).

For the secondary component in the 61 Cyg system, the spectroscopic T_{eff} included in Table 11 (Luck & Heiter 2005) is 360 K (3σ) higher than the fundamental value. An additional spectroscopic determination of 4120 ± 100 K was published by Tomkin & Lambert (1999), which agrees with the fundamental value of 4040 ± 30 K. No photometric T_{eff} value published after 2000 is available, but two earlier determinations by Alonso et al. (1996a) and di Benedetto (1998) resulted in 3800 K and 4000 K, respectively, close to the fundamental value. Furthermore, the line-depth ratio method gives $T_{\mathrm{eff}} = 3808 \pm 26$ K for 61 Cyg B (Kovtyukh et al. 2003). This is the coolest dwarf in our sample, and the same caveats with regard to equivalent width analyses as for 61 Cyg A hold.

5.2.3. δ Eri and ϵ Vir

For δ Eri and ϵ Vir, solar-metallicity (sub)giants with T_{eff} about 5000 K, the means of the spectroscopic T_{eff} determinations are higher than the fundamental values by 130 K, or about 2σ. In both cases, the photometric T_{eff} values show better agreement. The star δ Eri is the coolest subgiant in our sample[20]. Three of the nine spectroscopic T_{eff} values are within 1–2% of the fundamental value, and they agree with the latter within the uncertainties. These studies used three different methods. The first two were based on excitation equilibrium for 147 and 116 Fe I lines with abundances derived from equivalent-width modelling and line-profile fitting (Bensby et al. 2003 and Bruntt et al. 2010, respectively). The third study used model fits for the wings of the Balmer lines (Fuhrmann 2008). The discrepant studies are based on either excitation equilibrium for about 40 Fe I lines (Santos et al. 2001, 2004; Affer et al. 2005), excitation equilibrium for about 400 or 250 Fe I lines (Luck & Heiter 2005; Sousa et al. 2008), or on spectrum synthesis for a mixture of weak and strong lines (Valenti & Fischer 2005). In conclusion, for stars like δ Eri, it seems that the preferred method is Balmer-line fitting for spectroscopic T_{eff} determination. If the excitation equilibrium method is chosen, the Fe lines and atomic data should be carefully selected, possibly guided by the two studies above, which reproduced the fundamental T_{eff} value of δ Eri.

In the case of ϵ Vir, there are three discrepant studies, two of which are based on excitation equilibrium for either a few Fe I lines (20 lines by Hekker & Meléndez 2007) or numerous

---

[19] The symbol σ refers to the combined uncertainty (the uncertainties added in quadrature).

[20] For another subgiant, ϵ For, with a slightly higher T_{eff} and almost five times lower metallicity than δ Eri, we do not see any discrepancy between the different T_{eff} determinations. However, in this case, the input data for the fundamental value are based on calibrations.

lines (>350 by Luck & Heiter 2007)[21]. Our sample includes two stars with similar parameters to ϵ Vir. For β Gem (included in the same three studies), we see a similar tendency, but with lower significance. For ξ Hya, there is no discrepancy with the single spectroscopic T_{eff} value by Bruntt et al. (2010, line profile fitting for 99 Fe I lines). Ruland et al. (1980) analysed high-resolution spectra of β Gem and derived systematically lower abundances for low-excitation than for high-excitation Fe I lines (with differences up to 0.4 dex). On the basis of kinetic-equilibrium studies available at the time, they argued that this abundance separation could be caused by a combination of two non-LTE effects (non-thermal ionization and excitation). Recent studies of non-LTE line formation of Fe (Bergemann et al. 2012b; Lind et al. 2012) indeed predict differential non-LTE corrections for stars similar to β Gem and ϵ Vir in the sense described above; however, the magnitude of the effect is much smaller. Interpolation in these calculations, available at the *INSPECT database*[22], at T_{eff} = 5000 K, $\log g$ = 2.8, and [Fe/H] = 0.1 results in mean non-LTE corrections of 0.01 dex and 0.04 dex for lines with lower level energies above and below 3.5 eV, respectively.

5.2.4. Metal-poor stars with discrepant photometric T_{eff}

For HD 220009 the photometric T_{eff} is higher (4500 K) than the fundamental one (4200 K), while the two spectroscopic T_{eff} values (4400 K) almost agree with the fundamental one within the uncertainties. The photometric T_{eff} by Luck & Heiter (2007) was derived from theoretical calibrations of a variety of narrow- and broad-band colour indices. It might be affected by systematic errors, because earlier photometric T_{eff} determinations based on the IRFM resulted in lower values around 4200 K (di Benedetto 1998; Alonso et al. 1999a). The fundamental value is based on a preliminary direct angular diameter and a calibrated bolometric flux.

For the metal-poor giant HD 122563, a similar situation to that of HD 220009 is observed. Here, the photometric T_{eff} is from González Hernández & Bonifacio (2009) and is based on the IRFM and 2MASS colour indices. In this case, the 2MASS data have poor quality, and several other photometric T_{eff} determinations giving lower values around 4600 K can be found (e.g. Ryan et al. 1996; from theoretical $B - V$ and $R - I$ calibrations, Alonso et al. 1999a; from the IRFM and colour indices in the TCS[23] system, and Casagrande et al. 2014 from the IRFM using Johnson *JHK* photometry). The fundamental value is based on a direct angular diameter but a calibrated bolometric flux.

For the metal-poor subgiant HD 140283, the photometric T_{eff} value determined by seven authors is 250 K (2σ) higher than the fundamental one (5500 K). Three publications using the IRFM calibration by Alonso et al. (1996b) report T_{eff} values around 5700 K. Three other publications that apply more recent, 2MASS-based IRFM implementations (González Hernández & Bonifacio 2009; Casagrande et al. 2010) arrived at T_{eff} values around 5800 K. The highest value of ~5900 K is given by Masana et al. (2006), who used a spectral energy distribution fit method with V and 2MASS photometry. Discrepant T_{eff} values at low metallicities for the latter method were noticed by Casagrande et al. (2010). The spectroscopic T_{eff} value is higher

than the fundamental one by 170 K, which is not significant given the uncertainties. The published spectroscopic determinations span a wide range of values, even when using the same diagnostics (e.g. 5560 K and 5810 K by Gratton et al. 2003 and Korn et al. 2003, respectively, from Balmer line fitting). Casagrande et al. (2010) observe that for metal-poor stars, their T_{eff} scale is 100–200 K hotter than the spectroscopic one. They state that the IRFM is less model dependent than the spectroscopic T_{eff} determinations, but can be affected by reddening.

This star has the smallest measured angular diameter in our sample with an associated uncertainty larger than for all other stars, but still below 4%. The interferometric observations were obtained at optical wavelengths, and they sample the visibility curve well. The bolometric flux determination is somewhat problematic due to the possible effect of an unknown amount of interstellar extinction (see discussion in Creevey et al. 2015). We used the calibrated value from Alonso et al. (1996a), who estimated zero reddening for HD 140283 using two different photometric methods. Also, according to the maps of the local ISM by Lallement et al. (2014), HD 140283 should be located within a local cavity with negligible reddening. Furthermore, we did not detect any interstellar absorption in the high-resolution spectra of this star (Paper II), for neither the Na D lines nor the diffuse interstellar bands. The bolometric flux adopted here ($38.6 \pm 0.8 \times 10^{-9}$ mW m^{-2}) is similar to the flux adopted by Creevey et al. (2015) for zero extinction ($38.9 \pm 6.6 \times 10^{-9}$ mW m^{-2}), resulting in T_{eff} = 5500 ± 100 K. For the extreme case with an extinction A_V = 0.1 mag, Creevey et al. (2015) derived $F_{\mathrm{bol}} = 42.2 \pm 6.7 \times 10^{-9}$ mW m^{-2} and T_{eff} = 5600 ± 100 K.

5.2.5. The G dwarfs τ Cet and μ Ara

For τ Cet ([Fe/H] = -0.5), the mean of twelve spectroscopic T_{eff} determinations is about 90 K (1.7σ) lower than the fundamental one (5410 K), which is based on direct measurements of angular diameter and bolometric flux. However, this includes an individual value of 5420 ± 25 K by Takeda et al. (2005) with very good agreement. In fact, half of the spectroscopic measurements are consistent with the fundamental value within the uncertainties. The mean of the five photometric T_{eff} determinations agrees with the fundamental one, but includes individual values that are 100 K higher and lower. We cannot identify any systematic uncertainties affecting the fundamental determination.

For the metal-rich G dwarf μ Ara, both the mean spectroscopic and the mean photometric T_{eff} are lower than the fundamental one (5900 K) by 120 K (1.5σ) and 200 K (1.7σ), respectively. Eight of the nine spectroscopic determinations lie within the interval 5780 to 5820 K. Two of the photometric determinations (5700 and 5800 K) are by the same first author (Ramírez & Meléndez 2005; Ramírez et al. 2007). The third one, 5600 K by Bond et al. (2006), is based on a very rough relation between $B - V$ colour index and temperature derived from the assumption that a star radiates as a black body and used the absolute magnitudes of the Sun for calibration. However, the fundamental value is based on indirect determinations of both angular diameter and bolometric flux. Thus, we cannot currently conclude about the reliability of the non-fundamental values.

5.2.6. The metal-poor K dwarf Gmb 1830

The metal-poor K dwarf Gmb 1830 represents an extreme case where the spectroscopic and photometric temperatures agree

---

[21] The third study (da Silva et al. 2006) with T_{eff} closest to the fundamental value used the same method with an unspecified number of Fe I lines.

[22] http://www.inspect-stars.com/

[23] Telescopio Carlos Sánchez.

well (5100 K), but both are significantly higher than the fundamental one (4800 K). The 11 spectroscopic $T_{\rm eff}$ determinations can be divided into two groups. Five authors fit one or more synthetic Balmer line profiles to the observed spectra (Mashonkina & Gehren 2000; Zhao & Gehren 2000; Mishenina & Kovtyukh 2001; Korn et al. 2003; Gehren et al. 2006), and five others performed an equivalent width analysis of Fe I lines, with excitation equilibrium as a constraint for $T_{\rm eff}$ (Fulbright 2000; Stephens & Boesgaard 2002; Heiter & Luck 2003; Luck & Heiter 2005; Takeda et al. 2005). The analyses of the first group are based on similar spectra and theoretical models, while those of the second group differ in spectroscopic data, atmospheric models, and line data. Within the second group, the studies by Fulbright (2000) and Stephens & Boesgaard (2002) are the most alike regarding data and models; however, their results differ by 150 K. An additional method is applied by Valenti & Fischer (2005), who performed a global fit of synthetic spectra to observed spectra in several wavelength intervals containing weak lines of various elements and the strong Mg Ib triplet lines. All but two of these works obtain $T_{\rm eff}$ values in the interval of about 5000 K to 5100 K, and no systematic difference between methods can be discerned. The photometric determinations include three different approaches. Gratton et al. (2000) used theoretical calibrations for $B - V$ and $b - y$ colour indices, while Kotoneva et al. (2006) applied an empirical calibration of $R - I$ colour indices based on spectroscopic temperatures for GK dwarfs. The determinations by González Hernández & Bonifacio (2009) and Casagrande et al. (2011) are both based on the IRFM with 2MASS colour indices. Again, all values lie in a narrow interval of 5080 K to 5170 K, which is slightly higher than the spectroscopic values.

According to the discussion above, it seems that determinations using a wide variety of stellar atmosphere modelling and input data result in a consistent range of $T_{\rm eff}$ values. The quoted spectroscopic analyses could be affected by systematic uncertainties owing to unrealistic atmospheric models and model spectra, assuming hydrostatic and LTE. However, Ruchti et al. (2013) show, for somewhat warmer dwarfs and subgiants ($T_{\rm eff} > 5500$ K) at a metallicity of -1.5 dex, that including non-LTE corrections for Fe lines in the analysis results in about 100 K higher $T_{\rm eff}$ values than an LTE analysis. This points in a direction away from the fundamental value. Furthermore, effective temperatures derived from Balmer-line fitting by the same authors for two dwarf stars bracketing the metallicity of Gmb 1830 agree well with the fundamental values (HD 22879–5800 ± 100 K, HD 84937–6315 ± 100 K). See also the discussion in Paper III, where the line-by-line abundance determinations for Fe lines using the fundamental $T_{\rm eff}$ and $\log g$ values resulted in a considerable deviation from excitation and ionization equilibrium. It is therefore necessary to question the correctness of the fundamental value.

The fundamental $T_{\rm eff} = 4830 \pm 60$ K is based on direct measurements of both angular diameter (with a 2% uncertainty) and bolometric flux, and for each quantity there is an additional direct measurement that agrees within 2.5 and 1%, respectively (see Fig. 1). However, the angular diameter measurements are mostly based on the same interferometric data. An increase in $T_{\rm eff}$ of 200 K (4%) would require a decrease in $\theta_{\rm LD}$ by 8%, while an increase of 300 K (6%) would require a decrease in $\theta_{\rm LD}$ by 12%. Considering that the data for Gmb 1830 span only 6% of the first lobe of the visibility curve, it is conceivable that they could represent an angular diameter smaller than accounted for by the formal uncertainties. Figure 11 shows the data from Creevey et al. (2012, their Table 2) compared to model visibility
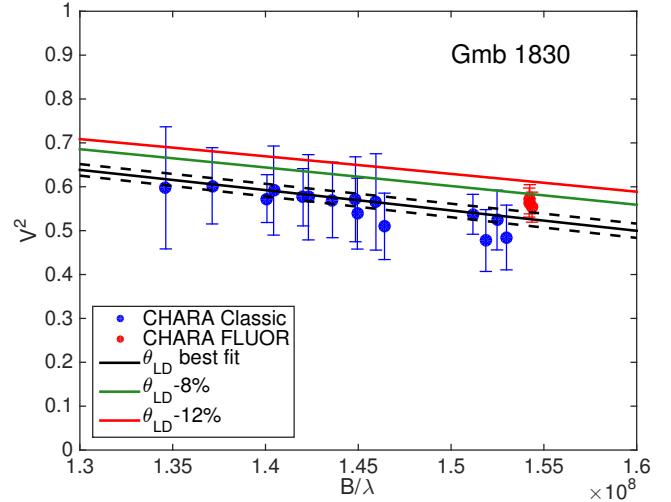

Fig. 11. Squared visibility measurements for Gmb 1830 from two instruments at the CHARA array (Creevey et al. 2012, their Table 2) compared to model visibility curves including limb darkening and assuming the best-fit angular diameter (black solid line) and its formal uncertainty (black dashed lines), as well as angular diameters that were decreased by 8 and 12% (green and red solid lines, respectively).

curves including limb darkening and assuming the best-fit or smaller angular diameters. A decrease of 12% is rather unlikely, as the model curve would only pass through one-third of the data points including error bars. For a decrease of 8%, the model curve would pass through two-thirds of the measurements. Furthermore, fitting the data from the two instruments separately results in angular diameters differing by about 7%. It is possible that the data are affected by additional uncertainties not included in the formal error, because of either the reduction procedure or the calibrator stars used. Further interferometric observations at longer baselines and/or shorter wavelengths are clearly needed to resolve or confirm the $T_{\rm eff}$ discrepancy for Gmb 1830.

5.3. Estimation of surface gravity from seismic data

Asteroseismic data provide an alternative way to estimate the surface gravity for stars with measurable p-mode oscillations. Here, we use a second global parameter derived from the power spectrum of oscillation frequencies (in addition to the large regular separation of frequencies $\Delta\nu$, see Sect. 4.2), namely the frequency where the power spectrum exhibits a global maximum, $\nu_{\rm max}$. It has been shown (e.g. Belkacem et al. 2011) that this parameter is proportional to the surface gravity and inversely proportional to the square root of the effective temperature. Thus, $\nu_{\rm max}$ measurements, together with the fundamental $T_{\rm eff}$ value, can be used for a *seismic* $\log g$ estimation:

$$\log g \approx \log \nu_{\rm max} + 0.5 \log T_{\rm eff} - \log \nu_{\rm max,\odot}, -0.5 \log T_{\rm eff,\odot} + \log g_\odot, \quad (3)$$

where $\nu_{\rm max,\odot} = 3160 \pm 40\ \mu$Hz (Barban et al. 2013, weighted mean of all data shown in their Fig. 3). Following Morel & Miglio (2012), we compiled measurements of $\nu_{\rm max}$ for about half of our sample from the literature. (The stars are the same as those listed in Table 9.) The data, references, and seismic $\log g$ values are given in Table 12. The precision of the $\nu_{\rm max}$ measurement varies from star to star, because the width of the peak in the power spectrum can be more or less narrow (see e.g. Fig. 11 in

Table 12. Seismic data (frequency of maximum power ν_{max}), $\log g$ estimates from Eq. (3), and their uncertainties (u), for a subset of *Gaia* FGK benchmark stars.

Name	$\log g$ [cm s^{-2}]	$u(\log g)$	ν_{max} [μHz]	$u(\nu_{max})$	Ref.
Procyon	3.92	0.24	900	500	1
HD 49933	4.19	0.01	1657	28	2
δ Eri	3.75	0.02	700	35	3
η Boo	3.83	0.02	750	38	4
β Hyi	3.94	0.02	1000	50	5
α Cen A	4.32	0.02	2400	120	5
τ Cet	4.58	0.02	4490	225	6
α Cen B	4.53	0.02	4100	205	5
18 Sco	4.44	0.02	3170	159	7
μ Ara	4.24	0.02	2000	100	8
β Vir	4.10	0.02	1400	70	9
Arcturus	1.44	0.01	3.7	0.1	10
β Gem	2.84	0.02	87.0	4.4	11
ξ Hya	2.87	0.01	92.3	3.0	12

Notes. References for ν_{max}: 1) Arentoft et al. (2008), Fig. 10, and Bedding et al. (2010), Fig. 8; 2) Gruberbauer et al. (2009); 3) Bouchy & Carrier (2003); 4) Carrier et al. (2005a), Figs. 2, 4, 5; 5) Kjeldsen et al. (2008); 6) Teixeira et al. (2009); 7) Morel & Miglio (2012); 8) Bouchy et al. (2005), Fig. 7; 9) Carrier et al. (2005b); 10) Retter et al. (2003), Fig. 4; 11) Hatzes et al. (2012); 12) Kallinger et al. (2010).

Arentoft et al. 2008 for a comparison of several stars). However, an uncertainty of 5% can be assumed in most cases (Morel & Miglio 2012).

For most stars, the seismic gravity value agrees with the one determined from the stellar mass and radius within ±0.06 dex or 15%. Larger deviations are obtained for Procyon, τ Cet, and Arcturus (-0.08, $+0.08$, and -0.2 dex, respectively). For Procyon, the ν_{max} determination has a large uncertainty (much larger than the deviation), because the peak in the power spectrum is very broad (referred to as a "plateau" in Arentoft et al. 2008). For τ Cet, our $\log g$ determination might be affected by an uncertain evolutionary mass (not consistent with a reasonable age), although it agrees with the seismic mass from $\Delta\nu$ within 10%. In the case of Arcturus, we have already found a deviation in its evolutionary mass from the seismic mass (Sect. 4.2). The nature of the variability of Arcturus seems to be unclear, and thus the scaling relations valid for solar-like oscillations might not be applicable. However, Tarrant et al. (2007) analysed seismic data for Arcturus obtained on a longer time scale than the data of Retter et al. (2003) and detected a peak in the power spectrum at ~3.5 μHz, which they ascribe to *p*-mode oscillations.

It should be noted that for seven dwarfs and subgiants in our sample Creevey et al. (2013, their Sect. 3) derived seismic $\log g$ values using a grid-based method with $\Delta\nu$, ν_{max}, T_{eff}, and [Fe/H] as constraints. Their seismic $\log g$ values agree with our fundamental $\log g$ values within 0.02 dex for all stars (Procyon, HD 49933, Sun, 18 Sco, α Cen A, α Cen B, β Hyi).

5.4. Comparison of fundamental $\log g$ to other determinations

Two main approaches to determining surface gravity are encountered in the literature – a spectroscopic analysis or a combination of V magnitude, parallax, bolometric correction, T_{eff}, [Fe/H], and stellar model isochrones (hereafter referred to as the parallax method). Spectroscopic gravity determinations are usually based on the requirement of ionization equilibrium of lines from neutral and singly ionized iron or on fitting the pressure-broadened wings of strong metal lines[24]. We queried the PASTEL catalogue for gravities of *Gaia* FGK benchmark stars published between 2000 and 2012. We supplemented the results with some additional data and classified the $\log g$ determinations by method. Duplicate values and those outside the two categories were removed. We compiled 192 $\log g$ determinations using spectroscopic methods and 89 values using the parallax method. Ten or more *Gaia* FGK benchmark stars were analysed spectroscopically by Valenti & Fischer (2005), Luck & Heiter (2005), and Bruntt et al. (2010), while the parallax method was applied for more than ten stars by Allende Prieto et al. (2004) and Ramírez et al. (2007).

In Table 11 we list the mean and standard deviation or quoted uncertainties of the compiled $\log g$ values, as well as the number of determinations used for each star and method. References are given in the table notes. These values are compared in Fig. 12, where we plot the difference between the spectroscopic and the fundamental $\log g$ values (cf. Table 10) in the top panel, and the difference between the parallax method and fundamental values in the middle panel. The uncertainties in the fundamental values and the σ values from Table 11 are represented as separate error bars. The bottom panel shows the difference between the mean spectroscopic and parallax method values with combined uncertainties. The stars are ordered by increasing fundamental temperature from left to right, and the colour of the symbol indicates the metallicity. As for T_{eff}, the stars ψ Phe and β Ara lack comparison data and are not included in this discussion.

There is in general good agreement between the gravity values obtained from the different approaches, when taking the uncertainties into account. For the coolest giants ($T_{eff} \lesssim 4300$ K), the spectroscopic gravities are systematically higher than the fundamental ones, although the differences are not significant. In the following, we discuss those stars with discrepant values (non-overlapping error bars), starting with the three dwarf stars 61 Cyg B, τ Cet, and μ Cas, followed by a subgiant and four giants.

5.4.1. The dwarf stars 61 Cyg B, τ Cet, μ Cas

For the secondary component in the 61 Cyg system, the spectroscopic $\log g$ included in Table 11 (Luck & Heiter 2005) is 0.5 dex (5σ) lower than the fundamental value. An additional determination of 4.4 ± 0.2 resulting from the parallax method was published by Tomkin & Lambert (1999), which is closer to the fundamental value of 4.67 ± 0.04. A mass of 0.46 $M_\odot$ inferred from astrometric observations (cf. Sect. 4.2) would give $\log g = 4.55$, decreasing the discrepancy even further. No other $\log g$ value published after 1980 is available. This is the coolest dwarf in our sample. The equivalent widths determined for such stars are uncertain due to blending. Fe II lines are weak and difficult to measure (see Paper III for an extensive discussion). The analysis of Luck & Heiter (2005) was based on Fe ionization balance, but included only one Fe II line (and 229 Fe I lines). Thus, we regard the spectroscopic $\log g$ as less reliable.

For τ Cet and μ Cas, the mean $\log g$ values from the parallax method are higher than the fundamental values by 0.1–0.2 dex (1–2σ), while the mean spectroscopic

---

[24] Examples for strong pressure-broadened lines are the Mg I b, the Fe I 5269.6 Å, the Na I D, and the Ca I 6162.2 Å lines in the optical, and the Ca II triplet, the Fe I 8688.6 Å, and the Mg I 8806.8 Å lines in the near-IR.
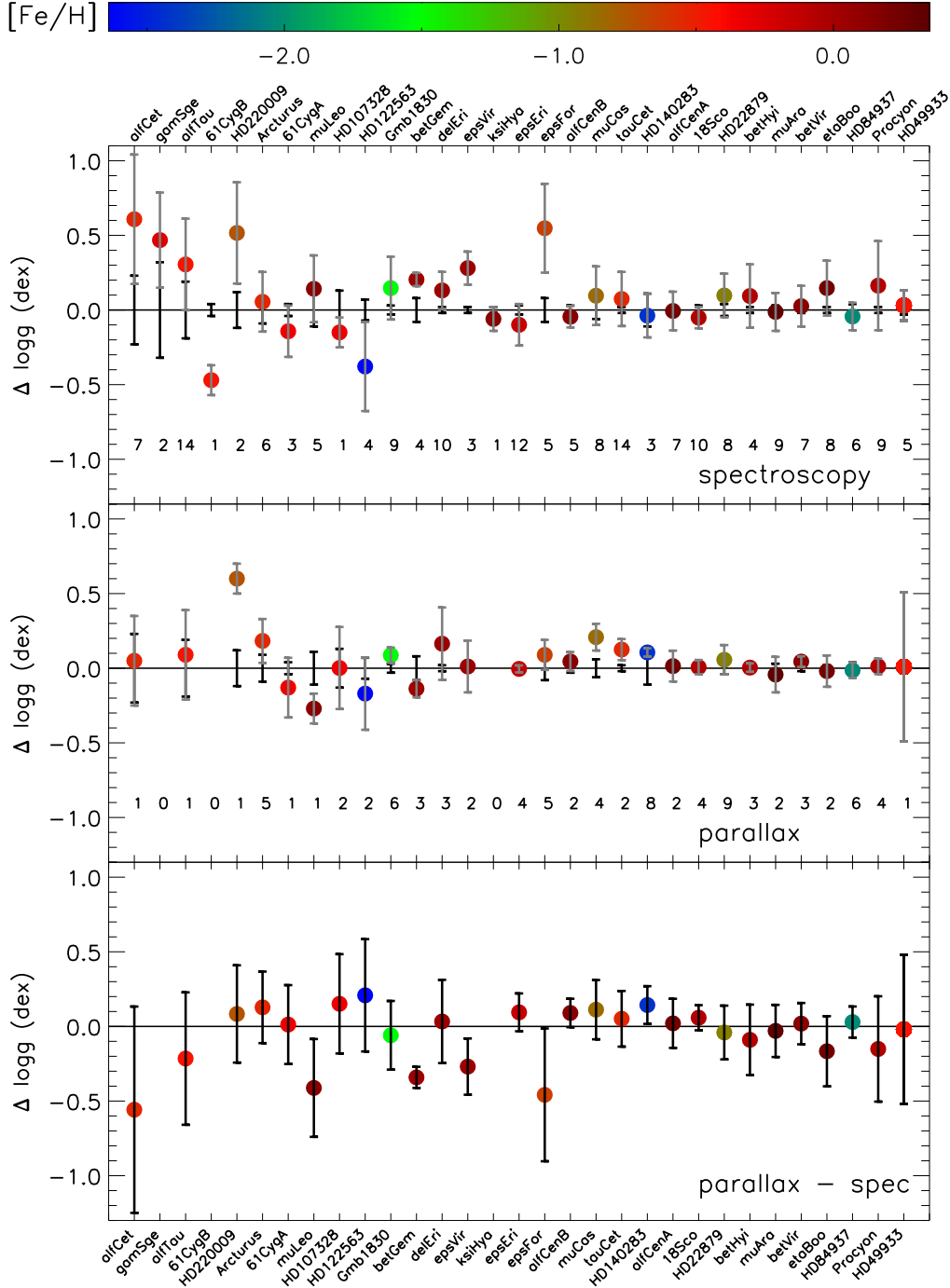
Fig. 12. Comparison of the fundamental surface gravity values with mean values of spectroscopic and parallax-based determinations compiled from the literature. The stars are ordered by increasing fundamental temperature from left to right. The *two upper panels* display the difference in the literature log *g* from the fundamental log *g*. Black error bars centred on zero represent the uncertainty in fundamental log *g* for each star, while grey error bars represent the standard deviation of the mean for $N \geq 3$, as well as combined linear uncertainties and individual uncertainties in the case of two and one determinations, respectively. The number of determinations for each star are indicated in the two panels. The *bottom panel* compares the parallax-based and spectroscopic gravity measurements with error bars representing combined standard deviations. Symbol colour indicates metallicity from Table 1. See text and Table 11 for data, references, and discussion.

determinations agree within the uncertainties[25]. These stars have very similar parameters (see e.g. Fig. 6), although μ Cas is somewhat more metal poor. Both stars have direct measurements of angular diameter and bolometric flux. However, the masses

used for the fundamental log *g* determination might be rather uncertain because they are derived from problematic evolutionary tracks predicting unreasonable ages (Sect. 4.1). For τ Cet, using the mass or log *g* from seismic data (see Tables 9 and 12) results in gravities of 4.53 and 4.58, respectively, which are compatible with the values by Allende Prieto et al. (2004) and Ramírez et al. (2007) from the parallax method. For μ Cas, using the dynamical mass (see Sect. 4.2) results in a gravity of 4.51 ± 0.04, which

---

[25] However, for μ Cas those of the spectroscopic determinations based on ionization balance of LTE Fe abundances could be too low by 0.2 dex due to non-LTE effects (Table 8 in Thévenin & Idiart 1999).

is closer to the values by Gratton et al. (2003), Allende Prieto et al. (2004), Reddy et al. (2006), and Ramírez et al. (2007) from the parallax method. In the first of these articles, a value of 4.46 ± 0.10 was derived, which is fully compatible with our fundamental value. In that publication, a more recent version of the *Padova* isochrones was used than in the other three (which quote log g values of 4.6 to 4.7 with uncertainties of 0.04 to 0.2).

5.4.2. The subgiant ϵ For

For the moderately metal-poor subgiant ϵ For, the mean spectroscopic log g is 0.5 dex higher than the fundamental value (about 1σ). The spectroscopic log g determinations show a large dispersion, compared to stars with similar $T_{\rm eff}$. The fundamental value is based on an angular diameter derived from a surface-brightness relation and has one of the largest uncertainties at $T_{\rm eff} \gtrsim 5000$ K, mainly due to the uncertainty of 17% in mass (caused by the close spacing of evolutionary tracks, see Fig. 6). The spectroscopic determination by Fulbright (2000), based on ionization equilibrium, agrees with the fundamental value. In all other publications, higher values have been presented, either using the same method (da Silva et al. 2006 by 0.3 dex; and Bond et al. 2006 by 0.9 dex), fitting the wings of strong Mg I, Ca I, and Fe I lines (Thorén et al. 2004, by 0.7 dex), or using a hybrid method (Valenti & Fischer 2005, by 0.4 dex). Including non-LTE effects in an Fe-line analysis would increase the derived log g (by about 0.1 dex at the metallicity of ϵ For, Ruchti et al. 2013). Three of the five log g values from the parallax method agree with the fundamental value (Gratton et al. 2003; Bensby et al. 2003; Ramírez et al. 2007), while the other two are about 0.2 dex higher (Reddy et al. 2006; Casagrande et al. 2011).

5.4.3. Four giants with discrepant gravities

For the K giants β Gem and ϵ Vir, the means of the spectroscopic log g determinations are 0.2–0.3 dex (2σ) higher than the fundamental values. In both cases, the dispersion of the three to four determinations is rather small (0.1 dex or less, see Table 11). The uncertainties of the fundamental values (based on measured angular diameters) are below 0.1 dex as well. The values from the parallax method agree better with the fundamental ones. This comparison indicates that for solar-metallicity giants with $T_{\rm eff} \approx 5000$ K and log $g \approx 2.8$, the spectroscopic approach can lead to overestimated gravities. On the other hand, for ξ Hya, a third giant in our sample with similar parameters as β Gem and ϵ Vir, the single spectroscopic log g determination by Bruntt et al. (2010) agrees very well with the fundamental value.

For the metal-rich giant μ Leo and the metal-poor (−0.7 dex) giant HD 220009, the log g values determined by Luck & Heiter (2007) with the parallax method differ from the fundamental one, by −0.3 dex (1σ) and by +0.6 dex (3σ), respectively. For μ Leo the mean of five spectroscopic determinations agrees with the fundamental value within the uncertainties, while for HD 220009 the two spectroscopic determinations are close to the one from the parallax method. The parallax-log g value by Luck & Heiter (2007) is based on isochrones from a previous version of the *Padova* models (Bertelli et al. 1994). Luck & Heiter (2007), Allende Prieto et al. (2004), and Ramírez et al. (2007) applied the same models to the solar-metallicity giant β Gem, resulting in lower-than-fundamental log g values. In fact, a systematic trend of discrepancy with metallicity becomes apparent when comparing the parallax-log g values determined by Luck & Heiter (2007) for six giants with the fundamental

Table 13. Comparison of log g values derived with the parallax method by Luck & Heiter (2007, LH07) for six giants with the fundamental values.

Name	[Fe/H]	log g(fund.)	LH07−fund.
μ Leo	0.3	2.5	−0.3
ϵ Vir	0.2	2.8	−0.1
β Gem	0.1	2.9	−0.1
HD 107328	−0.3	2.1	+0.1
Arcturus	−0.5	1.6	+0.1
HD 220009	−0.7	1.4	+0.6

values (see Table 13). On the other hand, Meléndez et al. (2008) used more recent model isochrones, similar to the ones used in the current work, for Arcturus and HD 107328, and derived log g values closer to the fundamental ones.

6. Discussion and conclusions

6.1. Atmospheric parameters quality for current sample

In this section, we summarise our current knowledge of $T_{\rm eff}$ and log g for each of the 29 FGK-type dwarfs, subgiants, and giants and refer to the discussions and comparisons in Sects. 3 to 5 as appropriate. We consider two comparison values to "agree well" if their error bars overlap. (These are the cases that have not been explicitly discussed in Sects. 5.2 and 5.4.) Based on these considerations, we assess for each star and each parameter whether they are suitable to be used as reference values for validation and/or calibration. Those of the fundamental values that we do not recommend as reference parameters are mentioned explicitly below and are indicated in Table 10 by square brackets.

Concerning the status of the M giants, we briefly note that all five of them have fundamental parameters based on directly measured input data (except for the bolometric flux of β Ara). Their masses are highly uncertain for various reasons discussed in Sect. 4.1. Both α Tau and α Cet have been discussed in Lebzelter et al. (2012). For a discussion of the $T_{\rm eff}$ for γ Sge see Sect. 5.2.1. For β Ara and ψ Phe the lack of comparison data prevents a comprehensive evaluation of their parameters.

Dwarfs.

Procyon: the quality of the available input data for the fundamental parameters is excellent. The interferometric diameter is based on 3D-RHD modelling of K-band visibilities. The mass is known to better than 10% from stellar evolution models, dynamical orbit modelling, and asteroseismic data. The mean spectroscopic and photometric determinations of $T_{\rm eff}$ agree with the fundamental one to less than 1%. We conclude that Procyon's $T_{\rm eff}$ is 6550 K with an uncertainty of 1%. The fundamental surface gravity agrees well with several other parallax-based determinations (the difference is 3%). Also in comparison to the spectroscopic log g determinations, the error bars overlap. However, the latter show a large dispersion of 0.3 dex (factor 2).

HD 84937: the fundamental $T_{\rm eff}$ and log g values are based on a calibrated angular diameter. Nevertheless, we recommend their use as reference values, since they show very good agreement in comparison with other determinations. For $T_{\rm eff}$, the means of the spectroscopic and photometric values differ by less than 1% from the fundamental one. For log g, the means of the parallax-based values differ by 3% and those of

the spectroscopic ones by 9%. In all cases the standard deviations of the comparison values are similar to the uncertainties of the fundamental value and larger than the differences quoted above.

HD 49933: the interferometric diameter for this sub-mas target was obtained from 3D-RHD modelling of optical visibilities. The resulting fundamental $T_{\rm eff}$ value agrees within 2% with all but one of the individual comparison values from the literature. The evolutionary mass and the fundamental $\log g$ values agree very well with the asteroseismic determinations (cf. Sects. 4.2 and 5.3), and there is a good agreement ($\approx$20%) with spectroscopic $\log g$ values.

α Cen A: apart from the Sun, α Cen A has the most precisely determined fundamental $T_{\rm eff}$ value of the sample (0.3% uncertainty), which agrees well with the literature spectroscopic measurements. Some of the photometric $T_{\rm eff}$ values are lower by 100 K to 300 K, but those by Ramírez & Meléndez (2005) and Ramírez et al. (2007) agree within 30 K (1%). The evolutionary, dynamic, and seismic masses agree well, as do the fundamental $\log g$ values with the asteroseismic, spectroscopic, and parallax-based $\log g$ determinations.

HD 22879: as for HD 84937 the fundamental $T_{\rm eff}$ and $\log g$ values based on a calibrated diameter agree well with all comparison values.

The Sun: based on the measured total solar irradiance (TSI, Kopp & Lean 2011) and the measured solar radius (Meftah et al. 2014, Sect. 3.1), the effective temperature of the Sun is 5771 ± 1 K, corresponding to a precision of 0.01%. A similar value has been derived by Ayres et al. (2006, their Sect. 2.4.2) based on an earlier measurement of the TSI with the same instrumentation (Kopp et al. 2005)[26]. The solar surface gravity based on the same radius measurement and the measured solar mass parameter (Konopliv et al. 2011, Sect. 4) is $\log g({\rm cm~s^{-2}}) = 4.4380$ with an uncertainty of 0.05%, which is dominated by the uncertainty in the radius.

μ Cas: all $T_{\rm eff}$ determinations agree well. The fundamental $\log g$ value based on the mass determined in Sect. 4.1 and given in Table 10 might be about 0.1 dex too low, and we do not recommend to use it as a reference value (see discussion in Sect. 5.4.1).

τ Cet: the fundamental $T_{\rm eff}$ value agrees well with the photometric determinations and with half of the spectroscopic determinations (see discussion in Sect. 5.2.5). For the fundamental $\log g$ value, the same case applies as for μ Cas.

α Cen B: the interferometric diameter is based on 3D-RHD modelling of K-band visibilities. The fundamental $T_{\rm eff}$ value agrees well with the literature spectroscopic measurements. For the photometric $T_{\rm eff}$ values, the comparison is the same as for α Cen A. All mass and $\log g$ values are consistent as in the case of α Cen A.

18 Sco: the fundamental $T_{\rm eff}$ value (based on the angular diameter measured at optical wavelengths by Bazot et al. 2011) agrees well with all comparison values (differences less than 1%). The evolutionary and seismic masses are consistent, as are the fundamental $\log g$ values with the

asteroseismic, spectroscopic, and parallax-based $\log g$ determinations.

μ Ara: this star has a very uncertain $T_{\rm eff}$, which should not be used as a reference value. The fundamental value is based on an indirect angular diameter, and the spectroscopic and photometric $T_{\rm eff}$ values are discrepant (see discussion in Sect. 5.2.5). The evolutionary and seismic masses differ by more than 20%, and the fundamental gravity from the seismic one by 13% (1.6σ). However, both the mean spectroscopic and the mean parallax-based $\log g$ agree well with the fundamental one (with differences of 3% and 9%, respectively).

β Vir: the fundamental $T_{\rm eff}$ value (based on an angular diameter measured at optical wavelengths) agrees well with the mean spectroscopic and photometric values. (The systematic difference seen in Fig. 10 is about 1%.) The evolutionary and seismic masses agree well (with a difference of about 5%). The fundamental $\log g$ agrees well with the seismic, the mean spectroscopic, and the mean parallax-based ones (differences of 0, 6, and 11%, respectively).

ϵ Eri: all $T_{\rm eff}$ and $\log g$ determinations are consistent. The mean differences are around 1%, except for the spectroscopic $\log g$ values, which are on average lower by 20%.

Gmb 1830: this star has a very uncertain effective temperature, which should not be used as a reference value. The interferometric diameter of this sub-mas object might be affected by calibration errors, and the spectroscopic and photometric determinations show a large dispersion (see discussion in Sect. 5.2.6). The mean spectroscopic and the mean parallax-based $\log g$ are 40% and 20% higher than the fundamental one, respectively, although they agree within the uncertainties.

61 Cyg A and B: the adopted fundamental $T_{\rm eff}$ values for both components agree with the photometric ones. For 61 Cyg B there are two different recent bolometric flux measurements (see Sect. 3.4), and we adopted the one by Mann et al. (2013) based on more realistic SEDs. The fundamental $\log g$ of 61 Cyg A is consistent with the single parallax-based comparison value. Using the dynamical mass by Gorshanov et al. (2006, see Sect. 4.2) instead of the evolutionary mass by Kervella et al. (2008) does not change the $\log g$ value. For 61 Cyg B the fundamental $\log g$ value based on the dynamical mass is 0.1 dex lower than that based on the evolutionary mass and given in Table 10. Determination of $T_{\rm eff}$ and $\log g$ based on equivalent width analysis seems to be unreliable in the temperature range of 61 Cyg A and B (see discussion in Sects. 5.2.2 and 5.4.1).

Subgiants.

δ Eri: the fundamental $T_{\rm eff}$ value is based on a precise (1%) interferometric measurement of the angular diameter with a good coverage of the visibility curve. The fundamental $T_{\rm eff}$ is about 1% lower than the mean photometric value and the closest spectroscopic determinations (see discussion in Sect. 5.2.3). The fundamental $\log g$ agrees well with the seismic $\log g$ estimate (0.01 dex difference). The mean spectroscopic and parallax-based determinations are larger by around 40% than the fundamental $\log g$, but the dispersions around the mean have similar magnitudes.

HD 140283: the fundamental $T_{\rm eff}$ of this sub-mas object is based on a direct angular diameter measured at optical

---

[26] The adopted TSI value is about 0.4% or 5 W m^{-2} lower than even earlier TSI measurements with different instruments (e.g. Fröhlich 2000), resulting in a downward revision of 0.1% or about 6 K from the previously used canonical value of 5777 K for the solar $T_{\rm eff}$.

wavelengths, but on a calibrated bolometric flux. The spectroscopic and photometric determinations are systematically higher, although they span a wide range of values (the lowest being within 1%, and the highest differing by 7% from the fundamental value, see discussion in Sect. 5.2.4). We do not currently recommend using HD 140283 as a reference star for $T_{\rm eff}$ validation.

The fundamental $\log g$ is consistent with the mean spectroscopic and parallax-based determinations within its rather large uncertainty of 0.1 dex and the large dispersion of the spectroscopic values. It is also compatible with the value of 3.65 ± 0.06 derived by Creevey et al. (2015). Two of the spectroscopic values (3.4 and 3.5 dex) are based on ionization balance of LTE Fe abundances (Fulbright 2000; Mishenina & Kovtyukh 2001) and could be too low by up to 0.5 dex owing to non-LTE effects (Table 8 in Thévenin & Idiart 1999). The third spectroscopic value (3.68 dex) is based on a fit of the wings of the Mg Ib triplet lines (Zhao & Gehren 2000) and is close to the mean of the eight parallax-based values (3.69 with a dispersion of only 0.03 dex, see Table 11).

ϵ For: the fundamental $T_{\rm eff}$ is consistent with the mean spectroscopic and photometric determinations, although it is based on indirect input data. The $\log g$ determinations, including the fundamental one (Table 10), span a wide range of possible values from 3.5 to 4.4 dex (see discussion in Sect. 5.4.2). These values, together with the adopted effective temperature, are consistent with the subgiant classification, but we cannot consider any of them to be a reference value for the $\log g$ of ϵ For.

η Boo and β Hyi: the fundamental $T_{\rm eff}$ values agree well with the mean literature spectroscopic and photometric measurements with differences of less than 1%. The evolutionary and seismic masses agree well (with differences of 2% and 8%, respectively). The fundamental $\log g$ values agree well with the seismic and the mean parallax-based values (<10% differences). The mean spectroscopic $\log g$ values are also consistent with the fundamental ones, although they are higher by about 40% and 20%, respectively.

Giants.

Arcturus: the fundamental $T_{\rm eff}$ agrees with the mean spectroscopic and photometric determinations of $T_{\rm eff}$ to less than 1%, and agrees perfectly with the independent determination by Ramírez & Allende Prieto (2011, see Sect. 5.2). We conclude that the effective temperature of Arcturus is 4290 K with an uncertainty of 1%.

The quality of the surface gravity is more uncertain. The seismic mass and $\log g$ are 40% lower than the evolutionary mass and the fundamental $\log g$ (which is 1.6 dex). However, the nature of the oscillations and the applicability of the seismic scaling relations are being debated (see Sects. 4.2 and 5.3). The mean spectroscopic $\log g$ value agrees well with the fundamental one with a 14% difference. The individual determinations range from 1.4 to 1.9 dex. The mean parallax-based $\log g$ value is 50% higher than the fundamental one with a narrower range from 1.7 to 2.0 dex. In conclusion, the uncertainty of the fundamental value (Table 10) seems underestimated, and we recommend to adopt $\log g = 1.6 \pm 0.2$ dex, if Arcturus is to be used as a reference star. Exactly the same value was derived by Edvardsson (1983) using the wings of strong pressure-broadened metal lines as constraints.

HD 122563: the interferometric diameter is based on 3D-RHD modelling of K-band visibilities. The resulting fundamental $T_{\rm eff}$ agrees well with the mean spectroscopic one (to within 2%). The single photometric $T_{\rm eff}$ value shown in Fig. 10 and given in Table 11 deviates significantly from the fundamental one, but several other determinations agree within the uncertainties (see discussion in Sect. 5.2.4).

The fundamental $\log g$ value agrees within 0.1 dex (30%) with two parallax-based determinations and with the spectroscopic determination by Mashonkina et al. (2008) based on ionization equilibrium of non-LTE Ca abundances. All cases have uncertainties of similar magnitude. Three other spectroscopic determinations based on ionization equilibrium of LTE Fe abundances are 0.3 to 1.0 dex too low. Ruchti et al. (2013) show that an LTE analysis underestimates the surface gravity by at least 0.3 dex at the metallicity of HD 122563 and up to 1.5 dex in combination with an erroneous $T_{\rm eff}$. This can easily explain the discrepancies.

μ Leo: the fundamental $T_{\rm eff}$ agrees well with the literature photometric determination (Luck & Heiter 2007), although it is based on indirect input data. The mean of the four spectroscopic $T_{\rm eff}$ determinations is about 3% higher, but is consistent with the fundamental $T_{\rm eff}$ within the uncertainties. The adopted $\log g$ value (Table 10) may serve as a reasonable reference. The discrepancy of about 50% with the single parallax-based comparison value (Fig. 12, Table 11) can be explained by inadequate isochrones (see discussion in Sect. 5.4.3).

β Gem: the fundamental $T_{\rm eff}$ is based on direct input data, and agrees well with the mean of the photometric values. The spectroscopic $T_{\rm eff}$ determinations are on average about 2% higher, but the difference has low significance. The evolutionary mass and the fundamental $\log g$ values agree with the seismic determinations within the uncertainties. The mean parallax-based and spectroscopic determinations are discrepant, in opposite directions, from the fundamental $\log g$ value. As discussed in Sect. 5.4.3, this may be explained by inadequate isochrones and a failure of the spectroscopic approach.

ϵ Vir: the fundamental $T_{\rm eff}$ and $\log g$ are based on direct input data and are consistent with the means of the photometric and parallax-based values. However, the mean spectroscopic determinations of $T_{\rm eff}$ and $\log g$ are significantly higher, by about 3% and 0.3 dex (90%), respectively. This indicates an inadequate application of the spectroscopic approach for this star (see discussions in Sects. 5.2.3 and 5.4.3).

ξ Hya: the fundamental $T_{\rm eff}$ and $\log g$ are based on direct input data. The fundamental $T_{\rm eff}$ value of 5040 ± 40 K agrees well with the single available literature spectroscopic determination, and the photometric determination of 5010 K by McWilliam (1990). The spectroscopic determination of $\log g$ deviates by 13% from the fundamental value, which is less than the quoted uncertainty of 20%. Also, the pre-HIPPARCOS parallax-based $\log g$ by McWilliam (1990, 2.93 ± 0.3 dex) is within 15% of the fundamental value. The seismic mass is consistent with the evolutionary one, and the seismic $\log g$ is equal to the fundamental one.

HD 107328: the fundamental $T_{\rm eff}$ and $\log g$ are based on indirect input data. However, the fundamental $T_{\rm eff}$ value agrees well (<2% difference) with the individual spectroscopic and photometric determinations, and the same applies to the fundamental in comparison with the parallax-based $\log g$ value.

The spectroscopic $\log g$ value deviates by 30%, which is, however, within the uncertainties. Thus, we consider the $T_{\rm eff}$ and $\log g$ in Table 10 to be reasonable reference values.

HD 220009: the fundamental $T_{\rm eff}$ and $\log g$ are based partly on preliminary direct and partly on indirect input data. All comparison values are inconsistent with the fundamental ones. The discrepancies may partly be explained by an erroneous photometric calibration in the case of $T_{\rm eff}$ and inadequate isochrones in the case of the parallax-based $\log g$ (see discussions in Sects. 5.2.4 and 5.4.3). In conclusion, the parameters remain uncertain for this star and are currently not recommended for using as reference values.

6.2. Conclusions

In the era of large Galactic stellar surveys, carefully calibrating and validating the data sets has become an important and integral part of the data analysis. Successive generations of stellar atmosphere models need to be subjected to benchmark tests to assess progress in predicting stellar properties. In this article we aimed at defining a sample of benchmark stars covering the range of F, G, and K spectral types at different metallicities. A set of 34 *Gaia* FGK benchmark stars was selected, based on the availability of data required to determine the effective temperature and the surface gravity independently from spectroscopy and atmospheric models as far as possible. Most of these stars have been subject to frequent spectroscopic investigations in the past, and almost all of them have previously been used as reference, calibration, or test objects. The stars are rather bright (V magnitudes ranging from 0 to 8), and about two thirds can be observed with telescopes on both hemispheres.

Fundamental values for $T_{\rm eff}$ and $\log g$ were determined from their defining relations (the Stefan-Boltzmann law and Newton's law of gravitation), using a compilation of angular diameter measurements and bolometric fluxes, and from a homogeneous mass determination based on stellar evolution models. Most of the available diameter measurements have formal uncertainties around 1% (see Table 4), which translate into uncertainties in effective temperature of about 0.5%. The measurements of bolometric flux seem to be accurate to 5% or better, which translates into uncertainties in effective temperature of 1% or less. This would enable accuracies for late-type stars used in Galactic studies of 2% (~100 K, e.g. Nissen 2005).

The derived parameters were compared to recent spectroscopic and photometric determinations and, in the case of gravity, to estimates based on seismic data. The comparison with literature data is in general satisfactory. In a few cases, significant systematic deviations are seen, most notably for cool stars and metal-poor stars. Some of them can be explained by shortcomings in the methods used in the literature, while others call for further improvement of the fundamental values: that is to say, their input data (angular diameters, bolometric fluxes, masses). The fundamental $T_{\rm eff}$ and $\log g$ values of all *Gaia* FGK benchmark stars are listed in Table 10, where those that need future adjustment are indicated by square brackets. In summary, 21 of the 29 FGK-type stars in our sample (including the Sun) have parameters with good quality, which may be used for testing, validation, or calibration purposes. There are four stars with good $T_{\rm eff}$ but uncertain $\log g$ (including Arcturus), and three stars with good $\log g$ but uncertain $T_{\rm eff}$. For one star (HD 220009), both parameters remain uncertain.

Additional interferometric observations are needed for Gmb 1830 and μ Ara (see Sects. 5.2.6 and 5.2.5, respectively).

Such observations are also desirable for the remaining stars with indirectly determined angular diameters (see Table 4), in order to verify the good quality of their fundamental $T_{\rm eff}$ and $\log g$. For most of these stars, we are planning observations with the CHARA array (Gmb 1830, ϵ For, HD 22879, μ Leo, HD 107328)[27].

For nine stars, the bolometric flux values are currently based on calibrations of broad-band photometry and bolometric corrections by Alonso et al. (1995, 1999b), see Table 4. More direct determinations should be obtained by compiling absolute flux measurements at numerous wavelength points distributed over a significant part of the spectrum for each star and integrating over the resulting SED (or over fitted model or template SEDs). It is also worth considering redetermining the measurements for the whole sample with the same method in order to obtain homogeneous bolometric fluxes.

Concerning mass determinations, a few metal-poor stars with masses less than about 0.7 $M_\odot$ lie at the limits of the model grids that we employed (μ Cas, τ Cet, HD 22879, HD 84937). Their masses should be verified using stellar evolution models tailored to their properties, applying codes such as CESAM2k (Morel 1997; Morel & Lebreton 2008) or the Dartmouth Stellar Evolution Program (Dotter et al. 2008; Feiden et al. 2011). The estimated mass uncertainties should be validated for the whole sample using statistical methods such as Monte Carlo simulations. In the long run, seismic data should be obtained and seismic modelling applied to all stars for which solar-type oscillations are expected.

The initial sample of *Gaia* FGK benchmark stars presented in this article should be extended in the future to improve the coverage of parameter space, in particular metallicity, and should be adapted to the needs of different surveys and studies. Detailed suggestions for future candidate benchmark stars are given in Appendix B.

Appendix A: HR-diagrams for individual stars

In Fig. A.1, we give examples for the results of mass determination for individual stars. Effective temperature and luminosity of each star are shown together with three evolutionary tracks interpolated in the *Yonsei-Yale* grid. The green lines correspond to a track for the derived mass (indicated in the figure) and the adopted metallicity (Table 1), while blue lines are tracks for both mass and metallicity increased by their uncertainties, and red lines are tracks for both mass and metallicity decreased by their uncertainties. The mass uncertainties were adapted such that one

---

[27] μ Ara and HD 84937 are not accessible to current interferometers, see Sect. 2.
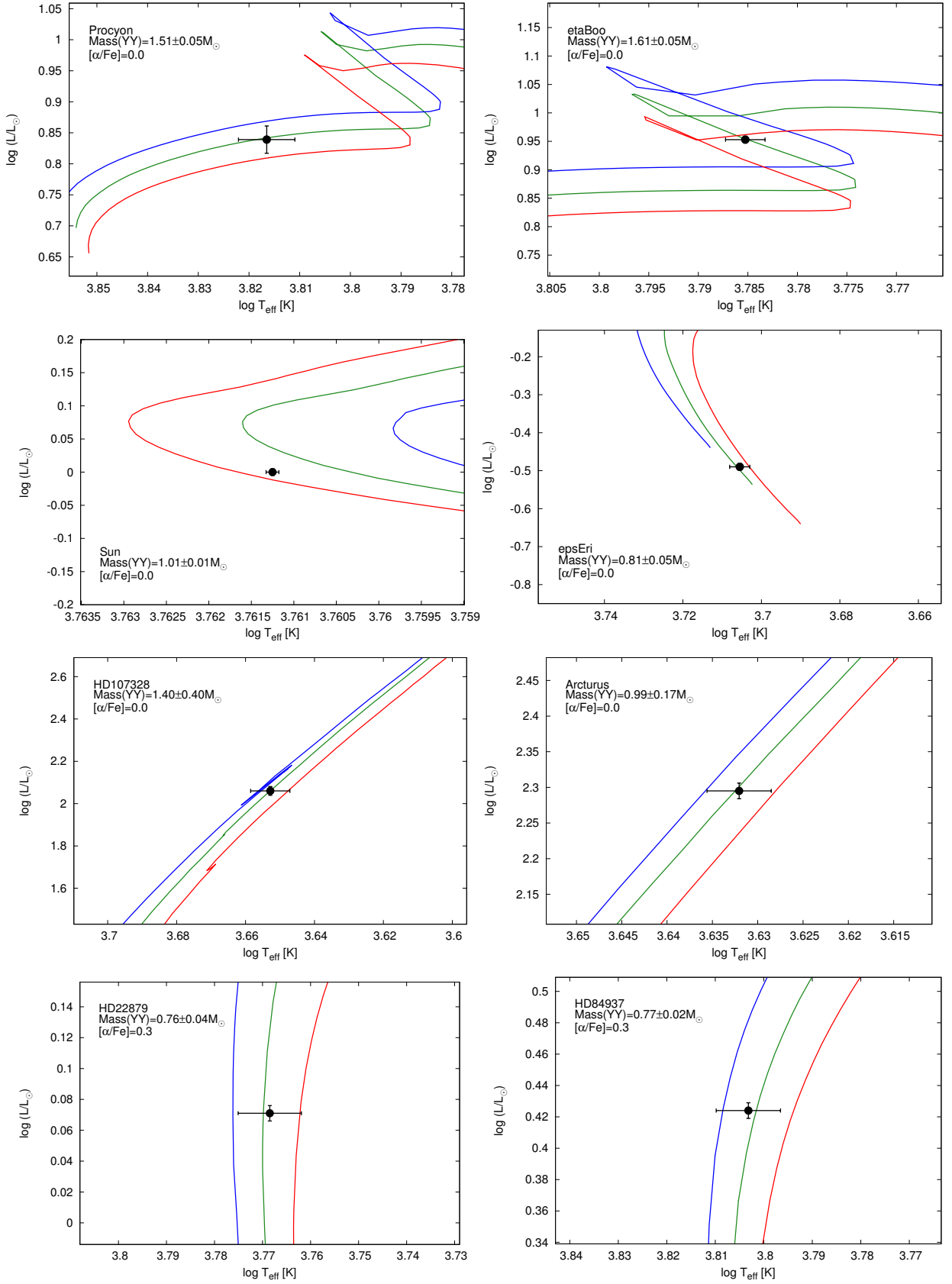
Fig. A.1. Evolutionary tracks for selected *Gaia* FGK benchmark stars, interpolated in the *Yonsei-Yale* grid for three different combinations of mass (given in each panel) and metallicity (taken from Table 1), see text for meaning of line colours. Metallicities decrease from top to bottom. Effective temperature and luminosity determined in this paper are indicated by the black filled circles. The α-element abundances [α/Fe] of the grids are indicated as well.

of the tracks with varied mass and metallicity was still consistent with the uncertainties in T_{eff} and L.

Appendix B: Future extension of the sample

In this section, we describe different categories of possible additional stars, and give a list of suggested future benchmark stars in Table B.1.

Four metal-rich dwarfs with magnitudes and angular sizes similar to μ Ara (cf. Sect. 2), but observable from the northern hemisphere, can be found in the PASTEL catalogue. These are HD 73752 (HR 3430, [Fe/H] = 0.4, Luck & Heiter 2006), a close visual binary (5.4 and 6.8 mag, period of 123 yr, semi-major axis of 1.7 arcsec, Malkov et al. 2012); HD 19994 (GJ 128) and HD 120136 (τ Boo, GJ 527), two planet-host visual binaries (semi-major axes 10 and 5 arcsec, Malkov et al. 2012; Poveda et al. 1994) with [Fe/H] = 0.3 (Takeda et al. 2005), each of which has an angular diameter of 0.79 ± 0.03 mas measured with the CHARA array (Baines et al. 2008); HD 161797 (μ Her, GJ 695 A, [Fe/H] = 0.3, da Silva et al. 2011), a star with asteroseismic data (Bonanno et al. 2008), for which Baines et al. (2014) measured an angular diameter of 1.96 ± 0.01 mas with the NPOI.

To find metal-poor candidate benchmark stars, we queried the PASTEL catalogue for stars with 4500 K < T_{eff} < 6500 K and −2 dex < [Fe/H] < −1 dex. The resulting list includes 14 stars that are brighter than $V = 9$ with at least four metallicity values published after 1990 with standard deviations less than 0.1 dex. Apart from Gmb 1830, these are HD 21581, HD 23439A, HD 23439B, HD 63791, HD 83212, HD 102200, HD 175305, HD 196892, HD 199289, HD 201891, HD 204543, HD 206739, and HD 218857.

Boyajian et al. (2012b, 2013) measured and compiled angular diameters with uncertainties of less than 5% for 125 main-sequence stars. Eighty-two of those are FGK stars not included in the *Gaia* FGK benchmark stars sample. Boyajian et al. (2012b, 2013) also determined bolometric fluxes and effective temperatures for all of these stars. Forty-seven of the 82 stars have T_{eff} determinations better than 1% and have a metallicity determination published 1990 or later (in the PASTEL catalogue). The mean literature metallicities of these stars range from −0.5 to +0.4 dex, with 80% between −0.3 and +0.1 dex. Candidate benchmark stars may be selected from 0.1 dex-wide metallicity bins as follows (ID, [Fe/H] bin centre, spectral type): HD 158633, −0.45, K0V; HD 128167, −0.35, F4V; HD 69897, −0.25, F6V; HD 4628, −0.25, K3V; HD 82328, −0.15, F7V; HD 16160, −0.15, K3V; HD 173667, −0.05, F6V; HD 10476, −0.05, K1V; HD 30652, +0.05, F6V; HD 149661, +0.05, K2V; HD 217014, +0.15, G3IV; HD 161797 (μ Her), +0.25, G5IV; HD 217107, +0.35, G8IV.

Recently, Baines et al. (2014) have published new interferometric diameters for several stars with seismic data (see below): β Aql, ϵ Oph, η Ser, κ Oph, ξ Dra, ζ Her, and HR 7349, as well as the *Gaia* FGK benchmark stars τ Cet and η Boo and the already mentioned μ Her. For several additional candidate benchmark stars, interferometric data have been obtained and are being processed (O. Creevey, priv. comm.). These are HD 148897, a metal-poor giant with [Fe/H] = −1.2 dex, and two solar-metallicity dwarfs with asteroseismic data: HD 52265 and HD 165341 (70 Oph). Furthermore, an observing programme at ESO's VLTI has been started to measure about 20 giant and subgiant stars with predicted angular diameters larger than 3 mas

(AMBER instrument, PI I. Karovicova)[28]. The stars were selected to fill gaps in the parameter space covered by the current *Gaia* FGK benchmark stars and have [Fe/H] from −0.5 to +0.5 dex. They are part of a sample of about 100 stars identified as possible targets for future proposals.

The stars θ Cyg and 16 Cyg A and B are the brightest dwarf stars with asteroseismic observations from the *Kepler* mission. Guzik et al. (2011) estimated a large frequency separation $\Delta\nu = 84$ μHz for θ Cyg. Metcalfe et al. (2012) derived $\Delta\nu = 103.4$ μHz for 16 Cyg A and $\Delta\nu = 117.0$ μHz for 16 Cyg B and determined the stellar parameters for these stars by modelling over 40 individual oscillation frequencies detected for each star. White et al. (2013) measured angular diameters of 0.753, 0.539, and 0.490 mas for θ Cyg, 16 Cyg A, and 16 Cyg B, respectively, with the CHARA array, each with a precision of 1%. In combination with the asteroseismic and other data, they determined the effective temperatures with precisions better than 1%. Bruntt et al. (2010) list 12 stars with seismic data in addition to those already included in the *Gaia* FGK benchmark stars sample (cf. Sect. 2). These are 70 Oph A, 171 Pup, α For, β Aql, γ Pav, γ Ser, δ Pav, η Ser, ι Hor, ν Ind, τ PsA, and HR 5803. We note that 70 Oph A was used as a standard star by Quirion et al. (2010, cf. Sect. 2). Additional stars with seismic data are listed in Morel & Miglio (2012): β Oph, β Vol, ϵ Oph, κ Oph, ξ Dra, μ Her, ζ Her, HD 49385, HD 52265, HD 170987, HD 175726, HD 181420, and HD 181906. Furthermore, Huber et al. (2012) measured the angular diameters of ten bright oscillating stars observed by *Kepler* or CoRoT with the CHARA array. The sample includes six dwarfs (HD 173701, HD 175726, HD 177153, HD 181420, HD 182736, HD 187637) and four giants (HD 175955, HD 177151, HD 181827, HD 189349).

Visual binary systems with well-defined orbits can be found in Table 2 of Malkov et al. (2012). Constraining the systems in that table to those with uncertainties in periods and semi-major axes of at most 5%, primary magnitudes less than 5, and to those where the spectral types of both components are given results in six systems containing at least one FGK dwarf component (including α Cen) and two systems with at least one FGK giant component, with periods between three months and 170 yr, and total dynamical system masses between 1.6 and 4.7 $M_{\odot}$. The systems (in addition to α Cen) are γ Vir (F0V+F0V), ψ Vel (F0IV+F3IV), α Equ (G0III+A5V), 10 UMa (F3V+K0V), 70 Oph (K0V+K4V), 113 Her (G4III+A6V), and ξ Boo (G8V+K5V).

Eclipsing binary systems with accurate mass and radius determinations (uncertainties lower than 3%) were compiled by Torres et al. (2010). Their Table 2 contains 85 FGK stars in 46 systems. Another catalogue of well-studied detached eclipsing binaries (Southworth 2014) is provided on-line[29]. The version of 2014-07-04 contained 100 systems with one or two FGK components, including 39 of those listed in Torres et al. (2010). This sample is dominated by F dwarfs. The brightest system with F-type components is VV Crv (F5IV+F5V, Fekel et al. 2013), the brightest systems with a G-type giant or dwarf are TZ For (G8III+F7IV, Andersen et al. 1991) and KX Cnc (G0V+G0V, Sowell et al. 2012), and the brightest system with a K-type component is AI Phe (K0IV+F7V, Andersen et al. 1988).

Several recent publications on automatic spectroscopic parameter determination have defined their own sets of FGK

---

[28] http://archive.eso.org/wdb/wdb/eso/sched_rep_arc/query?progid=094.D-0572(A)

[29] http://www.astro.keele.ac.uk/~jkt/debcat/

Table B.1. Basic information for stars suggested for future extension of the *Gaia* FGK benchmark stars sample.

HD	Name	RA (J2000)	Dec (J2000)	Spectral type	*V* mag	[Fe/H]	σ([Fe/H])
2665	HD 2665	00 30 45.446	+57 03 53.63	G5IIIw	7.7	−2.00	0.09
2796	HD 2796	00 31 16.915	−16 47 40.80	Fw	8.5	−2.32	0.13
4306	HD 4306	00 45 27.163	−09 32 39.79	KIIvw	9.0	−2.70	0.19
4628	HD 4628	00 48 22.977	+05 16 50.21	K2.5V	5.7	−0.26	0.05
6980	AI Phe	01 09 34.195	−46 15 56.09	K0IV+F7V	8.6	−0.14	0.10
6755	HD 6755	01 09 43.065	+61 32 50.19	F8V	7.7	−1.55	0.05
6860	β And	01 09 43.924	+35 37 14.01	M0III	2.0	−0.04	
6833	HD 6833	01 09 52.265	+54 44 20.28	G9III	6.7	−0.88	0.11
9826	υ And	01 36 47.842	+41 24 19.64	F9V	4.1	0.08	0.05
10476	HD 10476	01 42 29.762	+20 16 06.60	K1V	5.2	−0.04	0.04
	BD +44 493	02 26 49.738	+44 57 46.52	G5IV	9.1	−3.68	0.11
16160	HD 16160	02 36 04.895	+06 53 12.75	K3V	5.8	−0.12	0.06
17051	ι Hor	02 42 33.466	−50 48 01.06	F8V	5.4	0.13	0.10
20010	α For	03 12 04.527	−28 59 15.43	F6V+G7V	3.9	−0.28	0.06
19994	HD 19994	03 12 46.437	−01 11 45.96	F8V	5.1	0.19	0.07
20301	TZ For	03 14 40.093	−35 33 27.60	G8III+F7IV	6.9	0.10	0.15
21581	HD 21581	03 28 54.486	−00 25 03.11	G0	8.7	−1.69	0.09
23439	HD 23439A	03 47 02.113	+41 25 38.06	K1V	8.1	−1.06	0.09
23439	HD 23439B	03 47 02.636	+41 25 42.56	K2V	8.8	−1.03	0.13
25329	HD 25329	04 03 14.999	+35 16 23.79	K1V	8.5	−1.79	0.06
26297	HD 26297	04 09 03.418	−15 53 27.06	G5/G6IVw	7.5	−1.79	0.09
27697	HD 27697	04 22 56.093	+17 32 33.05	K0III	3.8	0.05	0.09
28305	HD 28305	04 28 36.999	+19 10 49.54	K0III	3.5	0.11	0.09
30652	HD 30652	04 49 50.411	+06 57 40.59	F6V	3.2	0.00	0.03
49385	HD 49385	06 48 11.503	+00 18 17.90	G0V	7.4	0.09	0.05
52265	HD 52265	07 00 18.036	−05 22 01.78	G0V	6.3	0.21	0.03
62345	HD 62345	07 44 26.854	+24 23 52.79	G8III	3.6	−0.02	0.17
63077	171 Pup	07 45 35.022	−34 10 20.51	F9V	5.4	−0.81	0.13
63791	HD 63791	07 54 28.724	+62 08 10.76	G0	7.9	−1.70	0.06
69897	HD 69897	08 20 03.862	+27 13 03.74	F6V	5.1	−0.27	0.06
71878	β Vol	08 25 44.195	−66 08 12.80	K2III	3.8	−0.01	
71369	HD 71369	08 30 15.871	+60 43 05.41	G5III	3.4	−0.10	0.14
73752	HD 73752	08 39 07.901	−22 39 42.81	G5IV	5.0	0.39	
74057	KX Cnc	08 42 46.211	+31 51 45.37	G0V+G0V	7.2	0.07	0.10
76943	10 UMa	09 00 38.381	+41 46 58.61	F3V+K0V	4.0	0.25	
82434	ψ Vel	09 30 42.000	−40 28 00.26	F0IV+F3IV	3.6	0.00	0.20
82328	HD 82328	09 32 51.434	+51 40 38.28	F7V	3.2	−0.18	0.06
83212	HD 83212	09 36 19.952	−20 53 14.76	G6/K0IIIw	8.3	−1.44	0.06
102200	HD 102200	11 45 34.235	−46 03 46.39	F2V	8.8	−1.22	0.06
110317	VV Crv	12 41 15.951	−13 00 50.03	F5IV+F5V	5.8	0.00	
110379	γ Vir	12 41 39.643	−01 26 57.74	F0V+F0V	2.7	−0.05	0.07
117176	70 Vir	13 28 25.809	+13 46 43.64	G5IV-V	5.0	−0.06	0.03
120136	HD 120136	13 47 15.743	+17 27 24.86	F6IV+M2	4.5	0.29	0.08
126681	HD 126681	14 27 24.911	−18 24 40.44	G3V	9.3	−1.21	0.12
128167	HD 128167	14 34 40.817	+29 44 42.46	F4V	4.5	−0.37	0.10
131156	ξ Boo	14 51 23.380	+19 06 01.70	G8V+K5V	4.6	−0.14	0.06
139211	HR 5803	15 39 56.543	−59 54 30.02	F6IV	6.0	0.00	0.06
140573	HD 140573	15 44 16.074	+06 25 32.26	K2III	2.6	0.05	0.11
142860	γ Ser	15 56 27.183	+15 39 41.82	F6IV	3.8	−0.20	0.04
146051	δ Oph	16 14 20.739	−03 41 39.56	M0.5III	2.8	−0.01	0.09
146791	ε Oph	16 18 19.290	−04 41 33.03	G8III	3.2	−0.10	0.10
148897	HD 148897	16 30 33.549	+20 28 45.07	G8III	5.2	−1.16	
149661	HD 149661	16 36 21.450	−02 19 28.52	K2V	5.8	0.04	0.04
150680	ζ Her	16 41 17.161	+31 36 09.79	G0IV	2.8	0.02	0.06
153210	κ Oph	16 57 40.098	+09 22 30.11	K2III	3.2	0.02	0.07
158633	HD 158633	17 25 00.099	+67 18 24.15	K0V	6.4	−0.49	0.07
161096	β Oph	17 43 28.353	+04 34 02.30	K2III	2.8	0.05	0.07
161797	μ Her	17 46 27.527	+27 43 14.44	G5IV	3.4	0.22	0.08
163588	ξ Dra	17 53 31.730	+56 52 21.51	K2III	3.8	−0.09	

Notes. Coordinates, *V* magnitudes, and spectral types are extracted from the SIMBAD database. Spectral types for binary stars were taken from the respective catalogues. [Fe/H] and σ are mean and standard deviations of metallicity determinations contained in the PASTEL catalogue (publications from 1990 and later), except for the following stars, for which individual measurements and uncertainties were taken from the sources in parentheses: HD 6980 (Andersen et al. 1988); HD 20301 (Andersen et al. 1991); HD 49385 (Deheuvels et al. 2010); HD 74057 (Sowell et al. 2012); HD 82434 (Fuhrmann & Chini 2012); HD 146051 (Smith et al. 2013); HD 170987 (Mathur et al. 2010); HD 181907 (Morel et al. 2014); HD 189349 (Huber et al. 2012); HD 217906 (Smith & Lambert 1985); BD +44 493 (Ito et al. 2009).

Table B.1. continued.

HD	Name	RA (J2000)	Dec (J2000)	Spectral type	V mag	[Fe/H]	σ([Fe/H])
165195	HD 165195	18 04 40.071	+03 46 44.73	K3p	7.3	–2.12	0.13
165341	70 Oph	18 05 27.285	+02 30 00.36	K0V+K4V	4.0	–0.02	0.12
168723	η Ser	18 21 18.601	–02 53 55.78	K0III-IV	3.2	–0.18	0.12
170987	HD 170987	18 32 01.731	+06 46 48.36	F5	7.5	–0.15	0.06
173701	HD 173701	18 44 35.119	+43 49 59.80	K0	7.5	0.28	0.09
173667	HD 173667	18 45 39.726	+20 32 46.72	F6V	4.2	–0.05	0.05
175305	HD 175305	18 47 06.440	+74 43 31.45	G5III	7.2	–1.41	0.08
175492	113 Her	18 54 44.872	+22 38 42.10	G4III+A6V	4.6	–0.16	
175955	HD 175955	18 55 33.327	+47 26 26.79	K0	7.0	0.12	0.08
175726	HD 175726	18 56 37.173	+04 15 54.47	G0V	6.7	–0.04	0.06
177151	HD 177151	19 01 06.548	+48 02 08.01	K0	7.0	–0.10	0.01
177153	HD 177153	19 01 39.678	+41 29 24.33	G0	7.2	–0.07	0.03
181827	HD 181827	19 19 55.068	+45 01 55.53	K0	7.2	0.14	
181420	HD 181420	19 20 27.072	–01 18 35.13	F6V	6.5	0.00	
181906	HD 181906	19 22 21.340	+00 22 58.74	F8	7.7	–0.11	
181907	HR 7349	19 22 21.545	–00 15 08.43	G8III	5.8	–0.15	0.12
182736	HD 182736	19 24 03.379	+44 56 00.74	G0	7.0	–0.10	0.06
185144	σ Dra	19 32 21.590	+69 39 40.24	G9V	4.7	–0.23	0.05
185395	θ Cyg	19 36 26.534	+50 13 15.96	F3+V	4.5	–0.03	0.05
232078	HD 232078	19 38 12.070	+16 48 25.64	K3IIp	8.7	–1.56	0.03
186408	16 Cyg A	19 41 48.953	+50 31 30.22	G2V	6.0	0.08	0.03
186427	16 Cyg B	19 41 51.972	+50 31 03.08	G3V	6.2	0.06	0.02
187111	HD 187111	19 48 39.574	–12 07 19.74	G8III/IV	7.8	–1.71	0.09
187637	HD 187637	19 49 18.139	+41 34 56.86	F5	7.5	–0.14	0.05
188512	β Aql	19 55 18.793	+06 24 24.34	G9.5IV	3.7	–0.19	0.07
189349	HD 189349	19 58 02.382	+40 55 36.64	G5	7.3	–0.56	0.16
190248	δ Pav	20 08 43.610	–66 10 55.44	G8IV	3.6	0.29	0.12
196892	HD 196892	20 40 49.380	–18 47 33.28	F6V	8.2	–1.03	0.10
199289	HD 199289	20 58 08.522	–48 12 13.46	F5V	8.3	–1.01	0.08
201891	HD 201891	21 11 59.032	+17 43 39.89	G5VFe-2.5	7.4	–1.05	0.08
202448	α Equ	21 15 49.432	+05 14 52.24	G0III+A5V	3.9	0.09	
203608	γ Pav	21 26 26.605	–65 21 58.31	F9V	4.2	–0.69	0.07
204543	HD 204543	21 29 28.213	–03 30 55.37	G0	8.3	–1.80	0.09
206739	HD 206739	21 44 23.945	–11 46 22.85	G5V	8.6	–1.57	0.02
210302	τ Psa	22 10 08.780	–32 32 54.27	F6V	4.9	0.05	0.04
211998	ν Ind	22 24 36.884	–72 15 19.49	G9VFe-3.1CH-1.5	5.3	–1.50	0.13
215665	HD 215665	22 46 31.878	+23 33 56.36	G8II-III	3.9	–0.12	0.08
216143	HD 216143	22 50 31.089	–06 54 49.56	G5	7.8	–2.20	0.06
217014	HD 217014	22 57 27.980	+20 46 07.79	G2.5IV	5.5	0.17	0.08
217107	HD 217107	22 58 15.541	–02 23 43.38	G8IV	6.2	0.36	0.04
217906	HD 217906	23 03 46.457	+28 04 58.03	M2.5II-III	2.4	–0.11	0.13
218857	HD 218857	23 11 24.596	–16 15 04.02	G6w	8.9	–1.88	0.04
221170	HD 221170	23 29 28.809	+30 25 57.85	G2IV	7.7	–2.13	0.05

standard stars for testing their routines. All of these may be considered for inclusion in an extended sample of *Gaia* FGK benchmark stars. The solar-metallicity G-type subgiant 70 Vir with an interferometric angular diameter of 0.93 mas (van Belle & von Braun 2009) was used for spectroscopic tests by Fuhrmann et al. (2011). In their Table 2 Cayrel et al. (2011, cf. Sect. 2) list four dwarfs between 5200 and 6100 K with interferometric angular diameters, which are not included in the *Gaia* FGK benchmark stars sample: υ And, σ Dra, ζ Her, and μ Her. (The last two have already been mentioned above.) Ruchti et al. (2013, cf. their Table 2) used four nearby giants between 4600 and 4900 K with interferometric $T_{\rm eff}$ to test effective

temperatures from Balmer-line fitting, in addition to several *Gaia* FGK benchmark stars and two stars from Cayrel et al. (2011): HD 27697, HD 28305, HD 140573, and HD 215665. The two solar-metallicity giants β And and δ Oph ($T_{\rm eff} \approx$ 3800 K) have been used as standard stars in the APOGEE survey (Smith et al. 2013; Mészáros et al. 2013) to test the pipeline for parameter determination and the line list for abundance measurements. Two metal-poor stars were among the reference stars used by Sbordone et al. (2014) for pipeline validation (cf. Sect. 2): the dwarf HD 126681, and the giant HD 26297. Morel et al. (2014) used three solar-metallicity giants with interferometric angular diameters to validate their abundance analysis of

red giants in the CoRoT asteroseismology fields, in addition to Arcturus and ξ Hya: β Aql, ϵ Oph, and η Ser. All of these have already been mentioned above. See their Table A.1 for a compilation of literature atmospheric parameters and abundances.

Finally, it could be worth considering the FGKM dwarfs and giants with Pδ and Hα observations contained in the catalogue of hydrogen line profiles by Huang et al. (2012) These include HD 2665, HD 2796, HD 4306, HD 6755, HD 6833, HD 6860 (β And), HD 25329, HD 62345, HD 71369, HD 165195, HD 187111, HD 216143, HD 217906, HD 221170, HD 232078, and BD +44 493.

Basic information for the 102 stars explicitly mentioned in this section is given in Table B.1. Furthermore, we extracted parallax measurements from the SIMBAD database for all stars except one. About half of these have uncertainties below 1.5%, and the uncertainties are below 10% for 80% of the stars. We also list the mean and standard deviations of metallicity determinations extracted from the PASTEL catalogue, except for a few stars for which metallicity references are given in the table notes. Twenty-eight of these stars have [Fe/H] < −1 dex.

References

Affer, L., Micela, G., Morel, T., Sanz-Forcada, J., & Favata, F. 2005, A&A, 433, 647

Allende Prieto, C., Barklem, P. S., Lambert, D. L., & Cunha, K. 2004, A&A, 420, 183

Allende Prieto, C., Majewski, S. R., Schiavon, R., et al. 2008, Astron. Nachr., 329, 1018

Alonso, A., Arribas, S., & Martinez-Roger, C. 1994, A&AS, 107, 365

Alonso, A., Arribas, S., & Martinez-Roger, C. 1995, A&A, 297, 197

Alonso, A., Arribas, S., & Martinez-Roger, C. 1996a, A&AS, 117, 227

Alonso, A., Arribas, S., & Martinez-Roger, C. 1996b, A&A, 313, 873

Alonso, A., Arribas, S., & Martínez-Roger, C. 1999a, A&AS, 139, 335

Alonso, A., Arribas, S., & Martínez-Roger, C. 1999b, A&AS, 140, 261

Andersen, J. 1999, Trans. Internat. Astron. Union, Ser. B, 23, 141

Andersen, J., Clausen, J. V., Nordstrom, B., Gustafsson, B., & Vandenberg, D. A. 1988, A&A, 196, 128

Andersen, J., Clausen, J. V., Nordstrom, B., Tomkin, J., & Mayor, M. 1991, A&A, 246, 99

Arentoft, T., Kjeldsen, H., Bedding, T. R., et al. 2008, ApJ, 687, 1180

Armstrong, J. T., Hutter, D. J., Baines, E. K., et al. 2013, J. Astron. Instrum., 2, 40002

Aufdenberg, J. P., Ludwig, H.-G., & Kervella, P. 2005, ApJ, 633, 424

Ayres, T. R. 2013, Astron. Nachr., 334, 105

Ayres, T. R., Plymate, C., & Keller, C. U. 2006, ApJS, 165, 618

Bailer-Jones, C. A. L., Andrae, R., Arcay, B., et al. 2013, A&A, 559, A74

Baines, E. K., McAlister, H. A., ten Brummelaar, T. A., et al. 2008, ApJ, 680, 728

Baines, E. K., Armstrong, J. T., Schmitt, H. R., et al. 2014, ApJ, 781, 90

Barban, C., Beuret, M., Baudin, F., et al. 2013, J. Phys. Conf. Ser., 440, 012031

Bazot, M., Ireland, M. J., Huber, D., et al. 2011, A&A, 526, L4

Bean, J. L., Sneden, C., Hauschildt, P. H., Johns-Krull, C. M., & Benedict, G. F. 2006, ApJ, 652, 1604

Beasley, A. J., & Cram, L. E. 1993, ApJ, 417, 157

Bedding, T. R., Kjeldsen, H., Arentoft, T., et al. 2007, ApJ, 663, 1315

Bedding, T. R., Kjeldsen, H., Campante, T. L., et al. 2010, ApJ, 713, 935

Belkacem, K., Goupil, M. J., Dupret, M. A., et al. 2011, A&A, 530, A142

Bensby, T., Feltzing, S., & Lundström, I. 2003, A&A, 410, 527

Bergemann, M., & Gehren, T. 2008, A&A, 492, 823

Bergemann, M., Pickering, J. C., & Gehren, T. 2010, MNRAS, 401, 1334

Bergemann, M., Hansen, C. J., Bautista, M., & Ruchti, G. 2012a, A&A, 546, A90

Bergemann, M., Lind, K., Collet, R., Magic, Z., & Asplund, M. 2012b, MNRAS, 427, 27

Bertelli, G., Bressan, A., Chiosi, C., Fagotto, F., & Nasi, E. 1994, A&AS, 106, 275

Bertelli, G., Girardi, L., Marigo, P., & Nasi, E. 2008, A&A, 484, 815

Bertelli, G., Nasi, E., Girardi, L., & Marigo, P. 2009, A&A, 508, 355

Bigot, L., Kervella, P., Thévenin, F., & Ségransan, D. 2006, A&A, 446, 635

Bigot, L., Mourard, D., Berio, P., et al. 2011, A&A, 534, L3

Blackwell, D. E., & Lynas-Gray, A. E. 1998, A&AS, 129, 505

Blanco-Cuaresma, S., Soubiran, C., Jofré, P., & Heiter, U. 2014, A&A, 566, A98 (Paper II)

Boeche, C., Siebert, A., Williams, M., et al. 2011, AJ, 142, 193

Bonanno, A., Benatti, S., Claudi, R., et al. 2008, ApJ, 676, 1248

Bond, J. C., Tinney, C. G., Butler, R. P., et al. 2006, MNRAS, 370, 163

Bouchy, F., & Carrier, F. 2001, A&A, 374, L5

Bouchy, F., & Carrier, F. 2003, Ap&SS, 284, 21

Bouchy, F., Bazot, M., Santos, N. C., Vauclair, S., & Sosnowska, D. 2005, A&A, 440, 609

Boyajian, T. S., McAlister, H. A., Baines, E. K., et al. 2008, ApJ, 683, 424

Boyajian, T. S., McAlister, H. A., van Belle, G., et al. 2012a, ApJ, 746, 101

Boyajian, T. S., von Braun, K., van Belle, G., et al. 2012b, ApJ, 757, 112

Boyajian, T. S., von Braun, K., van Belle, G., et al. 2013, ApJ, 771, 40

Britavskiy, N. E., Andrievsky, S. M., Tsymbal, V. V., et al. 2012, A&A, 542, A104

Bruntt, H. 2009, A&A, 506, 235

Bruntt, H., Bikmaev, I. F., Catala, C., et al. 2004, A&A, 425, 683

Bruntt, H., Bedding, T. R., Quirion, P.-O., et al. 2010, MNRAS, 405, 1907

Bruntt, H., Frandsen, S., & Thygesen, A. O. 2011, A&A, 528, A121

Carpenter, J. M. 2001, AJ, 121, 2851

Carrier, F., & Bourban, G. 2003, A&A, 406, L23

Carrier, F., Eggenberger, P., & Bouchy, F. 2005a, A&A, 434, 1085

Carrier, F., Eggenberger, P., D'Alessandro, A., & Weber, L. 2005b, New Astron., 10, 315

Casagrande, L., Ramírez, I., Meléndez, J., Bessell, M., & Asplund, M. 2010, A&A, 512, A54

Casagrande, L., Schönrich, R., Asplund, M., et al. 2011, A&A, 530, A138

Casagrande, L., Ramírez, I., Meléndez, J., & Asplund, M. 2012, ApJ, 761, 16

Casagrande, L., Portinari, L., Glass, I. S., et al. 2014, MNRAS, 439, 2060

Cayrel, R., van't Veer-Menneret, C., Allard, N. F., & Stehlé, C. 2011, A&A, 531, A83

Cayrel de Strobel, G., & Pasinetti, L. E. 1975, A&A, 43, 127

Chen, Y.-P., Trager, S. C., Peletier, R. F., et al. 2014, A&A, 565, A117

Chiavassa, A., Bigot, L., Kervella, P., et al. 2012, A&A, 540, A5

Claret, A. 2000, A&A, 363, 1081

Claret, A., Diaz-Cordoves, J., & Gimenez, A. 1995, A&AS, 114, 247

Cohen, M., Walker, R. G., Carter, B., et al. 1999, AJ, 117, 1864

Colavita, M. M., Wallace, J. K., Hines, B. E., et al. 1999, ApJ, 510, 505

Creevey, O. L., Thévenin, F., Boyajian, T. S., et al. 2012, A&A, 545, A17

Creevey, O. L., Thévenin, F., Basu, S., et al. 2013, MNRAS, 431, 2419

Creevey, O. L., Thévenin, F., Berio, P., et al. 2015, A&A, 575, A26

Cutri, R. M., Skrutskie, M. F., van Dyk, S., et al. 2003, VizieR Online Data Catalog: II/246

da Silva, L., Girardi, L., Pasquini, L., et al. 2006, A&A, 458, 609

da Silva, R., Milone, A. C., & Reddy, B. E. 2011, A&A, 526, A71

da Silva, R., Porto de Mello, G. F., Milone, A. C., et al. 2012, A&A, 542, A84

Davis, J., Tango, W. J., Booth, A. J., et al. 1999, MNRAS, 303, 773

Davis, J., Tango, W. J., & Booth, A. J. 2000, MNRAS, 318, 387

De Silva, G. M., Freeman, K. C., Bland-Hawthorn, J., et al. 2015, MNRAS, 449, 2604

Decin, L., Vandenbussche, B., Waelkens, C., et al. 2003, A&A, 400, 679

Deheuvels, S., Bruntt, H., Michel, E., et al. 2010, A&A, 515, A87

Demarque, P., Woo, J.-H., Kim, Y.-C., & Yi, S. K. 2004, ApJS, 155, 667

di Benedetto, G. P. 1998, A&A, 339, 858

di Benedetto, G. P., & Foy, R. 1986, A&A, 166, 204

di Benedetto, G. P., & Rabbia, Y. 1987, A&A, 188, 114

di Folco, E., Thévenin, F., Kervella, P., et al. 2004, A&A, 426, 601

di Folco, E., Absil, O., Augereau, J.-C., et al. 2007, A&A, 475, 243

Dotter, A., Chaboyer, B., Jevremović, D., et al. 2008, ApJS, 178, 89

Doyle, A. P., Smalley, B., Maxted, P. F. L., et al. 2013, MNRAS, 428, 3164

Drummond, J. D., Christou, J. C., & Fugate, R. Q. 1995, ApJ, 450, 380

Dyck, H. M., Benson, J. A., van Belle, G. T., & Ridgway, S. T. 1996, AJ, 111, 1705

Dyck, H. M., van Belle, G. T., & Thompson, R. R. 1998, AJ, 116, 981

Edvardsson, B. 1983, Uppsala Astronomical Observatory Reports, 27

Engelke, C. W., Price, S. D., & Kraemer, K. E. 2006, AJ, 132, 1445

Feiden, G. A., Chaboyer, B., & Dotter, A. 2011, ApJ, 740, L25

Fekel, F. C., Henry, G. W., & Sowell, J. R. 2013, AJ, 146, 146

Feltzing, S., & Gonzalez, G. 2001, A&A, 367, 253

Frandsen, S., Carrier, F., Aerts, C., et al. 2002, A&A, 394, L5

Fröhlich, C. 2000, Space Sci. Rev., 94, 15

Fuhrmann, K. 2004, Astron. Nachr., 325, 3

Fuhrmann, K. 2008, MNRAS, 384, 173

Fuhrmann, K., & Chini, R. 2012, ApJS, 203, 30

Fuhrmann, K., Chini, R., Hoffmeister, V. H., et al. 2011, MNRAS, 411, 2311

Fulbright, J. P. 2000, AJ, 120, 1841

Galeev, A. I., Bikmaev, I. F., Musaev, F. A., & Galazutdinov, G. A. 2004, Astron. Rep., 48, 492

Gatewood, G., & Han, I. 2006, AJ, 131, 1015
Gebran, M., Vick, M., Monier, R., & Fossati, L. 2010, A&A, 523, A71
Gehren, T., Shi, J. R., Zhang, H. W., Zhao, G., & Korn, A. J. 2006, A&A, 451, 1065
Gezari, D., Pitts, P., & Schmitz, M. 2000, Catalog of Infrared Observations (Version 5.1), available: http://ircatalog.gsfc.nasa.gov/cio_homepage.html [27-Mar.-2015], NASA/Goddard Space Flight Center, Greenbelt, MD
Gillon, M., & Magain, P. 2006, A&A, 448, 341
Gilmore, G., Randich, S., Asplund, M., et al. 2012, The Messenger, 147, 25
Girard, T. M., Wu, H., Lee, J. T., et al. 2000, AJ, 119, 2428
Gonzalez, G., Carlson, M. K., & Tobin, R. W. 2010, MNRAS, 403, 1368
González Hernández, J. I., & Bonifacio, P. 2009, A&A, 497, 497
Gorshanov, D. L., Shakht, N. A., & Kisselev, A. A. 2006, Astrophys., 49, 386
Gratton, R. G., Sneden, C., Carretta, E., & Bragaglia, A. 2000, A&A, 354, 169
Gratton, R. G., Carretta, E., Claudi, R., Lucatello, S., & Barbieri, M. 2003, A&A, 404, 187
Gray, D. F. 2010, ApJ, 710, 1003
Gray, R. O., Corbally, C. J., Garrison, R. F., McFadden, M. T., & Robinson, P. E. 2003, AJ, 126, 2048
Griffin, R. E. M., & Lynas-Gray, A. E. 1999, AJ, 117, 2998
Gruberbauer, M., Kallinger, T., Weiss, W. W., & Guenther, D. B. 2009, A&A, 506, 1043
Gustafsson, B., Edvardsson, B., Eriksson, K., et al. 2008, A&A, 486, 951
Guzik, J. A., Houdek, G., Chaplin, W. J., et al. 2011, ArXiv e-prints [arXiv:1110.2120]
Haberreiter, M., Schmutz, W., & Kosovichev, A. G. 2008, ApJ, 675, L53
Harmanec, P., & Prša, A. 2011, PASP, 123, 976
Hatzes, A. P., Zechmeister, M., Matthews, J., et al. 2012, A&A, 543, A98
Hauschildt, P. H., & Baron, E. 1999, J. Comp. Appl. Math., 109, 41
Heiter, U., & Luck, R. E. 2003, AJ, 126, 2015
Hekker, S., & Meléndez, J. 2007, A&A, 475, 1003
Hill, V., Lecureur, A., Gómez, A., et al. 2011, A&A, 534, A80
Huang, W., Wallerstein, G., & Stone, M. 2012, A&A, 547, A62
Huber, D., Ireland, M. J., Bedding, T. R., et al. 2012, ApJ, 760, 32
Hünsch, M., Schmitt, J. H. M. M., & Voges, W. 1998, A&AS, 132, 155
Ishigaki, M. N., Chiba, M., & Aoki, W. 2012, ApJ, 753, 64
Ito, H., Aoki, W., Honda, S., & Beers, T. C. 2009, ApJ, 698, L37
Jofré, P., & Weiss, A. 2011, A&A, 533, A59
Jofré, P., Panter, B., Hansen, C. J., & Weiss, A. 2010, A&A, 517, A57
Jofré, P., Heiter, U., Blanco-Cuaresma, S., & Soubiran, C. 2014a, in ASICS, 11, 159
Jofré, P., Heiter, U., Soubiran, C., et al. 2014b, A&A, 564, A133 (Paper III)
Jonsell, K., Edvardsson, B., Gustafsson, B., et al. 2005, A&A, 440, 321
Kallinger, T., Weiss, W. W., Barban, C., et al. 2010, A&A, 509, A77
Kervella, P., Gitton, P. B., Segransan, D., et al. 2003a, in Interferometry for Optical Astronomy II, ed. W. A. Traub, SPIE Conf. Ser., 4838, 858
Kervella, P., Thévenin, F., Ségransan, D., et al. 2003b, A&A, 404, 1087
Kervella, P., Thévenin, F., di Folco, E., & Ségransan, D. 2004a, A&A, 426, 297
Kervella, P., Thévenin, F., Morel, P., et al. 2004b, A&A, 413, 251
Kervella, P., Mérand, A., Pichon, B., et al. 2008, A&A, 488, 667
Kjeldsen, H., & Bedding, T. R. 1995, A&A, 293, 87
Kjeldsen, H., Bedding, T. R., Butler, R. P., et al. 2005, ApJ, 635, 1281
Kjeldsen, H., Bedding, T. R., Arentoft, T., et al. 2008, ApJ, 682, 1370
Koch, A., & McWilliam, A. 2008, AJ, 135, 1551
Konopliv, A. S., Asmar, S. W., Folkner, W. M., et al. 2011, Icarus, 211, 401
Kopp, G., & Lean, J. L. 2011, Geophys. Res. Lett., 38, 1706
Kopp, G., Lawrence, G., & Rottman, G. 2005, Sol. Phys., 230, 129
Korn, A. J., Shi, J., & Gehren, T. 2003, A&A, 407, 691
Korn, A. J., Grundahl, F., Richard, O., et al. 2007, ApJ, 671, 402
Kotoneva, E., Shi, J. R., Zhao, G., & Liu, Y. J. 2006, A&A, 454, 833
Kovtyukh, V. V., Soubiran, C., Belik, S. I., & Gorlova, N. I. 2003, A&A, 411, 559
Kovtyukh, V. V., Soubiran, C., & Belik, S. I. 2004, A&A, 427, 933
Lacour, S., Meimon, S., Thiébaut, E., et al. 2008, A&A, 485, 561
Lallement, R., Vergely, J.-L., Valette, B., et al. 2014, A&A, 561, A91
Laws, C., Gonzalez, G., Walker, K. M., et al. 2003, AJ, 125, 2664
Lebzelter, T., Heiter, U., Abia, C., et al. 2012, A&A, 547, A108
Lecureur, A., Hill, V., Zoccali, M., et al. 2007, A&A, 465, 799
Lee, Y. S., Beers, T. C., Allende Prieto, C., et al. 2011, AJ, 141, 90
Lind, K., Bergemann, M., & Asplund, M. 2012, MNRAS, 427, 50
Lindegren, L., Babusiaux, C., Bailer-Jones, C., et al. 2008, in IAU Symp. 248, eds. W. J. Jin, I. Platais, & M. A. C. Perryman, 217
Lobel, A. 2011, Canadian J. Phys., 89, 395
Luck, R. E. 1979, ApJ, 232, 797
Luck, R. E., & Heiter, U. 2005, AJ, 129, 1063
Luck, R. E., & Heiter, U. 2006, AJ, 131, 3069
Luck, R. E., & Heiter, U. 2007, AJ, 133, 2464

Maldonado, J., Eiroa, C., Villaver, E., Montesinos, B., & Mora, A. 2012, A&A, 541, A40
Malkov, O. Y., Tamazian, V. S., Docobo, J. A., & Chulkov, D. A. 2012, A&A, 546, A69
Mann, A. W., Gaidos, E., & Ansdell, M. 2013, ApJ, 779, 188
Martín-Fleitas, J., Sahlmann, J., Mora, A., et al. 2014, SPIE Conf. Ser. 9143, 91430Y
Martins, L. P., Coelho, P., Caproni, A., & Vitoriano, R. 2014, MNRAS, 442, 1294
Masana, E., Jordi, C., & Ribas, I. 2006, A&A, 450, 735
Mashonkina, L. 2013, A&A, 550, A28
Mashonkina, L., & Gehren, T. 2000, A&A, 364, 249
Mashonkina, L., & Zhao, G. 2006, A&A, 456, 313
Mashonkina, L., Korn, A. J., & Przybilla, N. 2007, A&A, 461, 261
Mashonkina, L., Zhao, G., Gehren, T., et al. 2008, A&A, 478, 529
Mashonkina, L., Gehren, T., Shi, J.-R., Korn, A. J., & Grupp, F. 2011, A&A, 528, A87
Mathur, S., García, R. A., Catala, C., et al. 2010, A&A, 518, A53
McWilliam, A. 1990, ApJS, 74, 1075
Meftah, M., Corbard, T., Irbah, A., et al. 2014, A&A, 569, A60
Meléndez, J., Asplund, M., Alves-Brito, A., et al. 2008, A&A, 484, L21
Mermilliod, J.-C., Mermilliod, M., & Hauck, B. 1997, A&AS, 124, 349
Mészáros, S., Holtzman, J., García Pérez, A. E., et al. 2013, AJ, 146, 133
Metcalfe, T. S., Chaplin, W. J., Appourchaux, T., et al. 2012, ApJ, 748, L10
Mishenina, T. V., & Kovtyukh, V. V. 2001, A&A, 370, 951
Mishenina, T. V., Kovtyukh, V. V., Korotin, S. A., & Soubiran, C. 2003, Astron. Rep., 47, 422
Mishenina, T. V., Soubiran, C., Kovtyukh, V. V., & Korotin, S. A. 2004, A&A, 418, 551
Mishenina, T. V., Soubiran, C., Bienaymé, O., et al. 2008, A&A, 489, 923
Morel, P. 1997, A&AS, 124, 597
Morel, P., & Lebreton, Y. 2008, Ap&SS, 316, 61
Morel, T., & Miglio, A. 2012, MNRAS, 419, L34
Morel, T., Miglio, A., Lagarde, N., et al. 2014, A&A, 564, A119
Mortier, A., Santos, N. C., Sousa, S. G., et al. 2013, A&A, 557, A70
Mosser, B., Bouchy, F., Catala, C., et al. 2005, A&A, 431, L13
Moultaka, J., Ilovaisky, S. A., Prugniel, P., & Soubiran, C. 2004, PASP, 116, 693
Mozurkewich, D., Armstrong, J. T., Hindsley, R. B., et al. 2003, AJ, 126, 2502
Nissen, P. E. 2005, in The Three-Dimensional Universe with Gaia, eds. C. Turon, K. S. O'Flaherty, & M. A. C. Perryman, ESA SP, 576, 121
Nissen, P. E., & Schuster, W. J. 2010, A&A, 511, L10
Nissen, P. E., Chen, Y. Q., Schuster, W. J., & Zhao, G. 2000, A&A, 353, 722
Nissen, P. E., Primas, F., Asplund, M., & Lambert, D. L. 2002, A&A, 390, 235
Nordgren, T. E., Sudol, J. J., & Mozurkewich, D. 2001, AJ, 122, 2707
North, J. R., Davis, J., Bedding, T. R., et al. 2007, MNRAS, 380, L80
North, J. R., Davis, J., Robertson, J. G., et al. 2009, MNRAS, 393, 245
Pasinetti Fracassini, L. E., Pastori, L., Covino, S., & Pozzi, A. 2001, A&A, 367, 521
Pavlenko, Y. V., Jenkins, J. S., Jones, H. R. A., Ivanyuk, O., & Pinfield, D. J. 2012, MNRAS, 422, 542
Perrin, G., Coudé du Foresto, V., Ridgway, S. T., et al. 1998, A&A, 331, 619
Perryman, M. A. C., de Boer, K. S., Gilmore, G., et al. 2001, A&A, 369, 339
Porto de Mello, G. F., Lyra, W., & Keller, G. R. 2008, A&A, 488, 653
Porto de Mello, G. F., da Silva, R., da Silva, L., & de Nader, R. V. 2014, A&A, 563, A52
Pourbaix, D., Nidever, D., McCarthy, C., et al. 2002, A&A, 386, 280
Poveda, A., Herrera, M. A., Allen, C., Cordero, G., & Lavalley, C. 1994, Rev. Mex. Astron. Astrofis., 28, 43
Prugniel, P., & Soubiran, C. 2001, A&A, 369, 1048
Prugniel, P., & Soubiran, C. 2004, ArXiv e-prints [arXiv:astro-ph/0409214]
Prugniel, P., Vauglin, I., & Koleva, M. 2011, A&A, 531, A165
Quirion, P.-O., Christensen-Dalsgaard, J., & Arentoft, T. 2010, ApJ, 725, 2176
Ramírez, I., & Allende Prieto, C. 2011, ApJ, 743, 135
Ramírez, I., & Meléndez, J. 2005, ApJ, 626, 446
Ramírez, I., Allende Prieto, C., & Lambert, D. L. 2007, A&A, 465, 271
Ramírez, I., Meléndez, J., & Asplund, M. 2009, A&A, 508, L17
Randich, S., Gilmore, G., & Gaia-ESO Consortium 2013, The Messenger, 154, 47
Reddy, B. E., Lambert, D. L., & Allende Prieto, C. 2006, MNRAS, 367, 1329
Retter, A., Bedding, T. R., Buzasi, D. L., Kjeldsen, H., & Kiss, L. L. 2003, ApJ, 591, L151
Richichi, A., & Roccatagliata, V. 2005, A&A, 433, 305
Richichi, A., Percheron, I., & Khristoforova, M. 2005, A&A, 431, 773
Robin, A. C. 2005, in The Three-Dimensional Universe with Gaia, eds. C. Turon, K. S. O'Flaherty, & M. A. C. Perryman, ESA SP, 576, 83
Roederer, I. U. 2012, ApJ, 756, 36
Roederer, I. U., Lawler, J. E., Sobeck, J. S., et al. 2012, ApJS, 203, 27

Roxburgh, I. W. 2008, Ap&SS, 316, 75
Roxburgh, I. W. 2015, A&A, 574, A45
Ruchti, G. R., Bergemann, M., Serenelli, A., Casagrande, L., & Lind, K. 2013, MNRAS, 429, 126
Ruland, F., Biehl, D., Holweger, H., Griffin, R., & Griffin, R. 1980, A&A, 92, 70
Ryan, S. G., & Smith, I. M. 2003, MNRAS, 341, 199
Ryan, S. G., Norris, J. E., & Beers, T. C. 1996, ApJ, 471, 254
Santos, N. C., Israelian, G., & Mayor, M. 2001, A&A, 373, 1019
Santos, N. C., Israelian, G., Mayor, M., Rebolo, R., & Udry, S. 2003, A&A, 398, 363
Santos, N. C., Israelian, G., & Mayor, M. 2004, A&A, 415, 1153
Santos, N. C., Israelian, G., Mayor, M., et al. 2005, A&A, 437, 1127
Sbordone, L., Caffau, E., Bonifacio, P., & Duffau, S. 2014, A&A, 564, A109
Shao, M., Colavita, M. M., Hines, B. E., et al. 1988, A&A, 193, 357
Smiljanic, R., Porto de Mello, G. F., & da Silva, L. 2007, A&A, 468, 679
Smith, G., & Ruck, M. J. 2000, A&A, 356, 570
Smith, V. V., & Lambert, D. L. 1985, ApJ, 294, 326
Smith, V. V., Cunha, K., Shetrone, M. D., et al. 2013, ApJ, 765, 16
Söderhjelm, S. 1999, A&A, 341, 121
Soubiran, C., Le Campion, J., Cayrel de Strobel, G., & Caillo, A. 2010, A&A, 515, A111
Sousa, S. G., Santos, N. C., Mayor, M., et al. 2008, A&A, 487, 373
Sousa, S. G., Santos, N. C., Israelian, G., et al. 2011, A&A, 526, A99
Southworth, J. 2014, ASP, Conf. Ser., submitted [arXiv:1411.1219]
Sowell, J. R., Henry, G. W., & Fekel, F. C. 2012, AJ, 143, 5
Steinmetz, M., Zwitter, T., Siebert, A., et al. 2006, AJ, 132, 1645
Stephens, A., & Boesgaard, A. M. 2002, AJ, 123, 1647
Takeda, Y., Ohkubo, M., Sato, B., Kambe, E., & Sadakane, K. 2005, PASJ, 57, 27
Takeda, Y., Kawanomoto, S., Honda, S., Ando, H., & Sakurai, T. 2007, A&A, 468, 663
Tarrant, N. J., Chaplin, W. J., Elsworth, Y., Spreckley, S. A., & Stevens, I. R. 2007, MNRAS, 382, L48
Teixeira, T. C., Kjeldsen, H., Bedding, T. R., et al. 2009, A&A, 494, 237
ten Brummelaar, T. A., McAlister, H. A., Ridgway, S. T., et al. 2005, ApJ, 628, 453

Thévenin, F., & Idiart, T. P. 1999, ApJ, 521, 753
Thévenin, F., Provost, J., Morel, P., et al. 2002, A&A, 392, L9
Thévenin, F., Kervella, P., Pichon, B., et al. 2005, A&A, 436, 253
Thorén, P., Edvardsson, B., & Gustafsson, B. 2004, A&A, 425, 187
Thygesen, A. O., Frandsen, S., Bruntt, H., et al. 2012, A&A, 543, A160
Tomkin, J., & Lambert, D. L. 1999, ApJ, 523, 234
Torres, G., Andersen, J., & Giménez, A. 2010, A&ARv, 18, 67
Traub, W. A., Ahearn, A., Carleton, N. P., et al. 2003, in Interferometry for Optical Astronomy II, ed. W. A. Traub, SPIE Conf. Ser., 4838, 45
Turon, C., O'Flaherty, K. S., & Perryman, M. A. C., eds. 2005, The Three-Dimensional Universe with Gaia, ESA SP, 576
Valenti, J. A., & Fischer, D. A. 2005, ApJS, 159, 141
Valentini, M., Morel, T., Miglio, A., Fossati, L., & Munari, U. 2013, in EPJ Web Conf., 43, 3006
van Belle, G. T., & von Braun, K. 2009, ApJ, 694, 1085
van Belle, G. T., Ciardi, D. R., & Boden, A. F. 2007, ApJ, 657, 1058
van Leeuwen, F. 2007, HIPPARCOS, the New Reduction of the Raw Data, Astrophys. Space Sci. Lib., 350
VandenBerg, D. A., Swenson, F. J., Rogers, F. J., Iglesias, C. A., & Alexander, D. R. 2000, ApJ, 532, 430
VandenBerg, D. A., Bond, H. E., Nelan, E. P., et al. 2014, ApJ, 792, 110
Verhoelst, T., Bordé, P. J., Perrin, G., et al. 2005, A&A, 435, 289
Westin, J., Sneden, C., Gustafsson, B., & Cowan, J. J. 2000, ApJ, 530, 783
White, T. R., Huber, D., Maestro, V., et al. 2013, MNRAS, 433, 1262
Wittkowski, M., Aufdenberg, J. P., & Kervella, P. 2004, A&A, 413, 711
Wittkowski, M., Aufdenberg, J. P., Driebe, T., et al. 2006a, A&A, 460, 855
Wittkowski, M., Hummel, C. A., Aufdenberg, J. P., & Roccatagliata, V. 2006b, A&A, 460, 843
Worley, C. C., de Laverny, P., Recio-Blanco, A., et al. 2012, A&A, 542, A48
Yi, S., Demarque, P., Kim, Y.-C., et al. 2001, ApJS, 136, 417
Yi, S. K., Kim, Y.-C., & Demarque, P. 2003, ApJS, 144, 259
Zhang, H. W., & Zhao, G. 2005, MNRAS, 364, 712
Zhang, H. W., & Zhao, G. 2006, A&A, 449, 127
Zhao, G., & Gehren, T. 2000, A&A, 362, 1077
Zhao, G., Chen, Y. Q., Qiu, H. M., & Li, Z. W. 2002, AJ, 124, 2224